Preparation of Substrates for Semiconductor Growth Using Atomic Hydrogen

Thesis

Submitted to the Eberly College of Arts and Sciences of West Virginia University
In Partial Fulfillment of the Requirements for
The Degree of Master of Science
in
Physics

By
Lauren S. Hirsch
Morgantown, West Virginia
March, 1998

Abstract

Atomic hydrogen is quite effective at cleaning substrate surfaces for subsequent growth of compound semiconductors by molecular beam epitaxy. Five different materials were cleaned *in-situ* using atomic hydrogen. Hydrogen cleaning was shown to remove oxides and other surface contaminants from CdTe, HgCdTe, GaAs, and sapphire. Hydrogen cleaning is compared to other methods of *in-situ* preparation which have been used in the past through the use of reflection high energy electron diffraction, atomic force microscopy, ultraviolet fluorescence microscopy, and Nomarski interference-contrast microscopy of substrate surfaces. The most detailed study, HgCdTe, also includes the use of x-ray photoelectron spectroscopy. Use of atomic hydrogen to prepare Si, however, was not effective in our MBE system. Reasons for the difficulty in cleaning Si are discussed, and possible solutions are presented.

To Mom, Dad, Rob, Faunne, Scott, and Kevin.
The six most important people in my life, I love you all.

ACKNOWLEDGMENTS

First I would like to thank Dr. C. Stinespring and Dr. D. Lederman for taking the time to serve on my committee. Most importantly want to thank Dr. T. Myers for serving as my advisor and for pushing me to do my best even when I just want to give up.

Special thanks to Zonghai Yu and Steve Buczkowski for taking time to get me started in the lab, and Matt Millecchia and Aaron Ptak for helping me out and keeping me sane, sort of. You guys are the best. A very special thanks to Dr. Stinespring's group for all of the XPS work, especially Katie Ziemer who compiled most of the data, and managed, somehow, to keep her spirits up under the most straining circumstances. Additional thanks also goes to Dr. N. Giles and Monica Moldovan for the photoluminescence data on the ZnSe. And to the numerous other friends I have in the department, thanks for your support - it really means alot.

Table of Contents

List of Figures

List of Tables

1. Introduction

1.1 Background

In recent years semiconductor research has seen rapid expansion. As this continues the quality of many compound semiconductors steadily improves. The development of II-VI semiconductors is fast approaching the level of the more advanced group IV and group III-V compound semiconductors. Interest in the wide bandgap III-V compounds is also growing. A recent accomplishment in this area was the production of a blue laser by Nichia Chemical that has a reported lifetime of 10,000 hours.[1] As researchers improve materials, device production expands at an equal if not greater rate. With each new technological achievement devices become quicker, cheaper, and smaller. They also run longer, perform better, and operate at higher speeds and temperatures.

Most intricate device structures require epitaxial growth of a succession or series of thin layers. This process is limited by a number of constraints. Material availability, compatibility between components, and the cost of starting materials must all be taken into account. As new structures are designed for commercial application, researchers scramble to solve the problems related to fabrication.

Of the numerous challenges facing researchers, many are related to problems at the interface of the two compounds. One of these is mismatch between the lattice constants of the two materials. If the lattice constants differ by more than a few percent, dislocations can be formed upon the initial nucleation of the film. Another challenge is understanding how the surface of one face interacts with the constituents of the other. If one of the elements is more reactive than the other, and consequently bonds to the substrate forming a compound that is not compatible with the crystal lattice, it can limit the quality of the subsequent film. Similarly, the

overall quality of the substrate surface can be a limiting factor. Rough surfaces, oxides, or etching remnants can all lead to poor film quality. New techniques to overcome these problems need to be explored.

As an example, an ongoing problem in heteroepitaxial growth of ZnSe and CdTe has been a high density of defects related to stacking faults originating at the substrate-epilayer interface. These defects serve as nucleation sites for dislocation generation during device operation, leading to degradation and ultimate device failure in an unacceptably short time.[2-4] It is believed that the stacking faults occur during initial layer growth and are due either to incomplete oxide removal or poor surface preparation that induces the formation of stoichiometry-related defects.[2,5]

Different techniques have been used to remove oxides from the surfaces of various substrates. These techniques include *ex-situ* etches as well as *in-situ* heating. However, such methods tend leave behind remnant oxides, and/or require buffer layers to be grown before the final film is deposited. Also, the temperatures required for *in-situ* heating can be quite high, while lower temperatures are often necessary for compatibility with the development of certain device technologies.

Contaminants and oxides can be removed from the surfaces of semiconductors with atomic hydrogen.[6-13] Early substrate preparation experiments were performed by reactive-ion etching. This is advantageous since the cleaning can be performed at much lower temperatures than conventional methods, however there tends to be some damage done to the surfaces due to ion bombardment.[14] Further experiments have been done using rf and electron-cyclotron-resonance (ECR) plasma sources to produce atomic hydrogen. This approach improved surface quality, yet the ions produced by the plasmas have the potential to degrade the surface electronic

2

properties.[5] The most recent work has been done using a thermal cracker to produce atomic hydrogen since it does not produce ions. Lou *et al.*[15] have cleaned CdTe surfaces with thermally-cracked atomic hydrogen, and examined the effects on stoichiometry. Other groups have used thermal sources to clean Si[10], GaAs[6,8], and InP[12].

1.2 Goals

A review of the literature shows that there is still a considerable amount of work remaining to be performed to understand the role of atomic hydrogen in the preparation of surfaces for epitaxial growth. It is the purpose of this thesis to investigate using atomic hydrogen to clean five different surfaces. The goals of this study are listed below.

(1) Study the effect of hydrogen cleaning of CdTe surfaces, and its effects on the resulting film growth.

(2) Investigate oxide removal from a HgCdTe surface using atomic hydrogen by looking at the effects of hydrogen cleaning on stoichiometry and on CdTe passivation.

(3) Build on previous hydrogen cleaning studies of GaAs surfaces by depositing ZnSe and CdTe layers, and looking at the quality of the epitaxial films.

(4) Use atomic hydrogen to prepare clean sapphire as a substrate for GaN deposition.

(5) Investigate the use of atomic hydrogen to prepare Si substrates for growth of ZnTe and CdTe.

2. Experimental Details

2.1 The Growth System

The oxide-removal experiments and epilayer growths were performed in a custom MBE system at West Virginia University, which is shown in Fig. 2.1 and 2.2.[16-18] The system consists of two chambers, the growth chamber and the load lock, which are separated by a gate valve. The growth chamber is evacuated with a CTI-Cryogenics CT-8 cryopump and the load lock with a Varian Turbo-V250 turbomolecular pump.

Initial pump down of the growth chamber is done with the turbomolecular pump through the load lock. Once the pressure reaches the 10^{-6} Torr range the gate valve is closed and the main chamber can be evacuated by the cryopump. Using the cryopump, the growth chamber pressure will reach pressures in the 10^{-9} Torr range without a bakeout. The background gases at this pressure tend to be water vapor, nitrogen, hydrogen, and carbon dioxide. These can all be monitored on the system's UTI-100C quadruple mass spectrometer. To further reduce the pressure in the chamber and suppress these background gases, the system is heated to temperatures between 120-150°C (the so-called "bakeout") until the levels of these gases reaches an acceptable range. After a bakeout the chamber reaches pressures in the 10^{-11} Torr range.

The gate valve at the main chamber allows the load lock to be brought up to atmospheric pressure without affecting the pressure in the growth chamber. This makes it possible to load and unload the substrate block in the following manner. If the gate valves to the turbo-molecular pump and the main chamber are both closed, the load lock can be vented with dry nitrogen gas to create an overpressure. Once the load lock is above 760 Torr it can be opened to the cleanroom environment without an excess of water vapor entering. A substrate block is then mounted on a
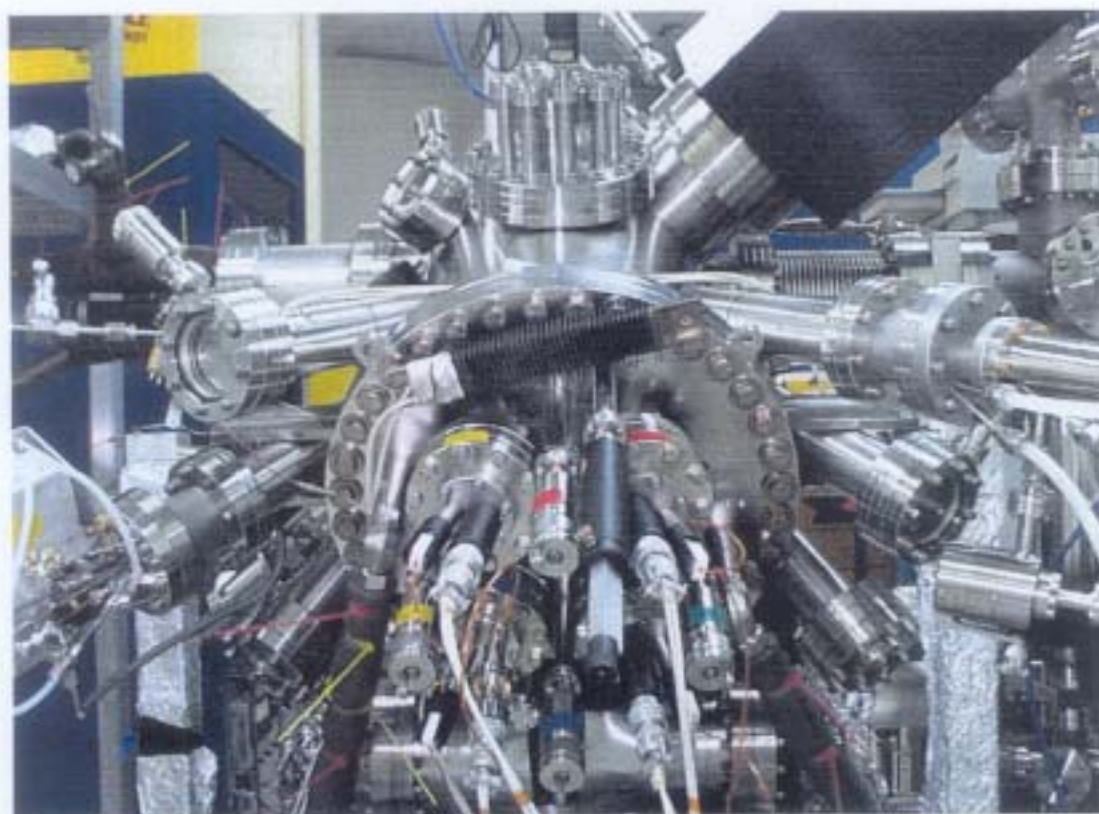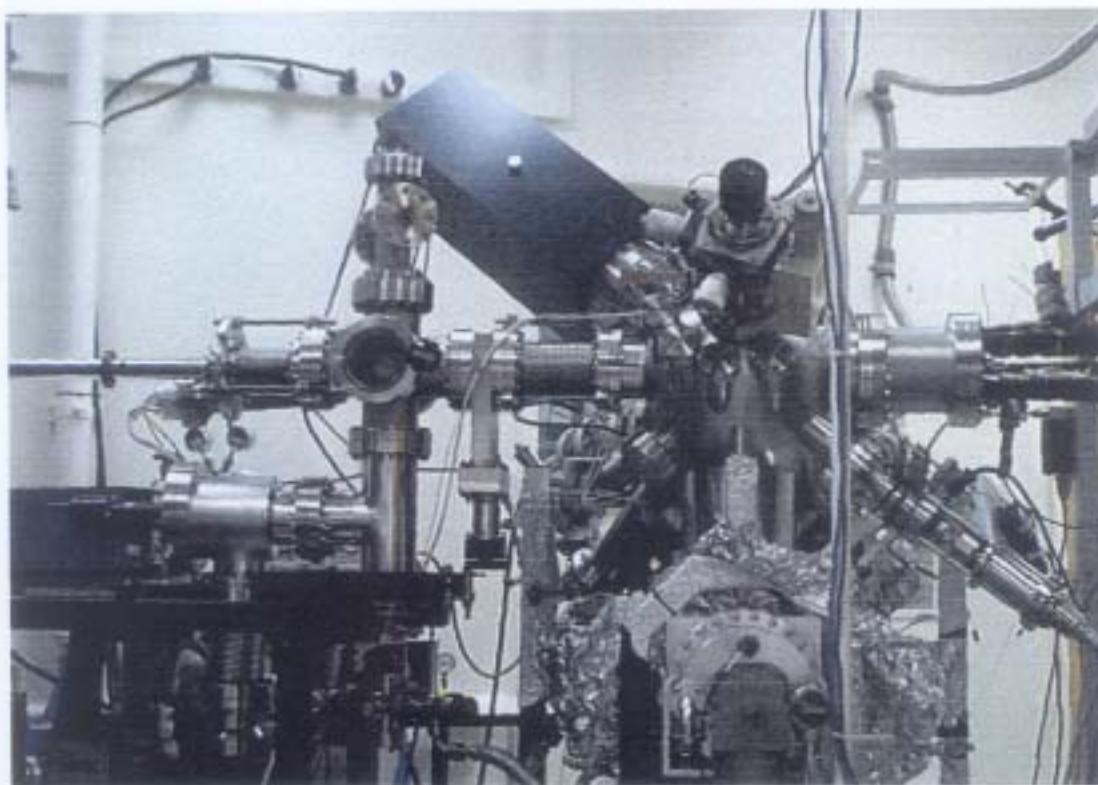
Fig. 2.1   Custom MBE chamber at West Virginia University.
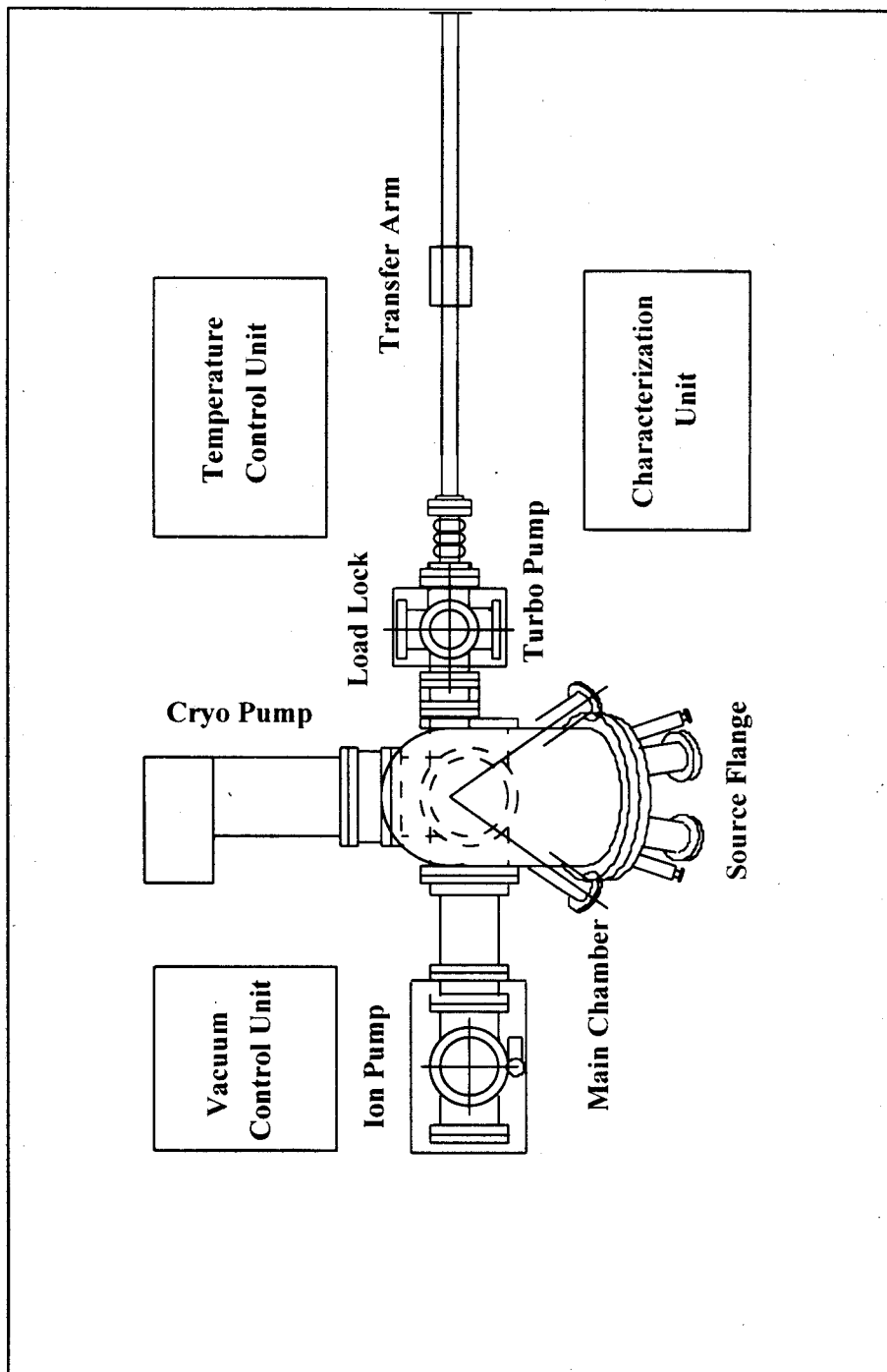
Fig. 2.2   Drawing of the MBE chamber at WVU, pointing out the major components discussed in this chapter.

transfer arm in the load lock, and the load lock is then pumped back down to the 10^{-7} Torr range. The transfer arm is then inserted into the growth chamber, and the substrate block can be positioned for growth.

The growth chamber is based on a cylindrically-shaped vessel tilted 30° away from horizontal. At the top of the growth chamber is the substrate manipulator. The manipulator directly controls the substrate heater and hence controls the position of the substrate block inside the chamber. Once the substrate block is brought into the system by the transfer rod, the manipulator can be used to bring down the heater assembly and grab the block. Once the block is transferred to the heater assembly, it is pulled back to the growth position using a micrometer. In addition to the Z coordinate, the X and Y coordinates can also be adjusted. Once in position the sample can be rotated 360° in the plane of the substrate. Due to the high substrate temperatures used for growths, the surrounding area is kept cool with a liquid nitrogen cooling shroud. The liquid nitrogen-cooled shroud also creates a cleaner vacuum in the volume immediately surrounding the substrate.

2.1.1 The Heater Assembly

The heater assembly consists of a molybdenum cup with three bayonet slots equally spaced around the cup used to lock the substrate block in place, and a fourth open slot used to ensure proper alignment. The substrate block itself is a cylindrical-molybdenum cup with three equally-spaced pins to hold the block in the bayonet slots, as well as a fourth pin for alignment purposes. This cup's outer diameter closely matches the inner diameter of the assembly cup. This geometry leaves a cylindrical cavity behind the substrate where the heater is mounted. A diagram of a substrate block on the heater assembly is given in Fig. 2.3.

To Manipulator

TC Spring Loading

Wire Connection Stub

Insulator Connection

Substrate Heater
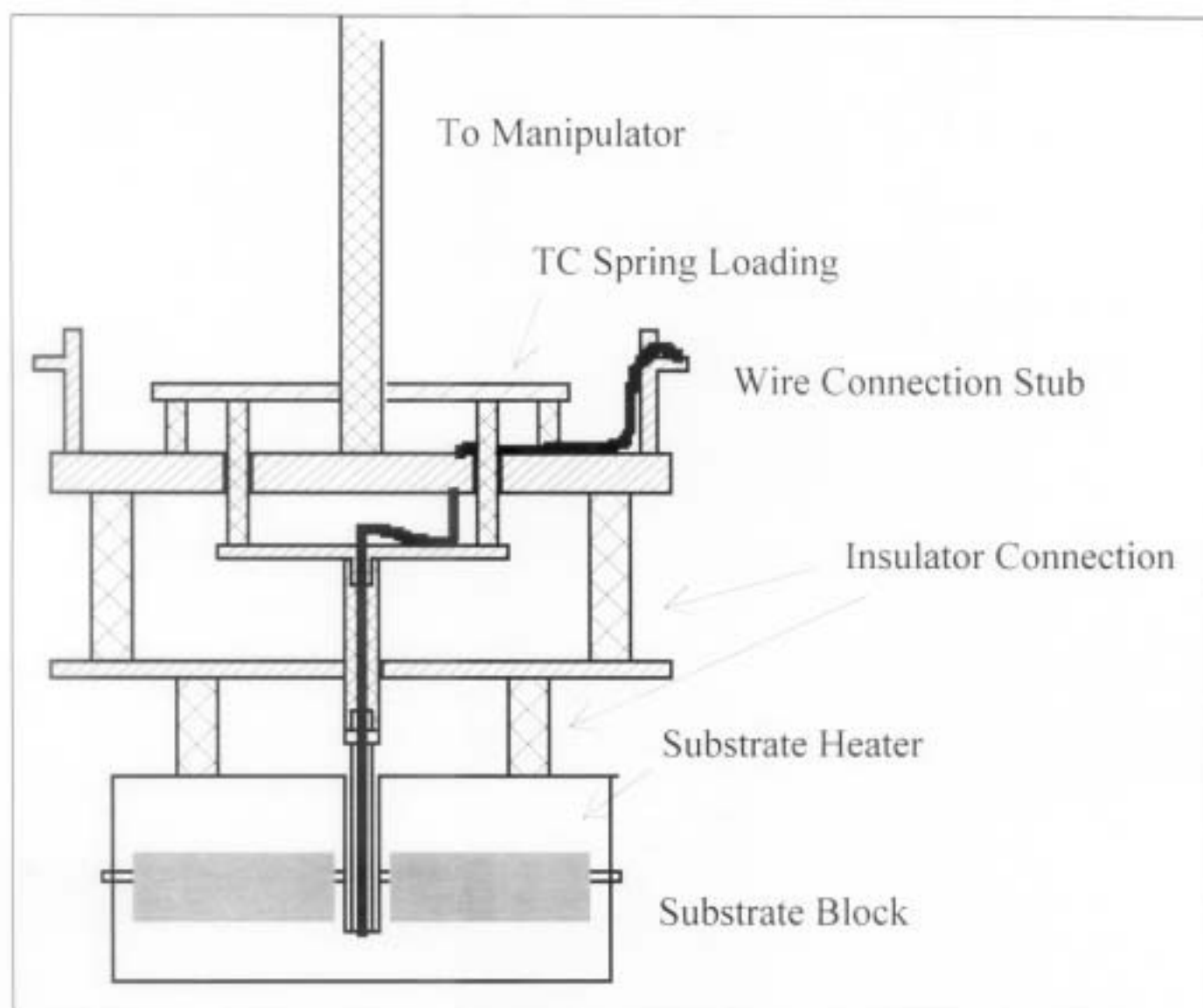
Substrate Block

Fig. 2.3   Diagram of the heater assembly and substrate block.

The heater is constructed of tantalum wire wound around a pyrolytic boron nitride (PBN) disk, and then situated between two more PBN disks which serve as insulators. These disks are then held in place by additional tantalum wire. The two ends of the wire in the windings are run to a ceramic feedthrough and connected to a power supply. Running through the center of the heater is a type K thermocouple used to regulate the heater power supply. This thermocouple comes in direct contact with the center of the back of the substrate block, and is held there by a spring mechanism. All wires, either from the heater or the thermocouple, are threaded with ceramic beads to ensure electrical isolation.

Because the thermocouple is not in direct contact with the substrate itself, it is important to know the temperature gradient between the surface of the block and the point of contact with the thermocouple. Three different experiments have been performed to calibrate the substrate temperature. In the first two cases a thermocouple was introduced to the system through a 1-1/3" flange, and brought into contact with the front surface. In the first experiment the thermocouple was attached directly to the block with colloidal graphite, and in the second a sapphire substrate was mounted on the block using indium with the thermocouple in contact with the surface of the substrate. The substrate temperature was raised in small increments, allowed to settle, and the two temperatures from the front and back thermocouples were recorded. The data points were then fit using a nonlinear regression in Jandel Scientific's Sigma Plot program. The resulting curve was then used in future experiments to determine a set point for the thermocouple in the heater assembly to achieve the proper temperature at the substrate.

After a large number of high temperature growths the spring loading of the thermocouple failed to work properly, and the thermocouple was not always in direct contact with the back of the block. This led to uncertainty in the temperature of the block. Because the temperatures

9

required at this point in time were relatively low, 80-300°C, accurate temperature readings were taken daily using a second technique. This calibration was performed by mounting a separate substrate piece to the block. Using a soldering iron, three to four indium spikes were attached to the surface of this second substrate. While slowly heating the block one could watch the spikes through a viewport, and record the temperature that the indium melted. Comparing this temperature with the actual melting temperature of indium, 156.7°C, one can determine the temperature differential, and thus make a good approximation of the temperature.

2.1.2 RHEED

An electron gun and phosphor screen are located 180° away from each other within the chamber, as shown in Fig. 2.4. These are used for reflection high energy electron diffraction (RHEED). The electron gun is aligned such that, when the sample is in the growth position, the electrons beam makes an angle of one degree with the surface of the sample. The scattered electrons incident on the phosphorous screen then form a diffraction pattern. The screen is surrounded on the outside of the chamber by a black box. Inside the box is a CCD camera which is connected to a computer and a video monitor. The computer controls the camera through a program called KSA-400, which was written by k-Space Associates, Inc. and is designed to acquire and manipulate RHEED images.

2.1.3 Source Ports

At the bottom of the chamber is the source flange. The source flange has four ports for solid-source ovens providing the growth species. Each oven is aimed toward the substrate block, and is 12° from an axis perpendicular to the substrate with a source-to-substrate distance of approximately 12". The sources are typically operated at temperatures ranging from 200 to
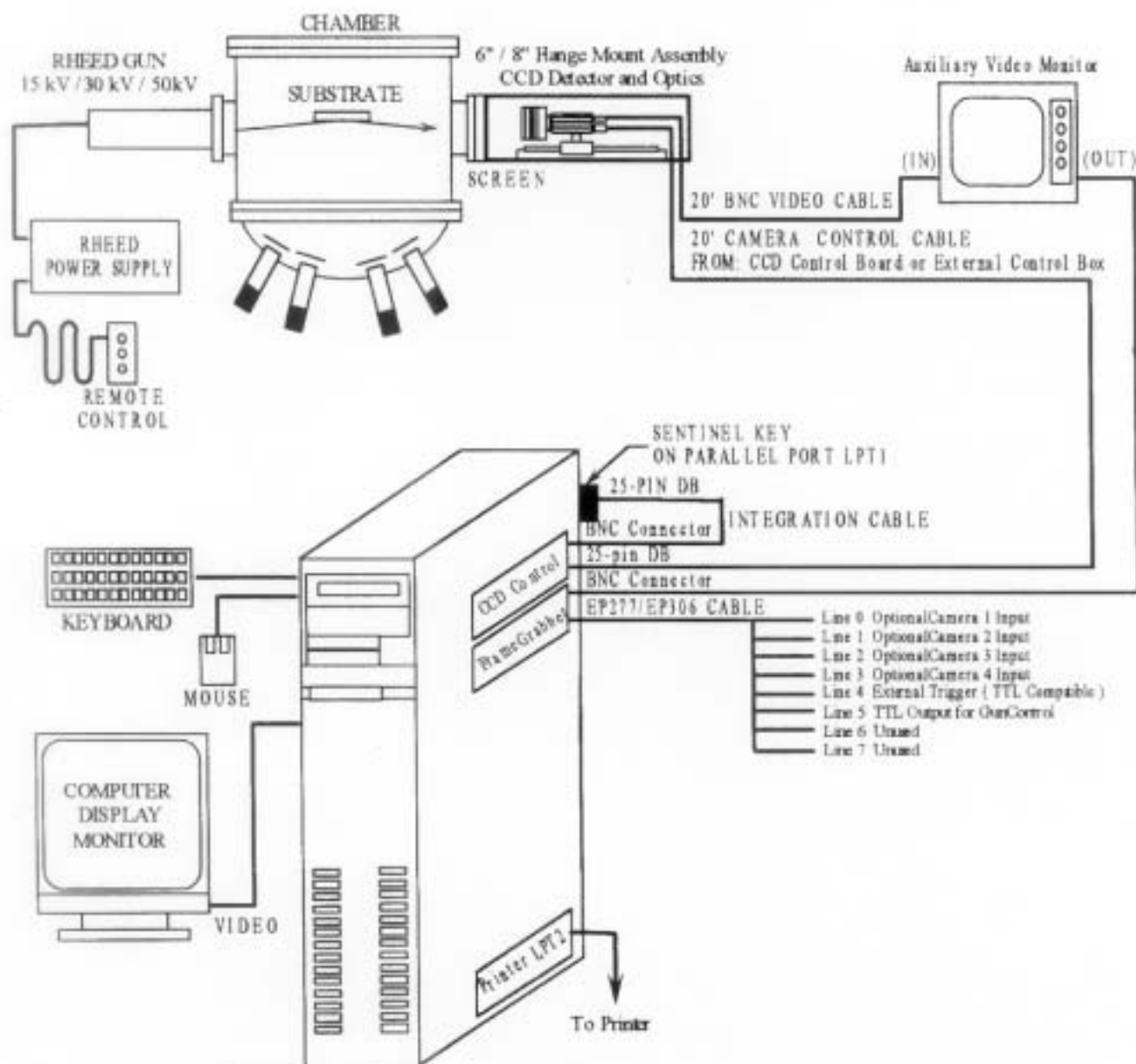
Fig. 2.4   Diagram of the RHEED system used on the MBE chamber, as well as the computer manipulation schematic used with the k-space program. (Taken from Ref. 19)

1000°C depending on the particular species. For this reason the sources are surrounded by a cooling shroud which contains a mixture of ethylene glycol and water. The solution is cooled to 5°C and circulated throughout the lower area of the chamber by a NESLAB HX-200 cooling system.

Surrounding these ports are a total of six 4.5" ports used for additional characterization, and for housing the nitrogen and hydrogen sources. Fig. 2.5 shows the chamber crossection with two of these ports shown at either side of the source flange port. These ports are each located at the end of 2 ½" OD stainless steel tube. The tubes are welded to the chamber such that their center line is approximately 8" above the source flange. The tubes are 10" along their center line, and 35° away from being inline with the sample. This gives a distance of 21.4" from the port to the substrate.

2.2 The Hydrogen Source

A commercial atomic hydrogen source (EPI-AHS-L), shown in Fig. 2.6, is used to generate atomic hydrogen. The source produces atomic hydrogen by thermal cracking of molecular hydrogen on a heated tungsten filament.[20] The filament is heated using a current-regulated power supply that can be adjusted up to 10 A. At currents of 7.0 to 10.0 A, the temperature varies between 1800 and 2400°C.[20] For this reason the source has its own water cooling lines located outside the cooling shroud. These lines are coiled around the cell, and supplied with water flowing at a rate of approximately 0.5 L/min. The hydrogen gas is inlet to the source cell through a VCR fitting. Connected to the inlet is a Fisons MD7 leakvalve. This valve employs a micrometer-calibrated knob, allowing the flow of gas to be controlled between 10^{-6} and 10^{-11} mbar/sec, or 7.5×10^{-7} and 7.5×10^{-12} Torr/sec.[21] Attached to the inlet side of the

Hydrogen
Source Port

Source Flange
Port

17.50"

10.0"

3.5°   3.5°

Location of Substrate
when in Growth Position

Substrate
Manipulator
Flange Port
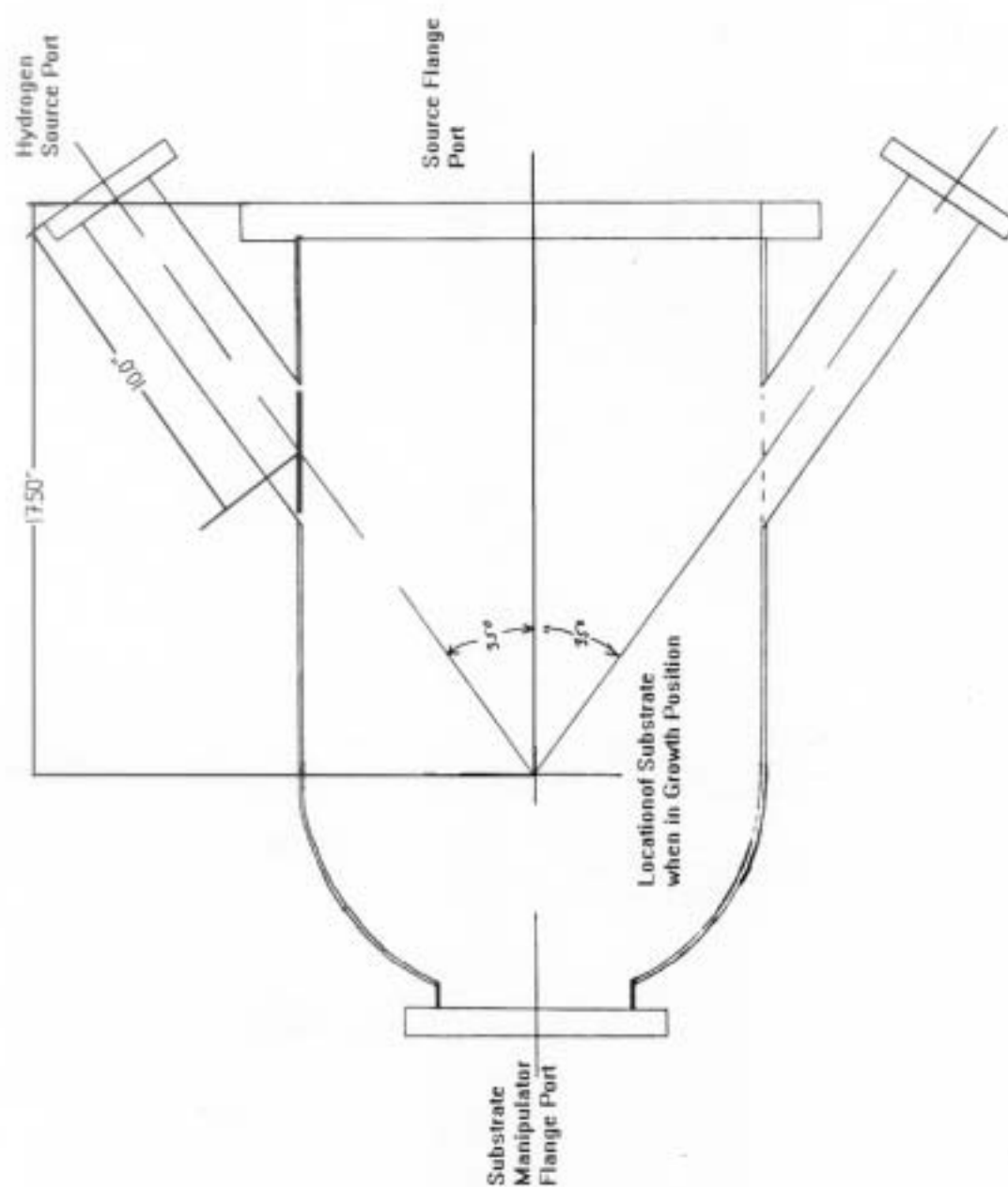
Fig. 2.5   MBE chamber showing the ports for the source flange, substrate manipulator flange, and the hydrogen source.
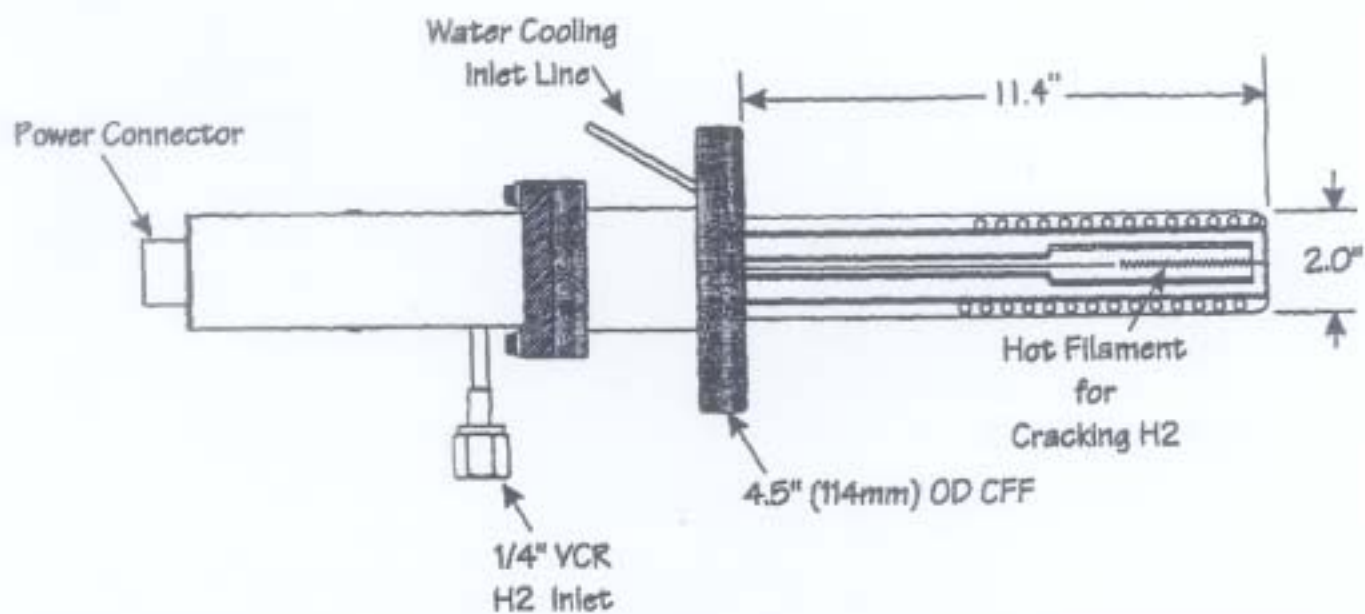
Fig. 2.6   Schematic of the hydrogen source, as well as a photograph of the source as it looks mounted to the system.
(Taken from Ref. 20).

valve is a tee connected to two on/off valves. These valves are connected by flexible, formed-bellows lines and regulators to hydrogen and deuterium tanks. During operation, the valve on the hydrogen tank and the valve leading to the tee are fully opened, and the regulator is set to supply 30 psi to the leak valve. Both valves to the deuterium tank are completely closed. For operation with deuterium, the order of open and closed valves is switched.

As stated in the previous section, the port for the hydrogen source is a 10" long, 2.5" diameter tube at the side of the chamber. Directly inside, at the point where the tube is welded to the chamber, are the water cooling lines for the source flange. Since the source is 11.4" in length, from tip to flange, a 4" nipple must be attached to the chamber's port to ensure that the source does not hit these cooling lines. This gives a source-to-substrate distance of 14".

Once inserted into the system, the source must be outgassed. To do this the filament current is slowly turned up to 9.5 A. This is typically accomplished by raising the current one amp every five minutes while watching the system pressure. If the pressure becomes too high due to the outgassing, the current is kept constant until the pressure falls to an acceptable level. Once the current reaches 9.5 A, the source is left to continue outgassing for several hours. The current is then brought down in steps of one amp every two minutes.

For operation the source is stepped up to 9.5 A, first in two amp increments every two minutes until the source reaches six amps. It is then raised in one amp increments every two minutes up to nine amps, at which point the final half amp step is made. The current is brought back down in the reverse step order.

Included with the source manual is a specification sheet which lists the temperatures the filament reached at specific currents prior to shipment, as measured with an optical pyrometer.

For the source used in this study, values of 1750°C and 2200°C were given for 7.0 A at 19.1 V and 10 A at 36.1 V, respectively.

This particular source was one of the first of its kind produced by EPI. Since then EPI has made some improvements in the production of their filaments, so that their performance is more consistent. It is noted that when newer filaments are used in this source, the voltage at 9.5 A is between 40.0 and 47.0 V. (As the filament is continually used the voltage rises from day to day, then drops significantly shortly before the filament fails.) Since the newer filaments operate at a higher power, one would expect the temperature to be higher as well. The MBE chamber does not have an optical port that could be used to measure temperature of the filament with an optical pyrometer, so no data could be directly taken for this source. However, a second source was purchased for a new MBE chamber currently being built at WVU. This newer source's specification sheet was supplied with data for a new filament, and has temperature values of 1870 and 2365°C corresponding to 7 A, 25.9 V and 10 A, 45.7 V, respectively. It was determined that while filament temperatures will vary slightly from source to source, the values on the second specification sheet were fairly typical and could be used to estimate the temperature of the new filament in the older source.[22] Stefan-Boltzmann's law is

$$\frac{P}{A} = \varepsilon \sigma T^4$$

where Stefan-Boltzmann's constant, σ, is 5.67×10^{-8} W m^{-2} K^{-4}. Using the values for power and temperature given on the specification sheet for 10 A, a value for emissivity times area, εA, can be determined and used as an estimated value for other filaments. Reverse substitution, assuming a power range of 380-447 W, yields an operating temperature range of 2248-2352 °C.

It is of interest to determine the number of hydrogen atoms reaching the surface of the substrate. The flux incident on the surface of the substrate, Φ, is given in MKSA units by [23]

$$\Phi = \frac{1}{2\pi^{1/2}} n_i v_o \qquad (2.1)$$

where n_i is the total number of molecules at a pressure p_i, and v_o is the most probable speed calculated from kinetic theory. The quantities n_i and v_o can be written as

$$n_i = \frac{2p_i}{M_i v_o^2} \qquad (2.2)$$

$$v_o = \left[\frac{2kT}{M_i}\right]^{1/2} \qquad (2.3)$$

where k is Boltzman's constant and M_i is molecular mass. Substitution into (1) gives

$$\Phi = \frac{p_i}{\sqrt{2kM_i T\pi}} \qquad (2.4)$$

The hydrogen flow used for substrate cleaning typically resulted in a system pressure of 1.2×10^{-6} Torr and a reading at our beam flux monitor of about 1.7×10^{-6} Torr. The ion gauge used in the beam flux monitor, however, is calibrated to nitrogen gas, and the sensitivity to hydrogen gas must be taken into account. The sensitivity for H_2 is approximately 0.5 which gives the actual pressure of hydrogen as 3.4×10^{-6} Torr, or 4.5×10^{-4} Pascals. For hydrogen (H_2), M_i is 2.0×10^{-3} kg/mole. Using k $=1.38062\times10^{-23}$ J/K and T = 300 K, a flux of 4.8×10^{19} m^{-2}s^{-1}, or 4.8×10^{15} molecules cm^{-2}s^{-1} is expected. The biggest uncertainty is what temperature to use. Using the operating temperature of our source, 2300K, would change this number to 1.7×10^{15} molecules cm^{-2}s^{-1}.

However, it is the number of atoms reaching the substrate that is of interest, so a cracking efficiency needs to be obtained. Information pertaining to the cracking efficiency for this source has been reported in two EPI application notes.[24,25] The first publication demonstrated that an inverse relationship existed between the cracking efficiency and the flow rate of hydrogen gas, but did not give enough information to accurately relate this to the amount of hydrogen flowing in the source.[24] The second EPI note gave a more specific relationship between a flow rate and the corresponding cracking efficiency. Fig. 2.7[25] is a graph of cracking efficiency versus temperature for a flow rate of 1.5 sccm.

The leak valve on the hydrogen source does not indicate a specific flow rate, so in order to complete the estimation of the cracking efficiency a flow rate must be determined. The pumping speed for hydrogen for the cryopump is 2500 L/sec.[26] Conductance calculations indicate that this should drop to about 2000 L/sec at the main chamber. A pressure of 1.2×10^{-6} Torr thus indicates a flow of approximately 1.5 sccm. This is important since this is the flow rate used to produce the graph in Fig. 2.7. The cracking efficiency for these operating conditions is approximately 10%. Every molecule cracked yields two atoms, so a cracking efficiency of 10% means that 9.6×10^{14} atoms cm^{-2}s^{-1} hit the substrate.

The time for one monolayer equivalent impingement of atomic hydrogen is given by

$$t_{mono} = \frac{1}{\Phi d^2}$$

(2.4)

where d is the distance between atoms. This distance will vary from substrate to substrate, but to get an approximate time the value of d can be taken as 3Å. Equation 2.4 then yields 1.2 sec as the time a monolayer equivalent of hydrogen atoms to arrive.
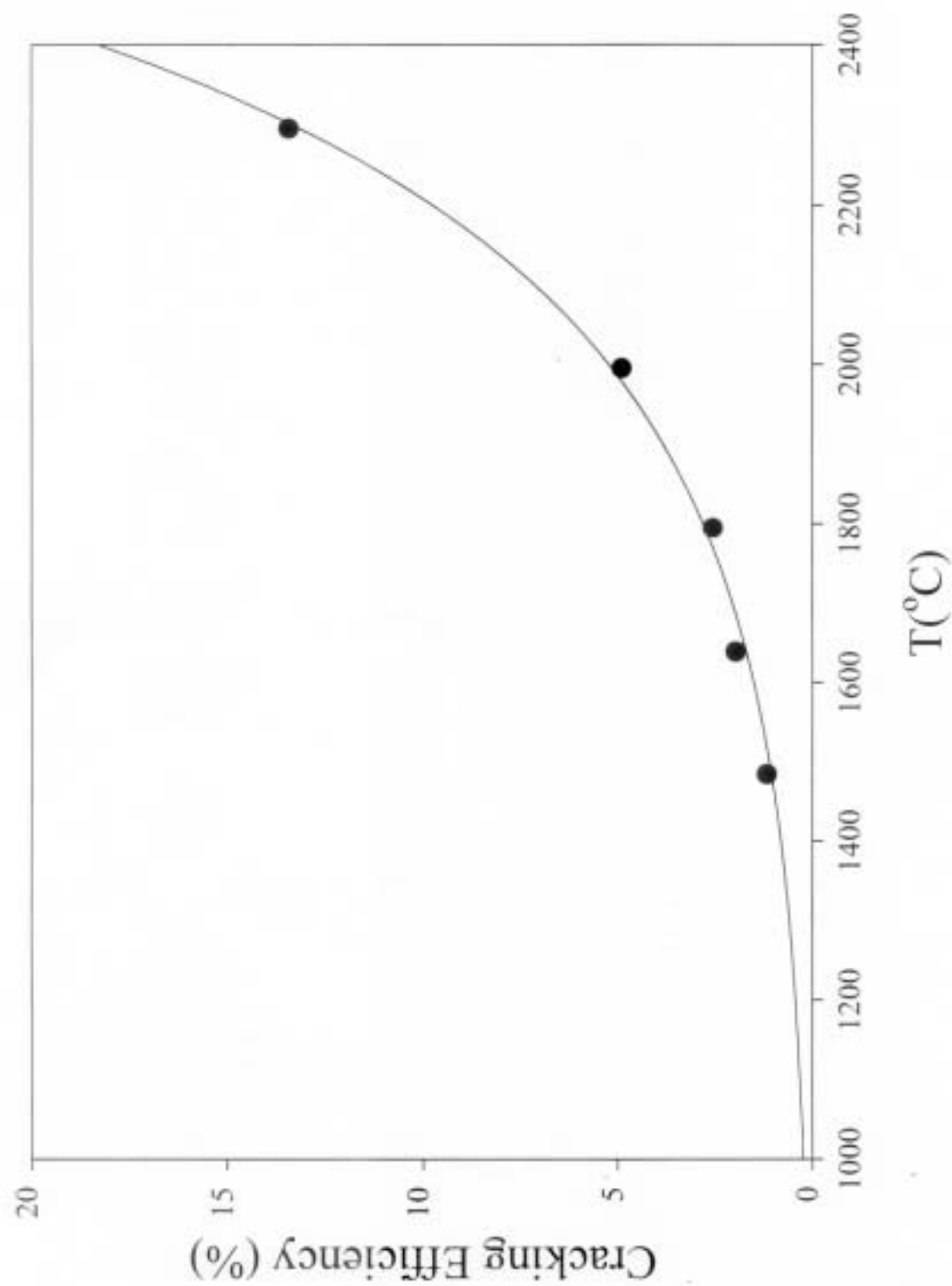
Fig. 2.7   Cracking Efficiency vs. Filament Temperature for the EPI cracker. (Taken from Ref. 25).

2.3 Procedure for Preparing Substrates

A typical cleaning sequence consists of several steps. Specific chemical and hydrogen etch conditions and times will be given in the individual sections if they do not apply to all substrates. In addition, Appendix A contains schematics describing all of the chemical etch procedures. The substrate first undergoes a solvent degreasing procedure. This consists of two immersions in trichloroethylene, each five minutes long. Next is a two minute immersion in acetone, followed by two five minute immersions in methanol. The five 100 ml beakers used for the degrease are filled with approximately 60 ml of their respective solvents. The beakers are warmed to a temperature of about 70°C on a hot plate prior to and during the degreasing. After the final bath in methanol, the substrate is rinsed in fresh methanol and dried with high purity nitrogen gas. Each type of substrate then undergoes a unique etch. After the etch, the substrate is mounted on the substrate block with either indium or colloidal graphite (Aqua-dag, Ladd Research Industries, Inc.), and inserted into the load lock. The loadlock is evacuated, at which point the substrate is transferred to the growth chamber and onto the substrate manipulator. Once on the manipulator, the substrate is pulled back to the growth position and shielded from the sources by the substrate shutter. If the substrate is mounted with Aqua-dag, a degassing time of approximately one hour from the time of insertion is allowed. After any necessary degassing the substrate is heated to its cleaning temperature, the hydrogen source is turned up slowly to its operating current, and the RHEED electron gun is slowly brought up to 13 kV and ~20 μA. It typically takes 20 minutes for the substrate temperature to stabilize, and the hydrogen source to be brought up to the operation current.

During this time it is important to rotate the substrate to a position where a known RHEED pattern exists. Practice and familiarity with the substrate allows one to find a particular pattern readily, even though at this point the substrate still has an oxide layer and may not exhibit a bright pattern. Once the current reaches 9.5 A, the hydrogen tank is opened. The leak valve is then slowly opened until there is a reading of 1.2×10^{-6} Torr above the background on the system's ion gauge. In order to monitor the RHEED diffraction patterns as a function of time the KSA-400 program is set up to take a RHEED image every thirty seconds. Once the first RHEED picture is taken of the substrate, the substrate shutter is opened, and a timer is started to monitor the exposure to hydrogen. The exposure time is determined from previous experiments on the particular substrate material being used, but can be modified based on RHEED observations. At the end of the predetermined cleaning time, the substrate shutter in closed. As the hydrogen cleaning progresses, the diffuse scattering associated with the oxide should disappear, and a streaky pattern indicative of a flat, two-dimensional surface should replace it. However, it has been shown that additional exposure of many of the substrate types can cause the surface to roughen. This is manifested by a breakdown of the streaks in the RHEED pattern into spots. If RHEED streaks appear to start breaking into spots before the general cleaning time expires the substrate shutter is closed, and the time elapsed is recorded in the notebook. If the pattern is still streaky, indicating a two dimensional surface, the substrate is cooled to growth temperature, and the experiment can proceed. If, on the other hand, the RHEED indicates a three dimensional pattern for any substrate other than HgCdTe, the experiment is terminated. After the substrate is shuttered, the gas is turned off, and the source's current is brought down.

2.4 *Ex-Situ* Characterization

Once the sample has been brought out of the system, there are a number of other experiments which can be performed. In device fabrication the substrate/epilayer interface needs to be as two-dimensional as possible to limit defects in the crystal. Therefore, a major concern is the topography of the substrate before and after hydrogen cleaning, as well as the surface of the epitaxial films that are ultimately deposited on the substrates. Atomic force microscopy (AFM) measurements were made in air using a Digital Instruments Nanoscope II. The AFM has been used to look at the surfaces of cleaned and uncleaned substrates as well as the surfaces of films deposited on these substrates.

Another topic of interest was the effect of hydrogen on the stoichiometry of the substrates. Maintaining the stoichiometry of the HgCdTe is of great importance, since small changes in stoichiometry will change the bandgap energy. Reflectance measurements have been performed in the visible region on HgCdTe using a Cary-14 spectrophotometer. Three room temperature scans were taken of each substrate and then referenced to sapphire scans taken on the same day. The E_1 reflectance peak in scans taken before and after hydrogen cleaning were then used to search for gross shifts in stoichiometry.

Nomarski microscopy and uv fluorescence microscopy were performed using an Olympus BX60M microscope. Nomarski microscopy was used to look for surface features such as hillocks, pits, or fractures, as well as surface roughness. Fluorescence microscopy was used to look for imperfections with a 100 W Hg lamp used to excite the fluorescence. For example, in ZnSe Frank dislocations or Schockley defects are easily seen with UV florescence. In GaN UV fluorescence can be used to locate possible sites for photoluminescence lines.

2.5 XPS System

X-ray photoelectron spectroscopy (XPS) measurements have been performed to study hydrogen cleaning. These experiments were performed in an effort to more clearly understand what occurs during hydrogen cleaning. The removal of oxides and changes in surface stoichiometry can be monitored as a function of cleaning time.

The experiments were performed in a two-chamber ultrahigh vacuum (UHV) system used for semiconductor processing studies, which is shown schematically in Fig. 2.8.[27] One chamber allowed atomic hydrogen etching with controlled sample heating, similar to that in the MBE chamber, while the second contained the facilities for XPS. (It is noted that the second hydrogen source mentioned earlier is used to perform experiments in this system.)

The Mg anode (1253.6 eV x-ray line) of a Fisons twin anode x-ray source, operating at 300 watts, was used in XPS analysis. Emitted electrons were analyzed using a VG100AX hemispherical analyzer in 1:1 lens mode, resulting in a sampling area slightly more than 4 mm wide. Spectra were taken in constant-analyzer-energy mode with a 20-eV pass energy with the work function determined by calibration on argon-etched silver foil. Data acquisition and analysis was performed with a VGX900 board and software. After further study it was determined that a more sophisticated analysis was necessary, and so the raw data was re-analyzed using Jandel Scientific's Peak Fit program to obtain a more accurate set of information.

2.5.1 Calibration of the Hydrogen Flux in the Second System

The hydrogen flow used for substrate cleaning in the MBE system typically resulted in a system pressure of 1.2×10^{-6} Torr representing a flux of about 9.6×10^{14} atoms sec^{-1} cm^{-2} for atomic hydrogen. In order to compare experiments in the two systems, the flux at the substrate in the XPS system needs to be determined.

Hemispherical Electron Energy Analyzer

X-ray Source

SAM Optics

Viewport

Extrel Mass Spectrometer

Radical Gas-Species Source

Linear Transfer

Hydrogen Source Port

Turbo Molecular Pump
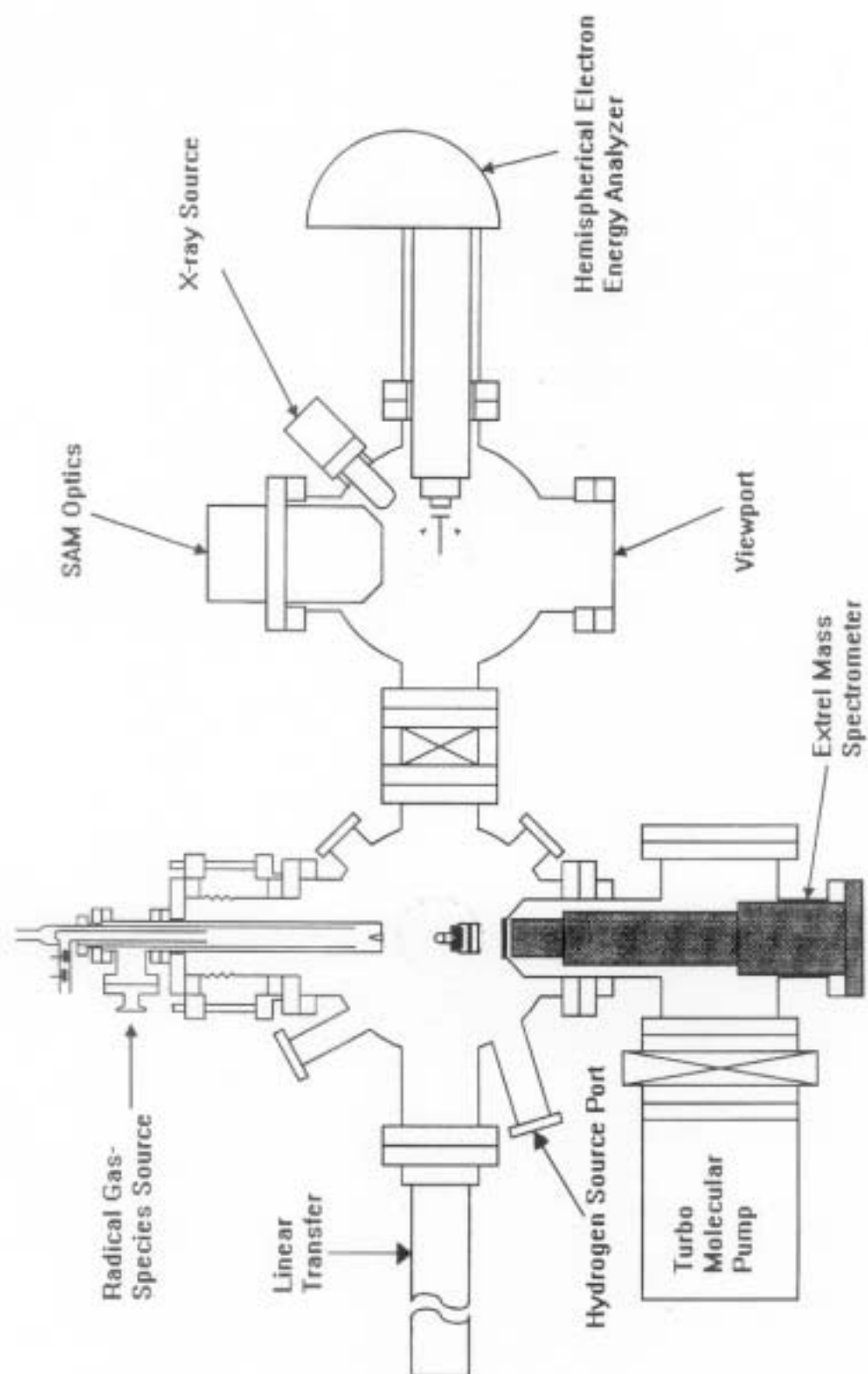
Fig. 2.8   Diagram of the system used for XPS investigations.

Three factors need to be taken into account when determining an equivalent system pressure for source operation (and hence an equivalent flux) for the second system. The first two factors are the source-to-substrate distance and the incident angle of the hydrogen with respect to the substrate surface. The source-to-substrate distance was 35 cm and 15 cm, while the angle of incidence was 35° and 73° in the growth system and the analysis system, respectively. Taking the ratio of the squares of the distances, then accounting for the angle of incidence gives a factor of about 1.9 more atoms at the surface of the substrate in the XPS system for a comparable pressure.

The third consideration is the difference in pumping speeds. The cryo pump on the MBE system has a pumping speed of 2500 L/sec[28] for hydrogen. The OsakaTG200 Turbo-molecular pump on the XPS chamber has a pumping speed of 150 L/sec[28] for hydrogen. Since both have similar conductance to the main chambers, the pumping rate in the XPS system is 6% of the pumping speed in the growth system. Taking 1.2×10^{-6} Torr multiplying by 16.7 and dividing by 1.9 indicates an XPS system pressure of 1.1×10^{-5} Torr should give a roughly equivalent flux of atomic hydrogen at the sample's surface.

However, a system pressure of 5.0×10^{-6} Torr was used throughout the experiments in the XPS chamber. This pressure was chosen prior to making the above detailed calculations. The system pressure, pumping speed, and conductance considerations, will again lead to a cracking efficiency of about 10%, so a simple ratio of pressures leads to a flux of 4.4×10^{14} molecules $cm^{-2}sec^{-1}$ at the surface of the substrate in the XPS system. This will lead to a monolayer equivalent impingement every 2.5 seconds. Thus, equivalent exposure times in the XPS chamber are a factor of 2.1 larger than in the MBE system in this study.

2.5.2 Comparison of Temperatures in the Two Systems

The filament used to dissociate hydrogen operates at an elevated temperature and produces a significant amount of heat and light. For this reason, surface heating should be considered. For example, it was observed that the temperature of substrates etched near room temperature (i.e. no power to the substrate heater) in the XPS system actually increased to 50°C during the etch. Since heating occurred from the front surface in this case, the HgCdTe surface could be significantly warmer. This will be important in interpreting the XPS spectra discussed later. Radiant heating due to the filament was not as much an issue for the MBE system due to the longer source-to-sample distance as well as the presence of a liquid nitrogen cooling shroud. In the growth chamber, the thermocouple indicated a temperature of ~30°C for "near-room temperature" experiments (no power to the substrate heater and operation with a liquid nitrogen cooling shroud) after a one-hour exposure to the filament.

To further investigate this phenomenon additional experiments were performed in the growth chamber. A HgCdTe sample was mounted on a substrate block, and an additional fine-gauge type-K thermocouple was attached to the center of the front of the sample with a small dot of indium to ensure good thermal contact. The substrate temperature and block temperature could then be measured simultaneously.

Four sets of measurements were taken at four different temperatures as shown in Table 2.1. The first two sets were taken before the liquid nitrogen shroud was cooled. One was taken with the hydrogen filament on, and the other while the filament was off. The third and fourth sets were again with and with out the hydrogen filament, but the liquid nitrogen shroud was cooled to -140°C.

Heater Setpoint (°C)	Temperature of Substrate/Temperature of Block (°C)			
	Cooling shroud at room temperature Source filament off	Cooling shroud at room temperature Source filament on	Cooling shroud at -140°C Source filament off	Cooling shroud at -140°C Source filament on
0	settled at 21.6/22.0	settled at 56.5/56.3	settled at 1.6/1.0	20 min. 18.0/15.7 1 hour 30.6/28.5
50	settled at 50.0/50.4	settled at 56.5/56.3	settled at 50.2/50.0	settled at 51.5/50.5
80	settled at 78.5/80.0	settled at 80.0/80.7	settled at 78.5/80.1	settled at 78.9/79.3
100	settled at 97.3/100.0	settled at 98.4/100.0	settled at 96.8/99.9	settled at 98.2/100.0

Table 2.1   Effect of the hydrogen filament on the substrate and block temperatures. Temperature measurements were taken both at the back of the block and the front surface of the HgCdTe sample for various conditions in the chamber, and for different substrate settings.

In addition to measuring the temperature gradients, it was of interest to determine if this heating was all radiant, or if some heat was transferred by the hydrogen atoms. For this reason, during the room temperature experiment the hydrogen gas was turned on. There was no discernible temperature difference with and without the hydrogen gas flowing, confirming that the heating is all radiant.

3. Preparation of CdTe for CdTe Deposition

3.1 Background

HgCdTe is an excellent candidate for fabrication of infrared detectors. One of the problems in its development has been the need for a suitable substrate. CdTe is an obvious choice, yet there were problems early on with its bulk growth. As these problems are resolved and bulk CdTe material improves, it will prove quite useful as a substrate for HgCdTe. In the meantime one possible solution to the problem of crystalline quality is growing a thin film of CdTe on a CdTe substrate.

This chapter discusses the use of atomic hydrogen to clean CdTe surfaces. Typical *in-situ* thermal treatments of CdTe to remove oxides and other unwanted elements from the surface require temperatures at or above 300°C. A prior study by Luo *et al.* has shown that atomic hydrogen is very effective at removing oxygen, chlorine, sulfur, and carbon from CdTe surfaces while preserving stoichiometry.[15] It will be shown that atomic hydrogen cleaning also results in smooth, 2-D surfaces appropriate for subsequent epitaxial growth.[29]

3.2 Surface Preparation

II-VI, Inc. (Saxonburg, PA) provided both (100) and (211)B-oriented substrates for this study. CdTe substrates underwent a chemical etching procedure typical of that used for MBE growth. The substrates were degreased and then etched for five minutes in a 0.5% Br:methanol solution, followed by two methanol dips. In between each solution the substrates were rinsed with methanol. After the second dip the substrates were blown dry with high purity nitrogen gas and rinsed in deionized (DI) H_2O for five minutes. The next step in this procedure was a thirty

second dip in 1:9 HCl:DI H$_2$O, followed by a five-minute rinse in DI H$_2$O and immediate blow-dry with nitrogen gas.

3.3 RHEED During Hydrogen Cleaning

When inserted into the MBE system and examined by RHEED, as-received substrates typically exhibited diffuse scattering. This is true even for those that were etched in HCl to strip surface oxides prior to insertion. This is consistent with previous LEED studies indicating a disordered surface on as-received substrates.[15] RHEED measurements on the as-etched substrates gave irregular, spotty patterns with superimposed rings, as seen in Fig. 3.1. This is indicative of a residual Te overlayer, probably from the Br:Methanol etch. In order to remove the Te, it was necessary to heat the substrate above 200°C. This was indicated by the disappearance of the diffraction rings. The surface, however, remained 3-D in nature, as the diffraction pattern exhibited only spots indicative of the textured surface. This pattern became two-dimensional only after the typical thermal treatment, which involved heating to 300°C for ten minutes.

The effect of atomic hydrogen cleaning was investigated at both room temperature and at elevated temperatures. At room temperature, both the diffuse scattering and the rings related to oxides and/or a Te-overlayer disappear after about a twenty minute exposure to atomic hydrogen. The bright, three-dimensional spot pattern shown in Fig. 3.2, is obtained after a total exposure of about thirty minutes, and similar to that observed for the 200°C thermal pretreatment. For temperatures above approximately 80°C, however, the oxide/Te overlayer was rapidly removed and a sharp two dimensional pattern with well-defined steaks was observed, like those shown in Fig. 3.3.
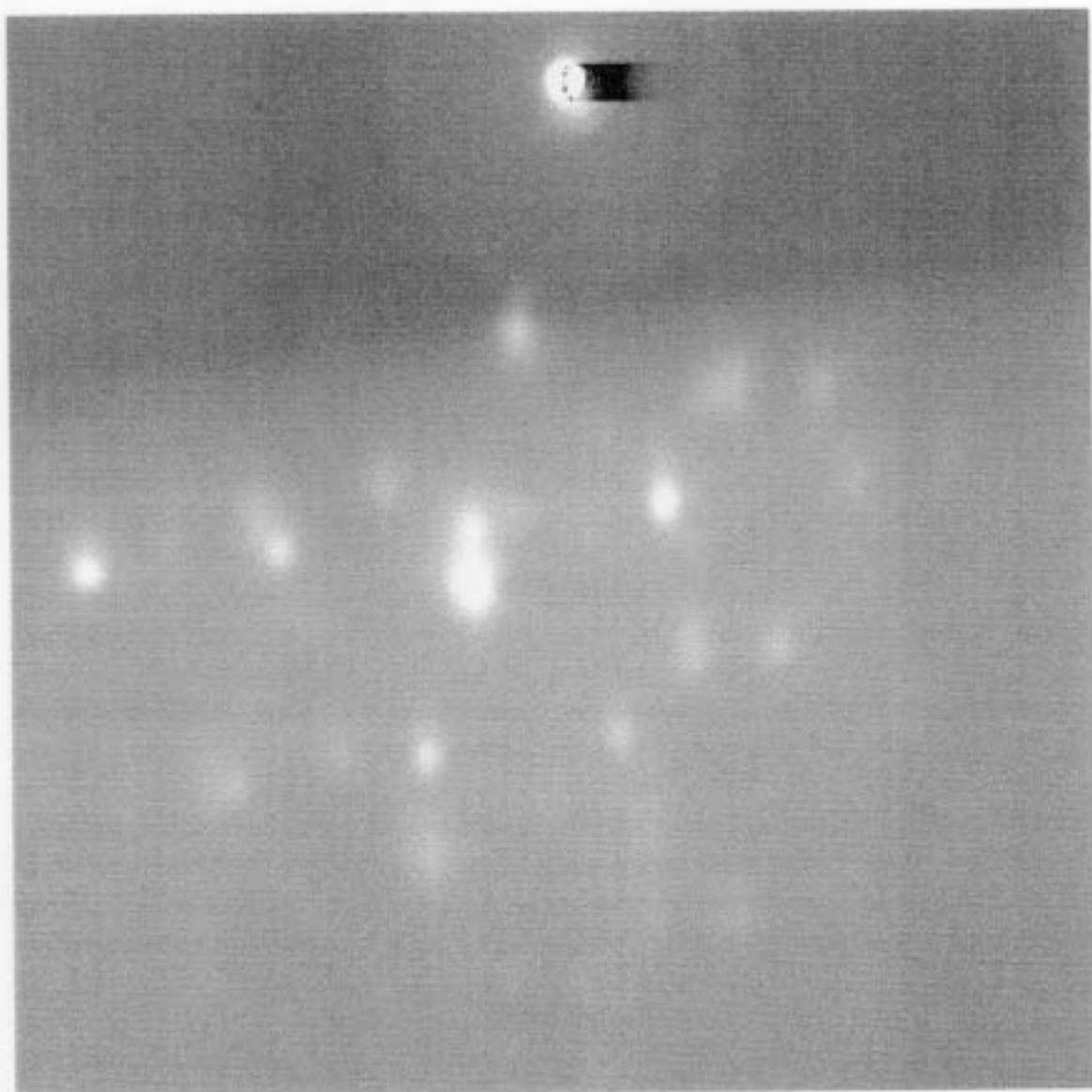
Fig. 3.1 RHEED of chemically etched CdTe

31
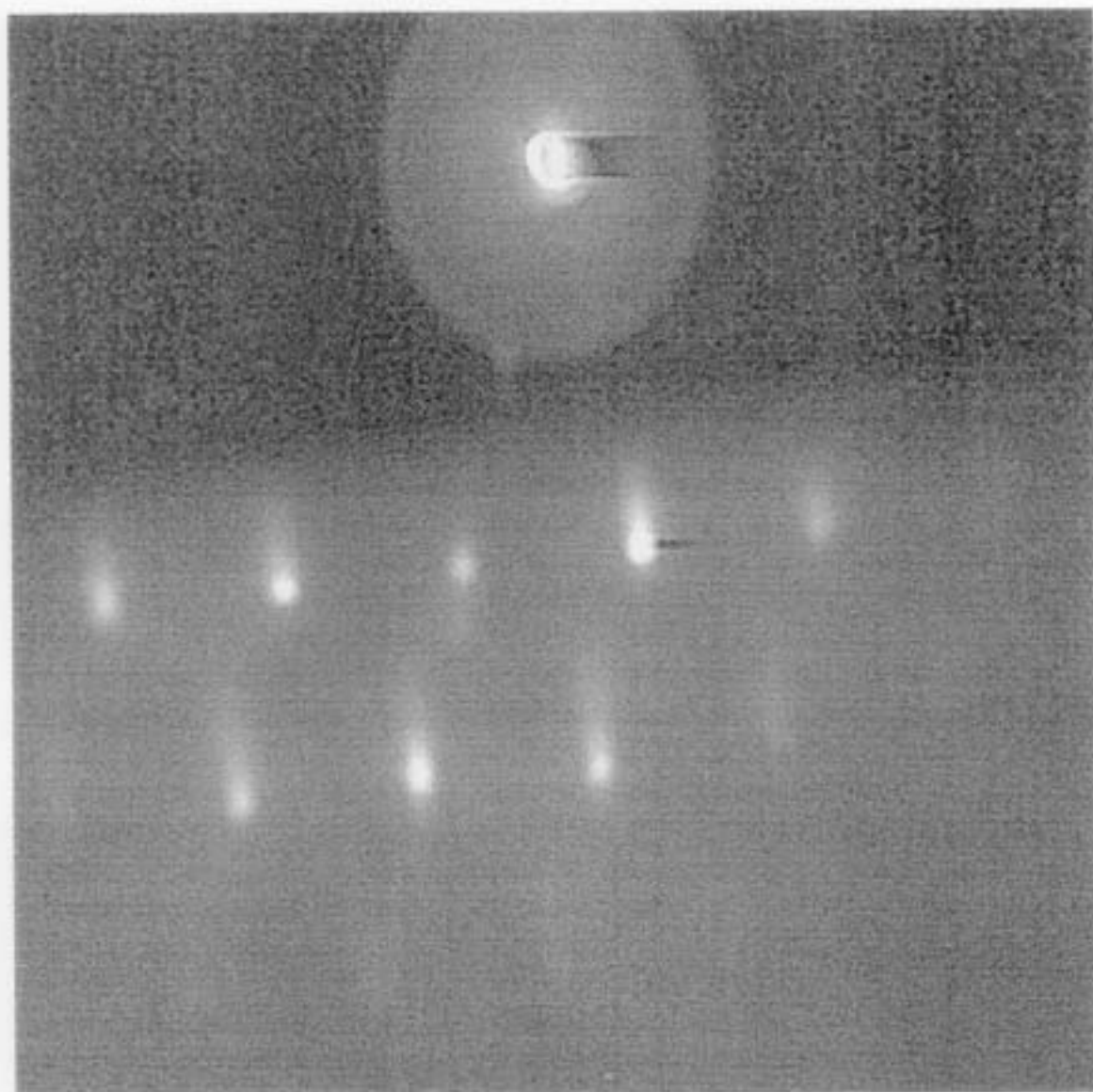
Fig. 3.2 RHEED of CdTe cleaned with atomic hydrogen at room temperature for 30 min.
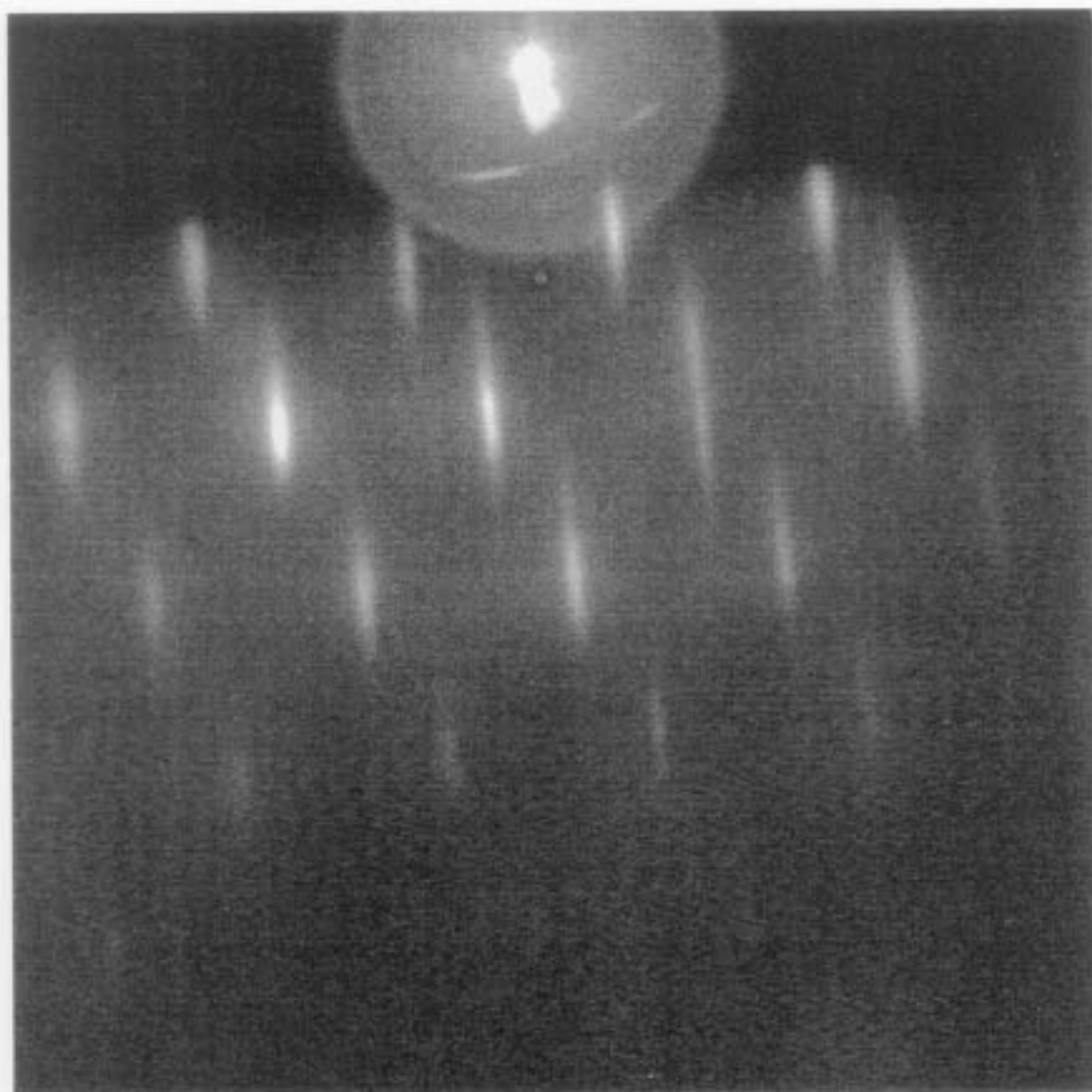
Fig. 3.3 RHEED of CdTe cleaned with atomic hydrogen above 80°C for 20 min.

3.4 Preliminary AFM Investigations

An AFM investigation of the as-received substrates indicated an atomically smooth surface with an rms. surface roughness of less than 0.5 nm. However, this surface was most likely due to a microscopically-thin disordered layer resulting from residual polishing damage. The surface tended to "smear" under the AFM probe tip, resulting in movement of material. By comparison, this smearing effect was never seen on epitaxial CdTe or etched CdTe surfaces.

Fig. 3.4 is an AFM micrograph of a typical (100) CdTe surface after the chemical etching procedure. It indicates a highly textured surface at the microscopic level, with features 50 nm in height and an rms. roughness of 4 nm. Similar roughness was observed for (211)B-oriented substrates. After a typical thermal treatment, AFM measurements still indicated a very rough surface, while AFM examination of the surface of substrates cleaned above 80°C with atomic hydrogen indicated a microscopically-flat, featureless surface with an rms. surface roughness of less than 0.5 nm.

3.5 Mechanisms

There are two primary candidates for surface oxides on CdTe. The first is $CdTeO_3$, and the second is TeO_2 which is the oxide formed with the tellurium overlayer.[5,30,31] Removal of these oxides using atomic hydrogen may proceed by reactions of the form:

$$CdTeO_3 + 6H \rightarrow CdTe + 3H_2O \uparrow \qquad (3.1)$$

$$TeO_2 + 4H \rightarrow Te + 2H_2O \uparrow \qquad (3.2)$$

Reaction (2) has the potential to leave behind a Te overlayer. This is consistent with RHEED which indicates the presence of a Te-overlayer after chemical etching. It is believed that the following mechanism is also important for atomic hydrogen cleaning of CdTe:

500 nm
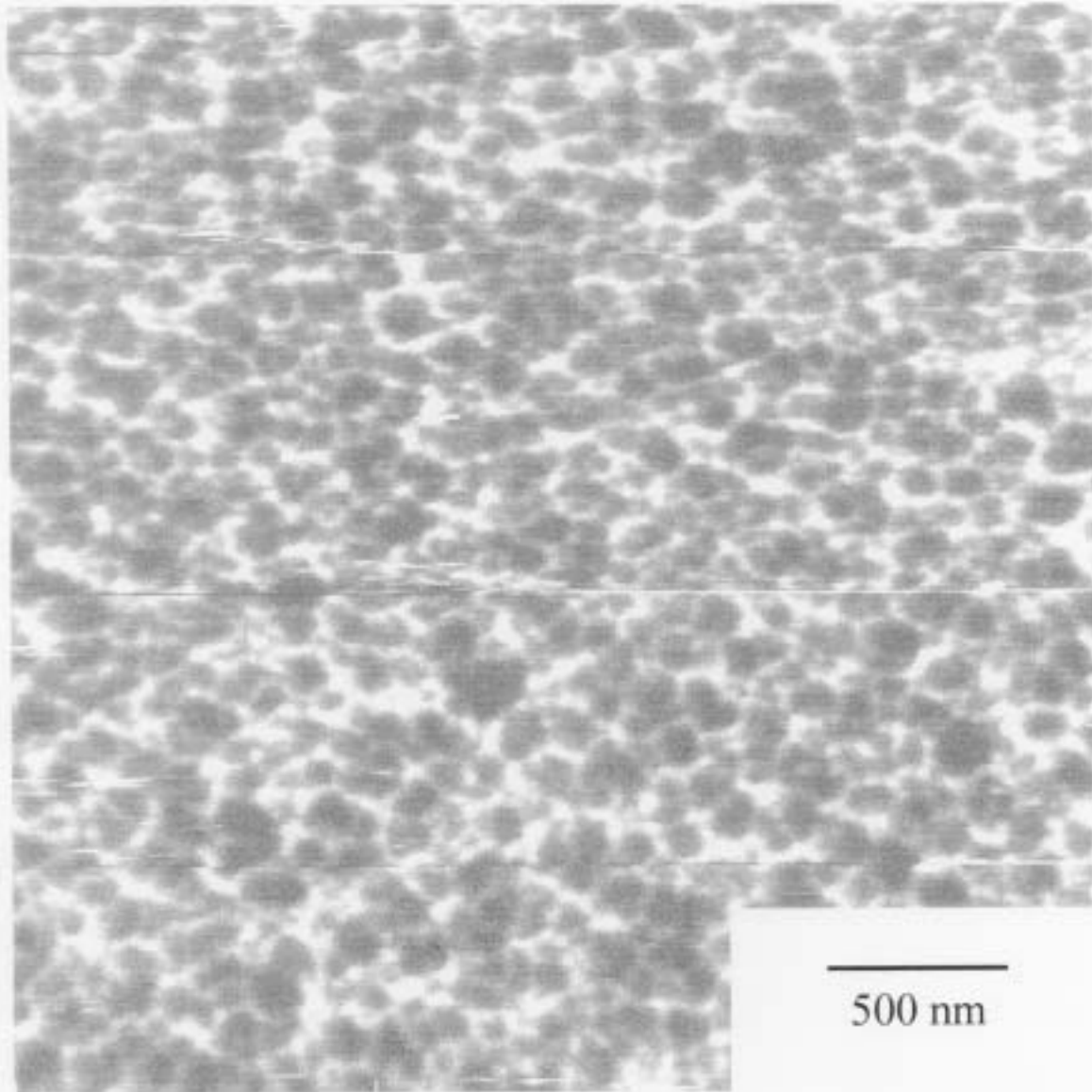
Fig. 3.4 AFM of chemically etched CdTe. The micrograph represents an area of $3\mu m \times 3\ \mu m$ and has a z-scale of 50nm.

$$Te + 2H \rightarrow TeH_2 \uparrow \qquad\qquad (3.3)$$
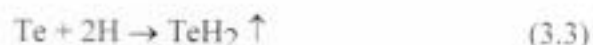
To test the possibility of the latter mechanism, a polycrystalline Te layer of about 30 Å thickness was deposited on a silicon substrate. At 80°C, this layer was removed by atomic hydrogen irradiation in about 300 s, indicating a Te etch rate of 0.1 Å/sec. Compared to the previously calculated arrival rate for atomic hydrogen, this corresponds to about a 4% efficiency in the use of atomic hydrogen, possibly limited by a kinetic barrier due to the need for two hydrogens to be available at a given Te atom for removal.

3.6 Etch Rates

We have not been able to directly measure an etch rate for CdTe (or ZnTe) due to atomic hydrogen by either direct exposure of thin layers deposited on silicon substrates or by observation of RHEED oscillations. However, etching must be possible as indicated by the smoothing of textured surfaces. An upper bound for the CdTe etch rate can be inferred from the difference in the CdTe growth rate observed when grown with and without the presence of atomic hydrogen. CdTe grown under an atomic hydrogen flux of 2×10^6 Torr exhibited a consistent decrease in growth rate of about 0.1 Å/s, which is comparable to the Te removal rate. The fairly rapid smoothing of the rough, as-etched CdTe surfaces may indicate that atomic hydrogen is more effective at etching three-dimensional structures since edge sites will be more reactive. Temperatures of 80°C or above may be required to thermally-desorb residual Cd, as there are no stable, volatile hydrides of Cd. Exposing thin ZnTe/Si epilayers to atomic hydrogen also indicated etch rates less than 0.1 Å/s.

4. Cleaning of HgCdTe for CdTe passivation

4.1 Background

One of the most common applications of HgCdTe is its use in infrared detectors. Before fabrication of a HgCdTe-based device, however, a passivation layer must be deposited on its surface. CdTe has been shown to be an effective surface passivation layer for HgCdTe. Although, unless the CdTe layer is grown as part of a heterostructure, it must be deposited after the HgCdTe surface has undergone exposure to air and/or chemical etching. This allows the formation of an oxide layer, and possibly an amorphous Te layer, which must be removed prior to CdTe growth.

Typical thermal oxide removal requires temperatures above 180°C in vacuum. Such temperatures can degrade the HgCdTe surface. It follows logically from the results of the previous chapter that HgCdTe might also exhibit a smooth, stoichiometric surface after cleaning with atomic hydrogen at low temperatures. Therefore, the thrust of this chapter is to show that oxides and other surface contaminants can be removed from HgCdTe at low temperatures by cleaning with atomic hydrogen.

4.2 Surface Preparation

The liquid phase epitaxy (LPE) $Hg_{1-x}Cd_xTe$ samples (with $x \sim 0.2$) used throughout these studies were provided by II-VI, Inc. (Saxonburg, PA) and had been chemi-mechanically polished to remove surface features related to the LPE process. Prior to insertion into the MBE system, the LPE layers were degreased and then etched for five seconds in 0.5 % Br:methanol. Upon removal from the Br:methanol, the sample was rinsed with methanol while being transferred to the first of two one-minute methanol baths. The sample was constantly agitated while submersed. Again the sample was rinsed with methanol while being transferred to the second

37

bath. After removal from the second bath the sample was rinsed a final time and then immediately blown dry with high purity nitrogen gas.

4.3 RHEED During Hydrogen Cleaning

The effect of atomic hydrogen cleaning was investigated at both room temperature and at elevated temperatures. Initial studies performed in the MBE system using RHEED were reported at the 1996 U. S. Workshop on the Physics and Chemistry of II-VI materials in Las Vegas, Nevada and published in the Journal of Electronic Materials, and are recounted here.[32]

Results were similar to that observed for CdTe. Fig. 4.1 contains the time-evolution of RHEED patterns observed for cleaning at near room temperature (the sub-ambient temperature is due to the liquid N_2 shroud) and 80°C. As discussed in Chapter 2, the substrate temperature was not constant during the "room-temperature" experiments. The definition of the "room-temperature" scans is that there is no power to the heater, and so any temperature change comes solely from the radiant heat of the tungsten filament in the hydrogen source. While the substrate is exposed to the filament for longer amounts of time the substrate temperature is constantly rising, and so the temperature quoted for a particular image is the temperature at the time the scan was taken.

Fig. 4.1a shows the diffuse pattern characteristic of as-prepared HgCdTe. A brief (~ 5 minute) exposure to atomic hydrogen eliminated most of the diffuse scattering and rings while raising the temperature of the HgCdTe to about 10°C. The RHEED then consisted of a highly irregular spot pattern, indicative of a rough surface with a possible partially polycrystalline overlayer. Only after 60 minutes of exposure to atomic hydrogen, which produced a substrate temperature of ~30°C, did distinct RHEED patterns emerge, indicating

38
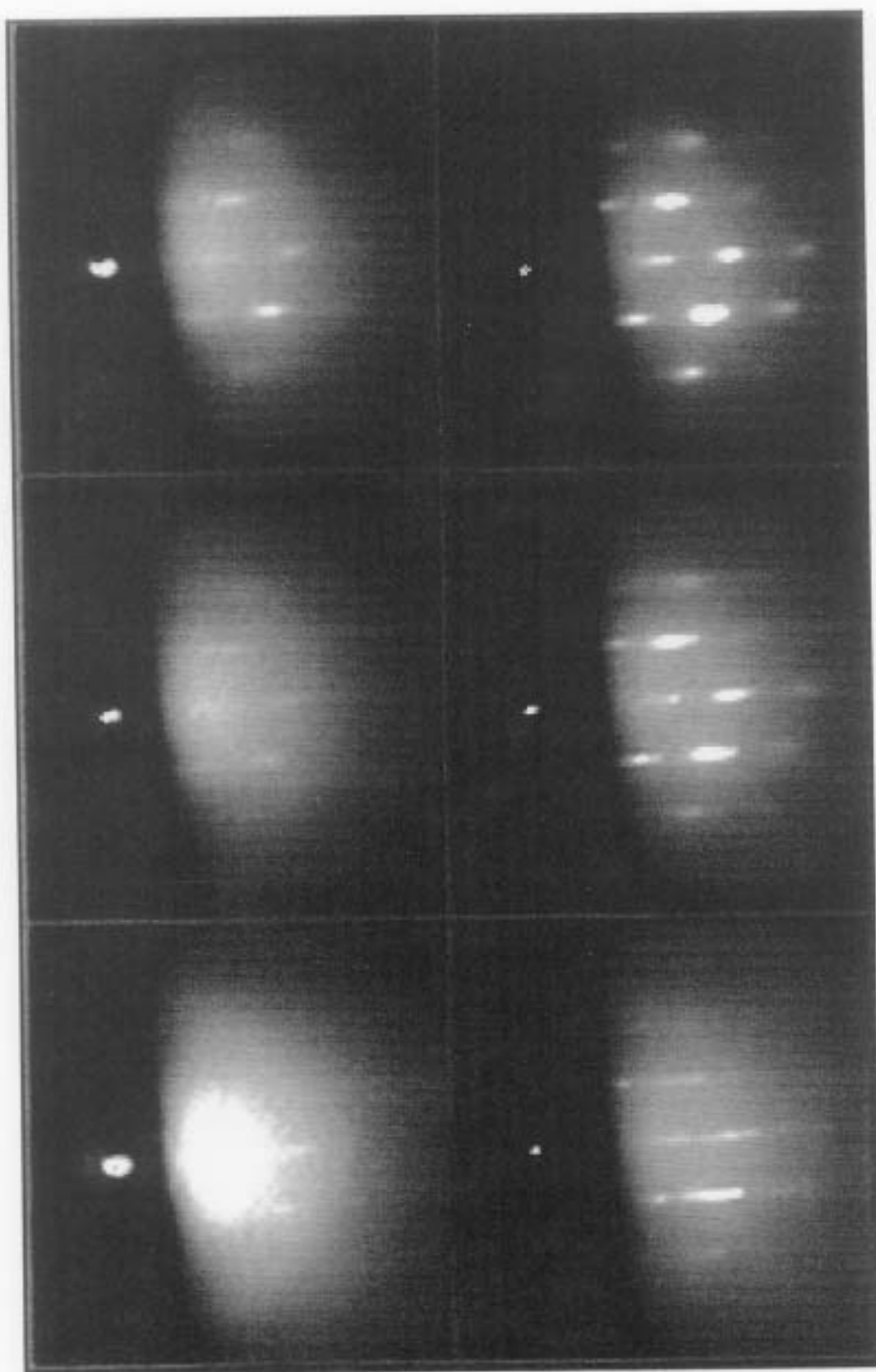
Fig. 4.1   RHEED evolution of an LPE HgCdTe surface under atomic hydrogen (a) after 20 min (~18°C), (b) after 40 min (~24°C), (c) after 60 min (~30°C), (d) after 20 min (~80°C), (e) after 40 min (~80°C), and (f) after 60 min (~80°C).

removal of the oxide overlayer. As shown in Fig. 4.1c, the patterns remained spotty, indicative of a rough surface, and there is still diffuse scattering. Raising the sample temperature to 80°C dramatically changed the process. Again, a brief exposure to the hydrogen source appeared to remove an initial oxide layer. In contrast to the "room-temperature" etch, a well-defined two-dimensional (2-D) pattern exhibiting sharp streaks was observed after a 20 minute exposure, as shown in Fig.4.1d. Continued exposure to atomic hydrogen eventually resulted in the evolution of the streak patterns into the ordered 3-D spot pattern similar to that obtained for extended exposure at ~30°C.

4.4 AFM Investigations and CdTe Passivation

AFM examination of a HgCdTe surface cleaned with atomic hydrogen and exhibiting a RHEED pattern similar to that shown in Fig. 4.1d indicated a microscopically-smooth surface with an rms. surface roughness less than 0.5 nm, with a suggestion of monolayer steps. A representative AFM micrograph is shown in Fig. 4.2. CdTe grown at 80°C on such a surface at a rate of 0.1 μm/hr (using a single effusion cell) maintained the sharp, streaky RHEED pattern, as indicated by Fig. 4.3. The resulting CdTe epilayer surface exhibited the same atomic-level smoothness when examined by AFM, Fig. 4.4, again with an rms. surface roughness less than 0.5 nm.[32] This demonstrates that atomic hydrogen can be used to obtain a HgCdTe surface suitable for low-temperature epitaxial growth of CdTe.

As stated earlier, Luo *et al.*[15] have demonstrated that atomic hydrogen can be used for low temperature oxide removal and cleaning of CdTe while preserving surface stoichiometry. Since the smallest shifts in composition will greatly change the operation of a fabricated device, it is very important that the stoichiometry of the HgCdTe be maintained during cleaning. Therefore,
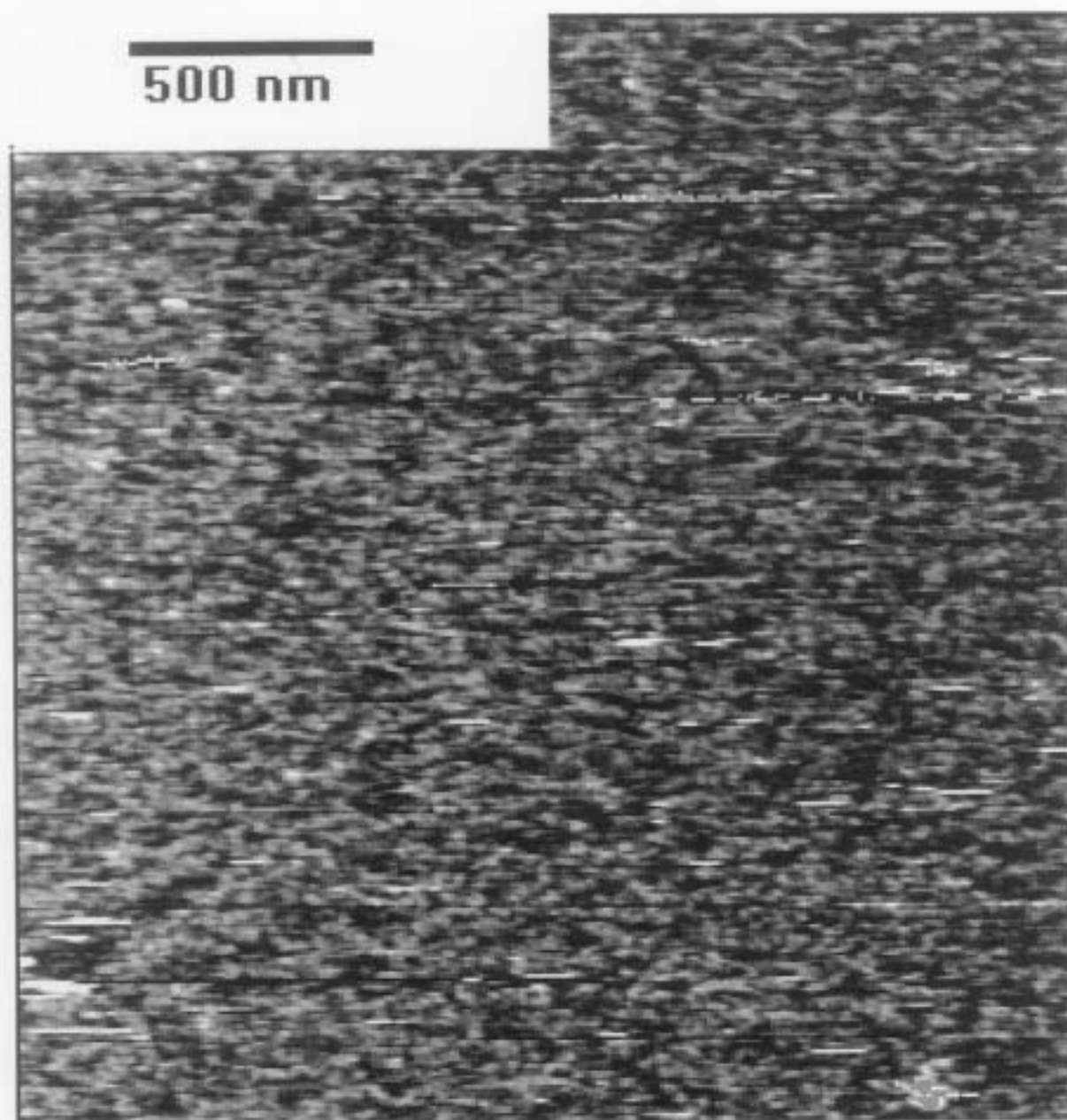
Fig. 4.2   AFM of HgCdTe cleaned with atomic hydrogen at 80°C for 20 min. The micrograph represents an area of 2×3 μm and has a z-scale of 10 nm.
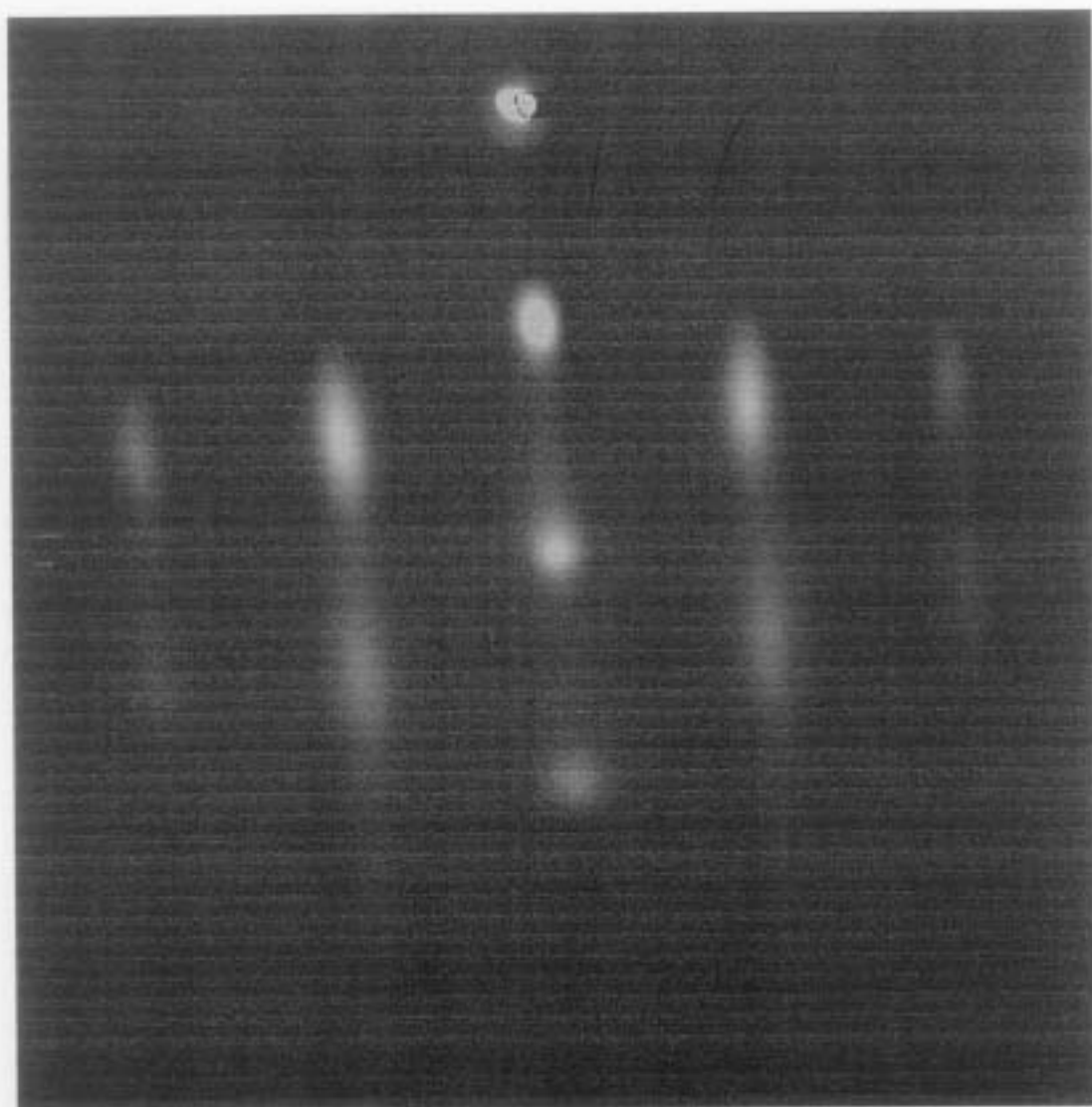
Fig. 4.3   RHEED of a 0.3 μm film of CdTe grown on a hydrogen cleaned HgCdTe substrate.
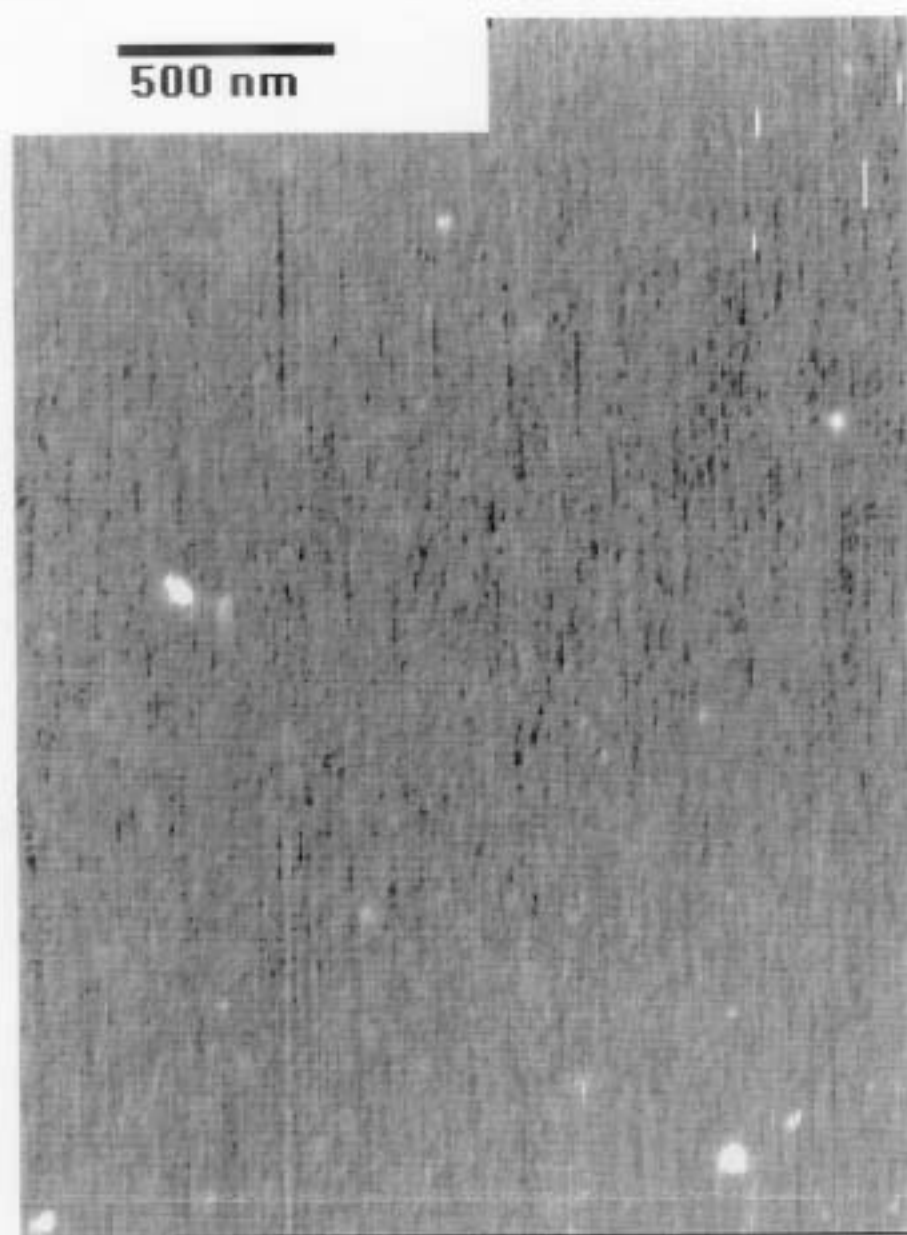
Fig. 4.4   AFM micrograph of a 0.3 μm CdTe layer deposited on a hydrogen cleaned HgCdTe substrate. The micrograph represents an area of 2 × 3 μm and has a z-scale of 10 nm.

an experiment was performed to look for stoichiometric changes in HgCdTe during atomic hydrogen cleaning.

XPS Investigations

4.5.1 Background

In order to better understand the processes occurring during atomic hydrogen etching, a series of etch experiments which allowed XPS measurements as a function of etch time were performed in the second system described in Chapter 2.[33] The composition and chemical state of the surface were determined by monitoring the Te $3d_{5/2}$, Cd $3d_{5/2}$, and Hg $4f_{7/2}$ photoelectron peaks. Surface composition was determined in a standard manner[34] using peak areas and elemental sensitivity factors established by Nitz et al.[35] and subsequently discussed by Christie et al.[36] A detailed discussion of the derivation can be found in Appendix B. In addition a complete analysis of XPS data for hydrogen cleaning at 50°C and 80°C can be found in appendix C.

4.5.2 Analysis Techniques

The peak areas were initially determined using the VGX900 software. The software automatically fit the data with a combination of Gaussian and Lorentzian curves, then used this fit to report the area under the curve as well as the peak positions. These areas and positions are a good approximation, but upon careful inspection one will notice flaws in the software's approach.

For instance, it will be shown that the tellurium curve shifts during cleaning. The VGX900 software tended to report this as a single peak that shifted up in energy as the etch time increased. However, it is more realistic to think of this case as two neighboring peaks, where one dominates over the other. Then as time progresses, the smaller peak becomes more prominent,

until it begins to dominate and suppress the larger one. Fitting this particular curve with two peaks instead of one, leads to a noticeable change in area, and also slightly different peak positions.

Another noticeable problem with the VGX900 software is its inability to fit curves that are either short and broad, or just slightly above the background. The tellurium oxide tends to be just such a feature. In some cases looking only at the numerical data from the VGX900 software, one might be led to the conclusion that there is no oxide on a particular substrate. However, if instead one looks at the plot of the raw data, they would notice a definite feature above the background. Surprisingly, the opposite scenario can also take place. For instance, on one occasion the software reported a tellurium oxide peak as being 1/3 the area of the tellurium peak, and inspection of the raw data clearly showed that this was not the case. It is for these reasons that Jandel Scientific's Peak Fit program was used to reanalyze the data.

As was alluded to earlier, each substrate has a series of XPS scans as a function of time. Each scan was individually entered into the Peak Fit program. Next, a linear baseline was chosen to best fit each portion of the data. Then the curves were fit using a combination of Gaussian and Lorentzian curves. The cadmium and mercury scans were relatively easy to fit because there was no associated oxide with these peaks. Therefore the focus of this discussion will be the tellurium and tellurium-oxide peaks.

Fig. 4.5 is the first of a series of graphs of a tellurium scan as it is being fit. In order to get the best fit, while remaining consistent over a series of scans taken of the same substrate, the last scan taken is analyzed first. An initial assumption is made, that the tellurium peak is made up of only the tellurium peak associated with the binding energy of tellurium in a HgCdTe matrix. (Later this will be shown to be a valid assumption.) For this reason, the left curve is fit
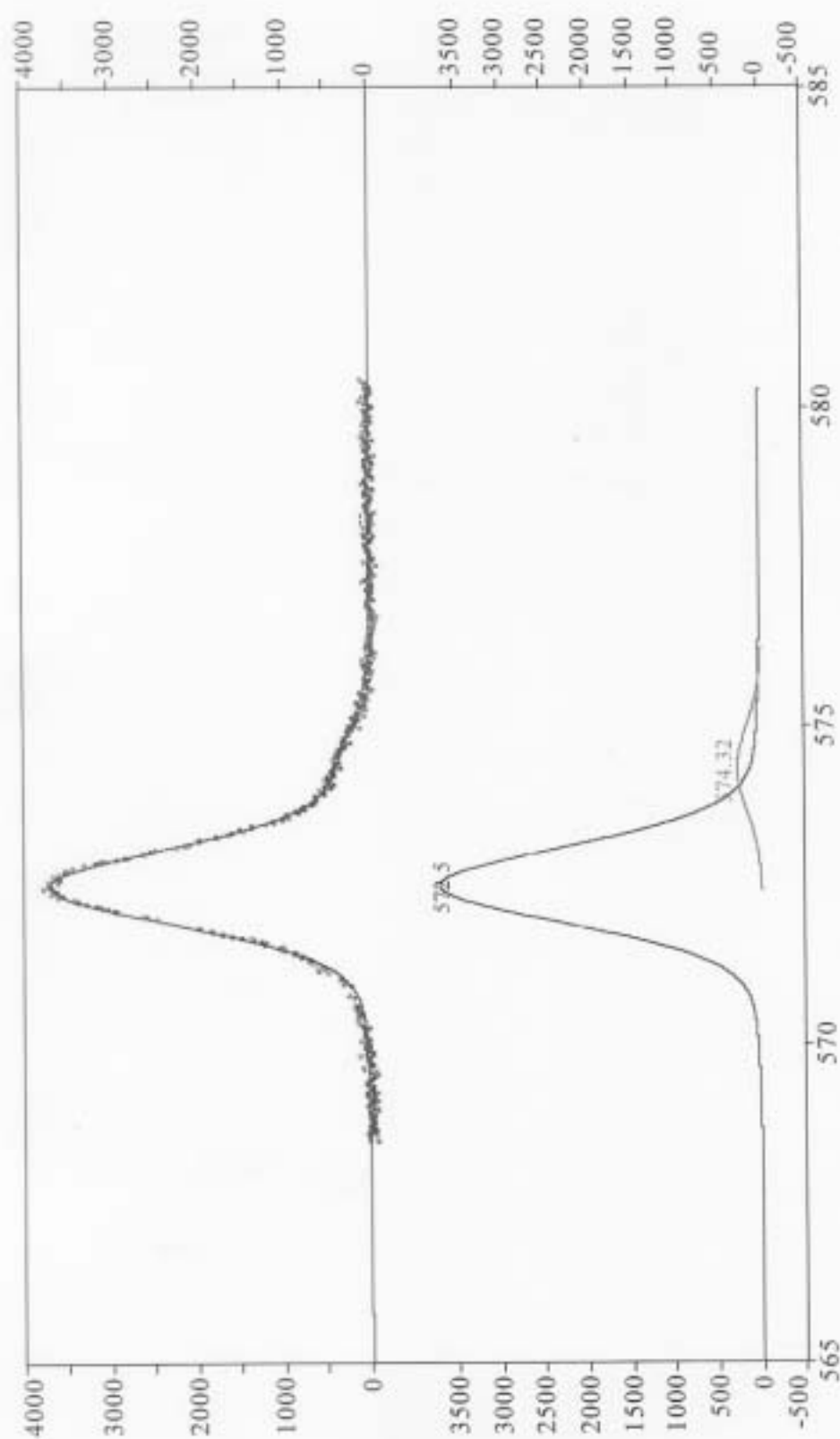
Fig. 4.5   The XPS spectra of sample WVUD after a series of atomic hydrogen etches showing the Te $3d_{5/2}$ peak and its oxide. The top graph, (a), contains the raw data and the final fit. The lower graph, (b), shows the peaks that, when added together, make up the final fit. The large curve is fit with one peak, and the shoulder is fit with a satellite for the $3d_{3/2}$ peak.

with only one peak. The peak is found to be centered at 572.5 eV, therefore this value is now used as the binding energy of tellurium in a HgCdTe matrix. (Two additional parameters are given to describe the peak, the width and the shape. It is noted that these numbers are monitored, and fixed so that associated peaks will not differ in width or shape. For the sake of brevity this will not be noted again.) The next peak to the right is the satellite of the $3d_{3/2}$ peak, and is located 1.8 eV from the $3d_{5/2}$ peak at 574.3 eV. As shown in Fig. 4.5b, these two peaks appear to account for all of the signal above the background, and this will be proven after further analysis.

The next scan to be analyzed is the one taken of the substrate after only the bromine etch. This scan contains the Te oxide, as shown in Fig. 4.6a. Since the peak position for tellurium in a HgCdTe matrix is now known, the first peak can be fixed at 572.5 eV. Also, the satellite associated with the $3d_{3/2}$ peak is placed 1.8 eV to the right of the $3d_{5/2}$ peak, at 574.3 eV. These two peaks, however, do not account for all of the scan, so additional peaks are added for the following reasons. RHEED indicates metallic tellurium exists at this point, so another peak is placed about 0.6 eV higher than the first tellurium peak. Again there will be a satellite from the $3d_{3/2}$ oxide peak located near 574.9 eV. Finally we will put in peaks for the tellurium oxide and its associated satellite. All of the peaks are now allowed to adjust their amplitude to best fit the data. In addition, the four new peaks are permitted to adjust their positions, since there are no concrete positions for these peaks yet.

When the fit for the curve is obtained, the positions for the six peaks are defined. These peaks can now be used to fit all of the other graphs in that set. This includes showing that the final scan is devoid of metallic Te, as well as the oxide, as shown in Fig. 4.7.
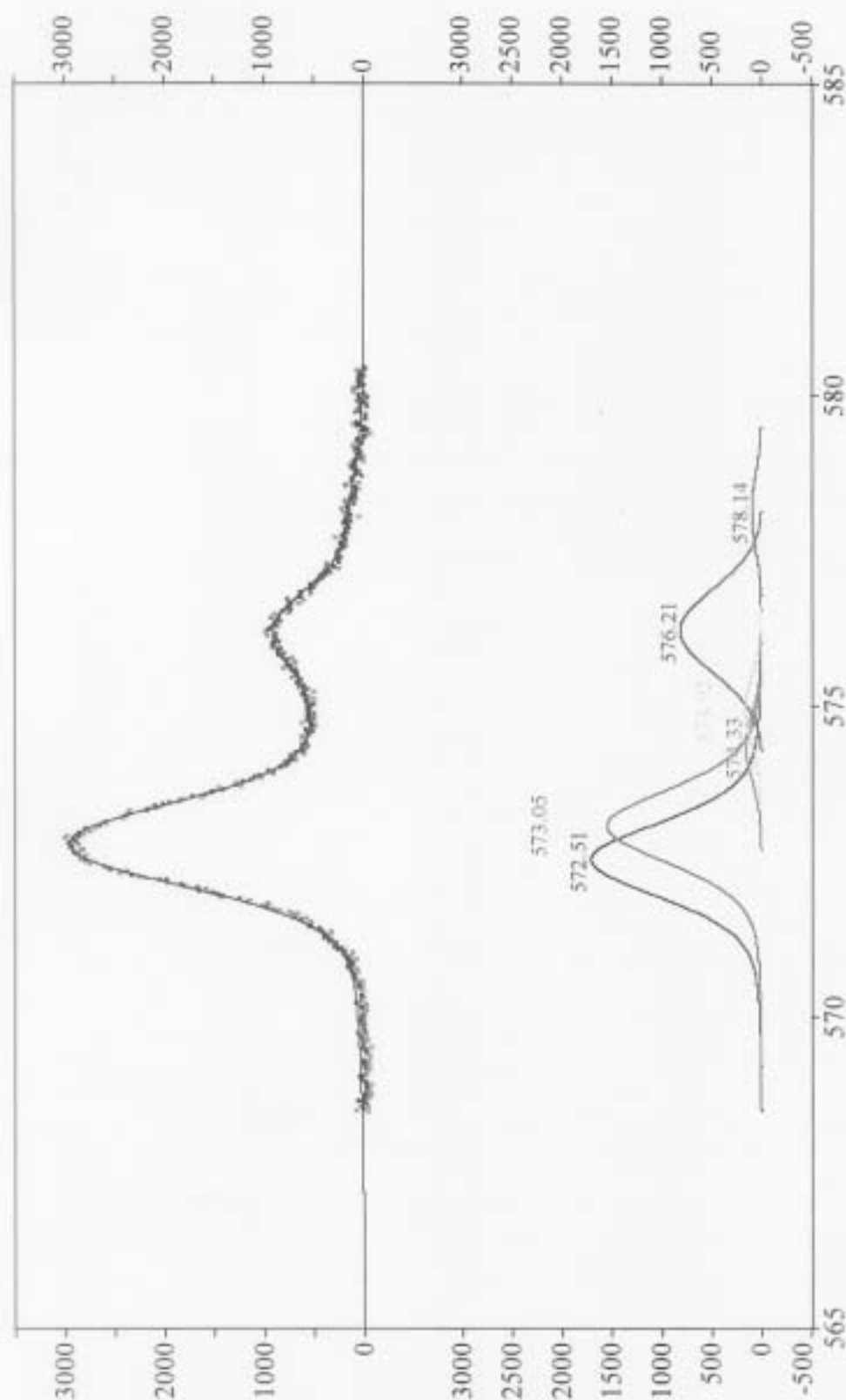
Fig. 4.6   The first XPS spectra of sample WVUD after only an *ex-situ* etch showing the Te $3d_{5/2}$ peak and its oxide. The top graph, (a), contains the raw data and the final fit. The lower graph, (b), shows the peaks that, when added together, make up the final fit. The large curve is fit with two peaks representing metallic Te and Te in a HgCdTe matrix, and the shoulder is likewise fit with two peaks. The oxide is fit with one peak as well as a satellite.

48
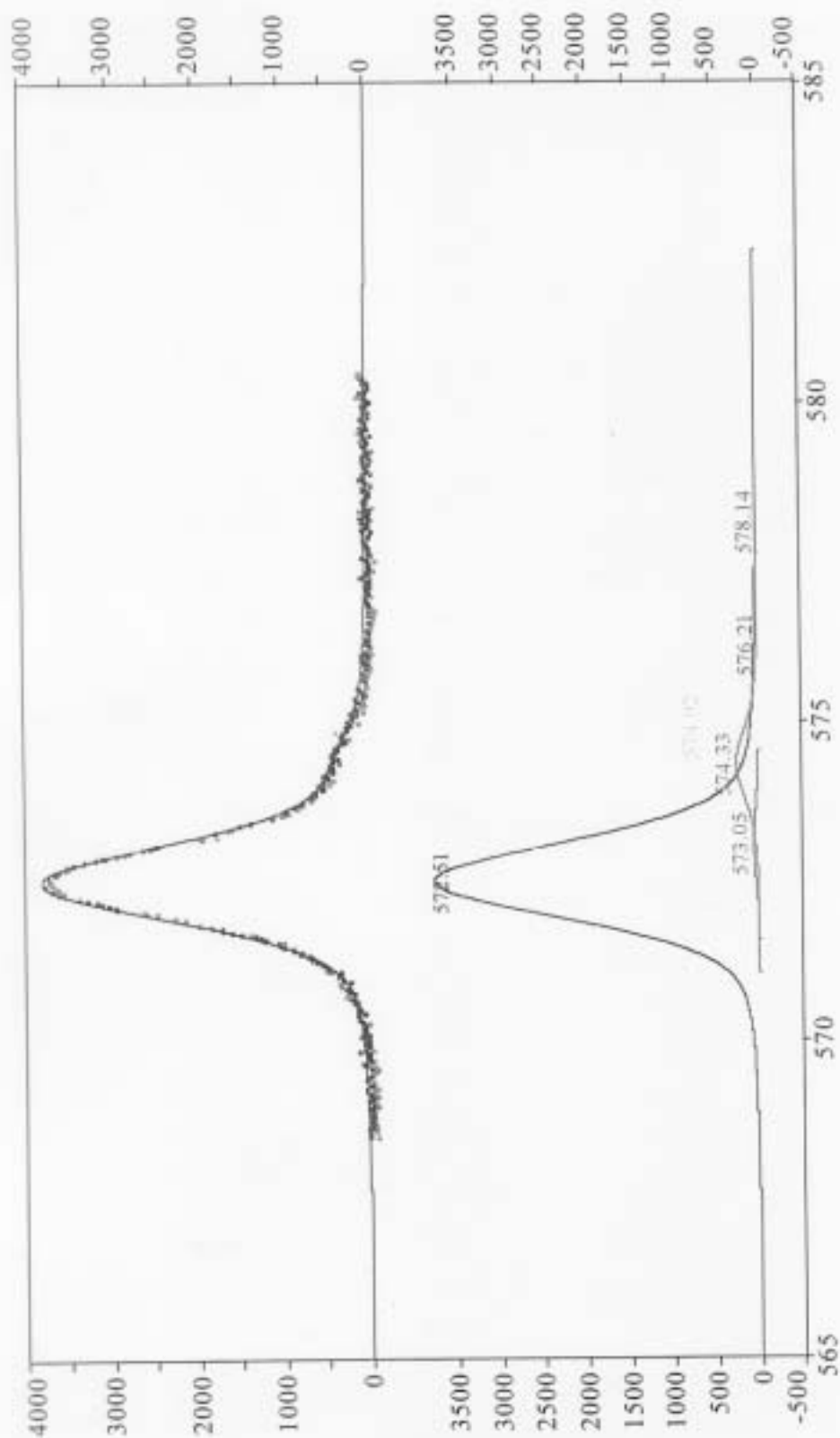
Fig. 4.7   The same XPS spectra as Fig. 4.5, except this time the curves are fit with six peaks. The top graph, (a), contains the raw data and the final fit. The lower graph, (b), shows the peaks that, when added together, make up the final fit. Note that the addition of the oxide and metallic tellurium peaks is unnecessary, and therefore the initial assumptions are correct.

49

4.5.3 Oxide and Tellurium Overlayer Removal

Fig. 4.8 shows a series of Te $3d_{5/2}$ photoelectron spectra for increasing exposures to atomic hydrogen. These spectra were obtained from a substrate etched at 80°C, but they are similar to those obtained for near room temperature. The t = 0 spectrum is typical of all Br-methanol etched samples analyzed in this study. The photoelectron peak at 576.3 eV has been previously associated with Te in the oxide state, while the peak at 572.7 eV is a combination of two peaks centered at 572.5 eV and 572.8 eV. The first peak is associated with tellurium in a HgCdTe matrix[37] and is the smaller of the two peaks. The second peak, which dominates, is associated with metallic tellurium.[38,39] As the etch proceeds, the peak centered on 572.5 eV begins to dominate, and by the end of the etch, the metallic tellurium peak is completely suppressed. The corresponding Cd $3d_{5/2}$ and the Hg $4f_{7/2}$ photoelectron spectra did not exhibit a characteristic oxide peak, and indicated binding energies consistent with values reported for CdTe and HgCdTe, which are 403.2 and 100.2 eV respectively.[38,39,40] Combined with the prior discussion of RHEED, these results suggest that the Br-methanol etch leaves behind a thin amorphous-Te overlayer which is oxidized in transit to the XPS system. After a five minute exposure the oxide peak is dramatically reduced, however it is not completely gone, which is consistent with the reduction of diffuse scattering seen in RHEED.

4.5.4 Oxide Thickness

An estimate of the oxide thickness can be obtained from the ratio of the oxide-Te and Te peaks[41] from the t = 0 spectrum in Fig. 4.8. (For further explanation see Appendix B.) For all the Br-methanol etched samples analyzed here, the thickness was estimated to be on the order of 0.3 nm. That is, the oxide appears to be on the order of only a monolayer or less in thickness.
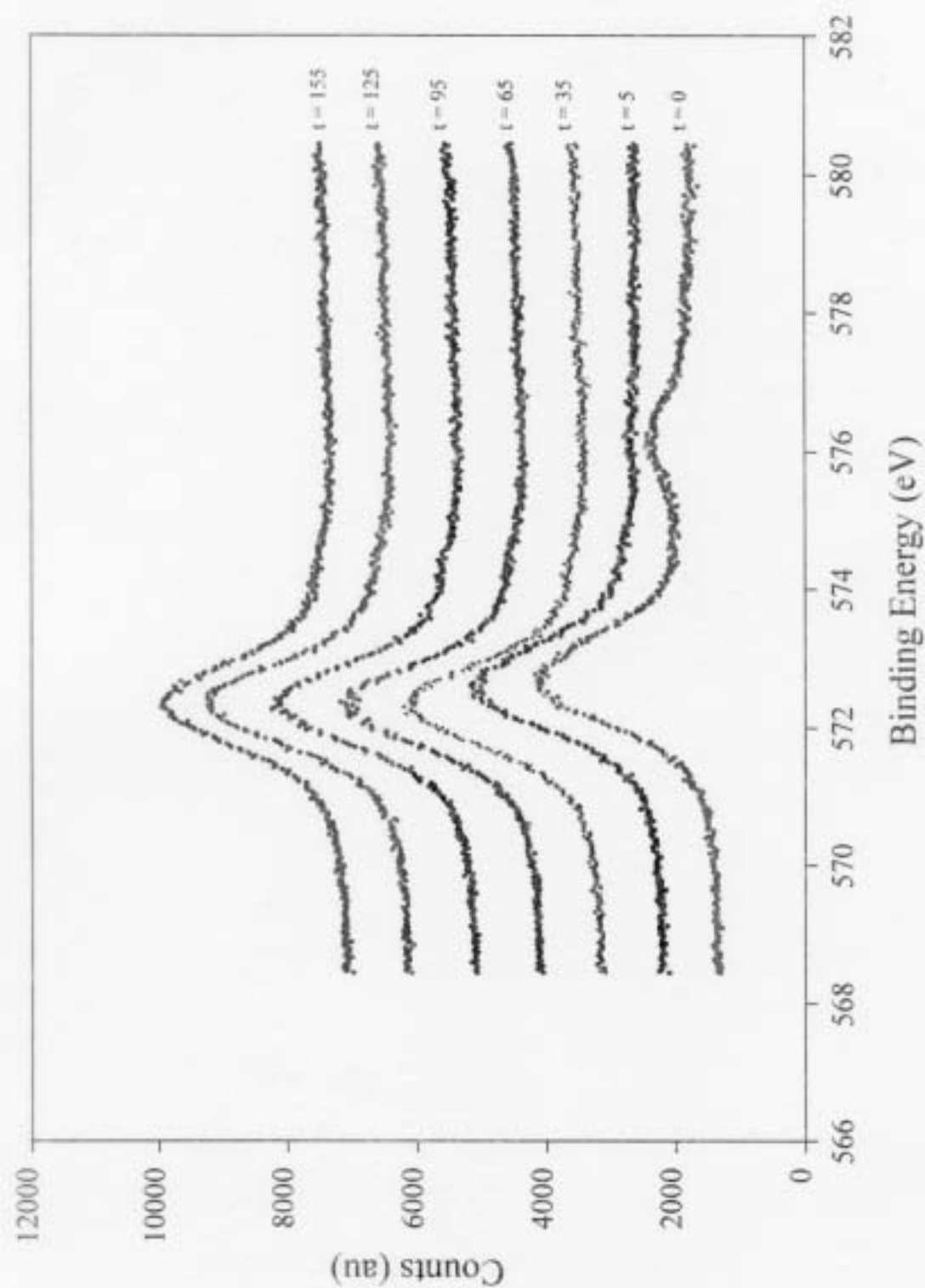
Fig. 4.8   XPS spectra of Te $3d_{5/2}$ peaks after various hydrogen cleaning times. The t = 0 and t = 5 min scans show a Te binding energy of 572.7 eV, indicative of mostly metallic Te, while the remaining scans show a binding energy of 572.5 eV which is representative of mainly Te in a HgCdTe matrix. Also shown is the Te-O peak at 576.1 eV.

This result applies to samples which had been exposed to the atmosphere for several days before being loaded into the UHV system as well as samples transferred as rapidly as possible (~20 minutes) into the system. Oxide formation appears to be self-limited due to both the low diffusion of the oxide constituents into the near surface layers and to a relatively low number of reactive surface sites on a Br-methanol etched surface. Using this thickness (0.3 nm) and etch times to remove the oxide determined from both RHEED and XPS, approximately five minutes, we estimate an oxide etch rate of 0.6 Å/min.

4.5.5 Stoichiometry

There is always concern that the use of atomic hydrogen may lead to non-stoichiometric etching of HgCdTe.[42,43] We performed *ex-situ* reflectance measurements to look for gross shifts in stoichiometry due to hydrogen etching.[32,44] The E_1 reflectance peak is characteristic of HgCdTe composition,[45] and probes a region approximately 100 to 200-nm thick. Measurements of the E_1 reflectance peak before and after atomic hydrogen cleaning were identical within instrumental resolution, as seen in Fig. 4.9, indicating that any stoichiometry change over the depth probed by this measurement is less than $\Delta x = 0.01$.

The near-surface case as probed by XPS, however, is quite different. Fig. 4.10 shows typical changes in the surface composition indicated by XPS as the atomic hydrogen etch proceeds. In all cases, an increase in the surface concentration of Cd, typically from an x-value of 0.2 to 0.6, was observed following the removal of the oxide overlayer. With continued etching, the Te decreased slightly to a relatively constant value which was typically within a few percent of its initial concentration, while the Hg decreased to a value significantly lower than either its initial or nominal bulk concentration. The relative atomic concentrations approximately indicated one Te for each remaining Hg and Cd, implying Te removal as well as

52

HgCdTe Sample G from Tray 2
Reflectance Data

λ_{max} = 539 nm
x = 0.223

λ_{max} = 540.5 nm
x = 0.216

— Before Hydrogen Cleaning
— After Hydrogen Cleaning

Wavelength (nm)
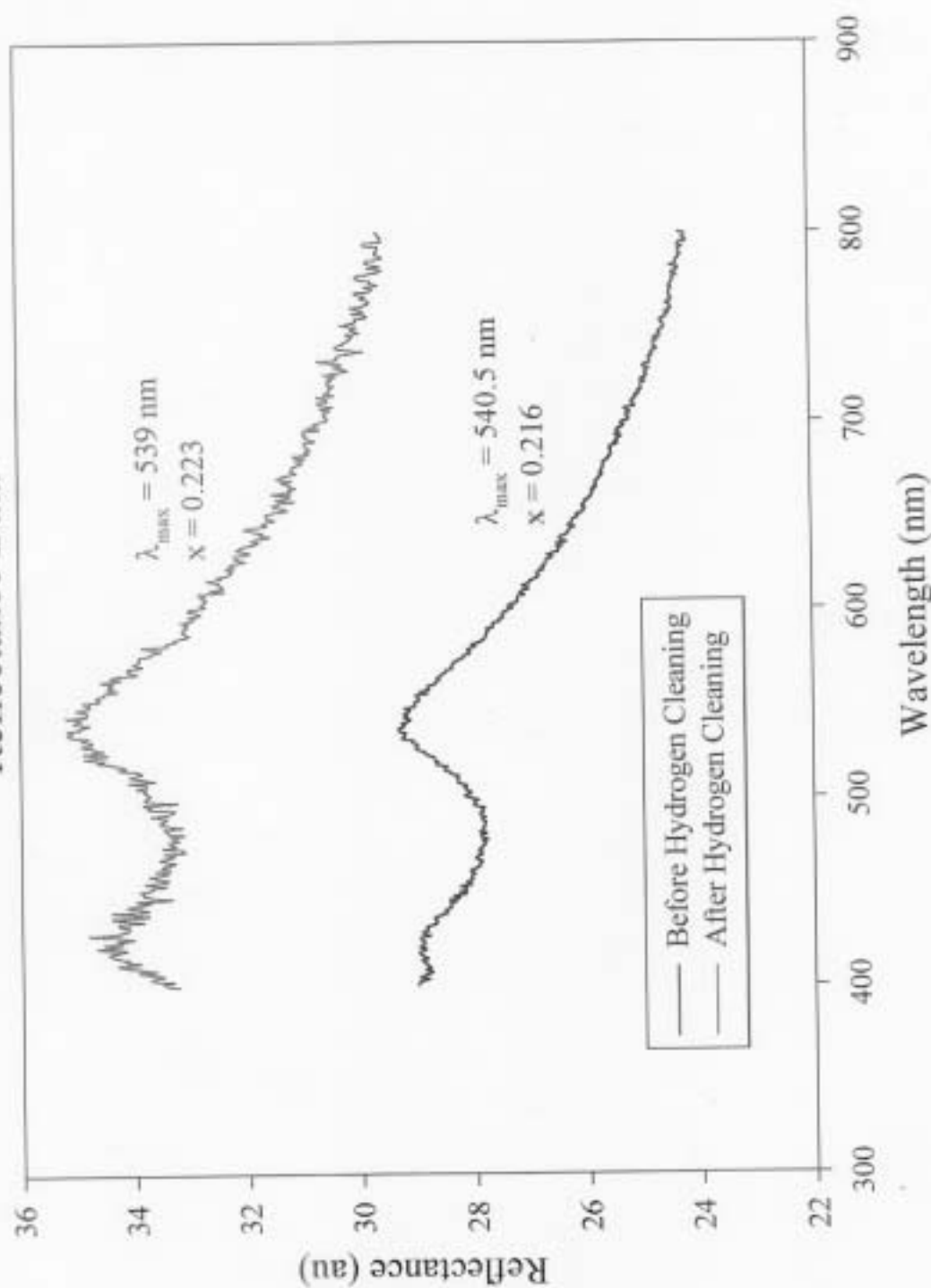
Reflectance (au)

Fig. 4.9   Reflectance data from a HgCdTe sample before and after hydrogen cleaning. Shown are the wavelengths associated with the E_1 reflectance peaks to indicate that there are no stoichiometry changes after atomic hydrogen cleaning.
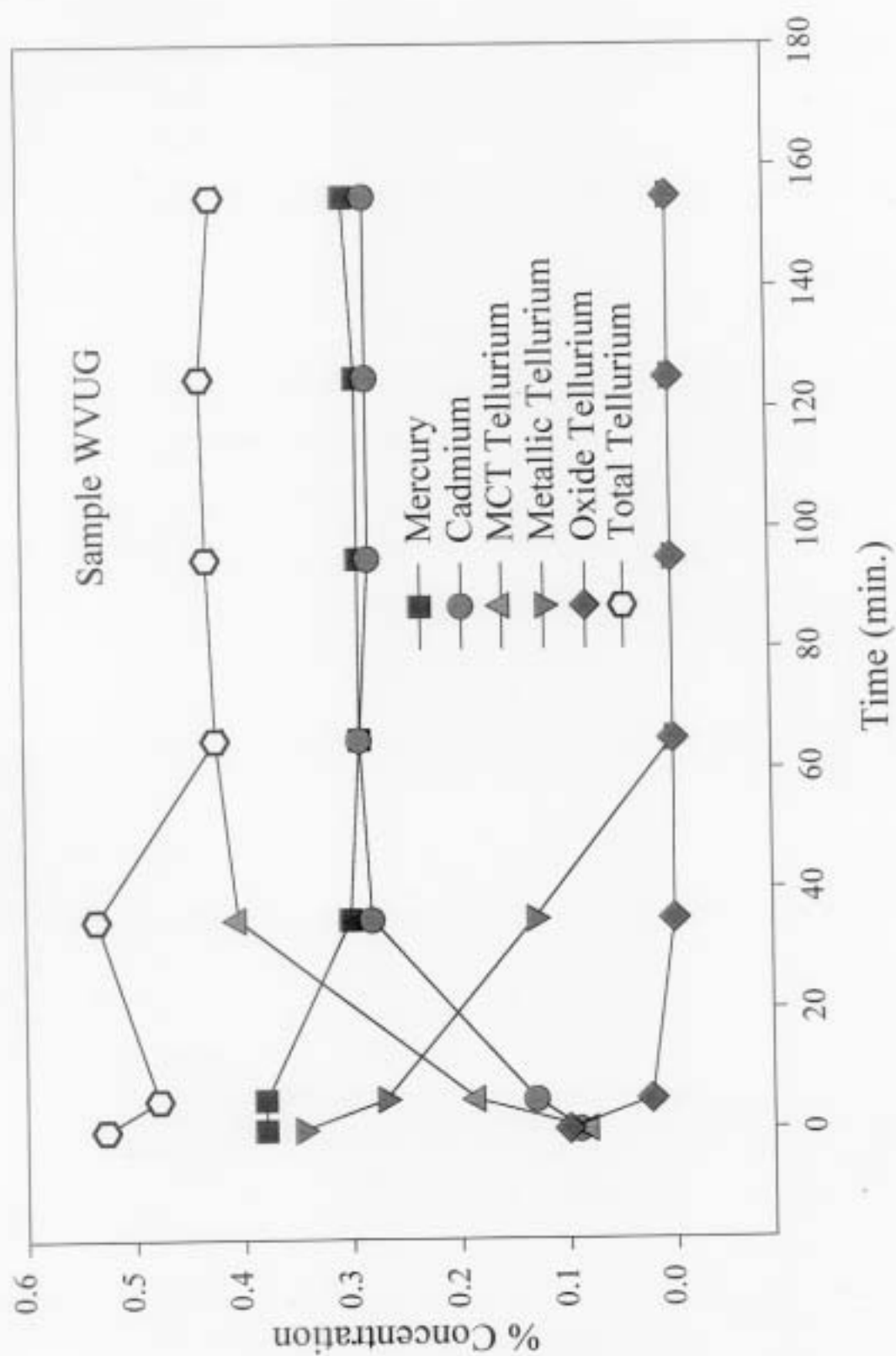
Fig. 4.10   The graph shows the changes in the composition of HgCdTe as a function of atomic hydrogen cleaning time.

Hg removal. In all cases, the steady state composition of the atomic hydrogen-etched HgCdTe surface was HgTe depleted, and reached a limiting x value of 0.6 after ~ 40 minutes.

The data shown in Fig. 4.10 were obtained for a substrate etched at 80°C. Analyses for substrates etched near room temperature produced similar results with any differences being traceable to differences in bulk composition or the initial composition of the oxide/Te overlayers. This is not surprising recalling the substrate block temperature was observed to rise to 50°C during "room-temperature" etching.

4.6 Mechanisms

Surface oxides on CdTe have been reported to contain TeO_2 or $CdTeO_3$.[46-48] It is believed that similar oxides are present on HgCdTe. Removal of these oxides may proceed by reactions similar to those given in Chapter 3 as equations 3.1-3.3. Again reaction 3.2 has the potential to leave behind a Te overlayer, and both XPS and RHEED indicate the presence of a Te-overlayer after chemical etching. Therefore, it is believed that the equation 3.3 is also important for atomic hydrogen cleaning of HgCdTe.

A reaction involving breaking the relatively weak HgTe bond must also occur since HgTe depletion is observed in the near-surface region. Schematically, we could write:

$$HgTe + 2H \rightarrow Hg \uparrow + TeH_2 \uparrow \qquad (4.1)$$

where the Hg is thermally desorbed. Since the Te is actually in a HgCdTe matrix and is potentially bonded to a Cd, this mechanism should be quite sensitive to alloy composition and depth. Indeed, the steady-state composition we observe after extended atomic hydrogen exposure may be due to the extraction of all the Te bound primarily to Hg. That is, steady state is attained as the etch produces a composition that is resistant to further HgTe bond breaking and

removal. We have no evidence for Cd extraction. One possible measure for the removal of Cd in conjunction with mechanism 4.1 would be the total etch rate.

4.7 Etch Rates

We attempted to measure an etch rate for HgCdTe as follows. The Norwegian Defense Research Establishment, in Kjeller, Norway, under the direction of Dr. Stian Lovold, provided three HgCdTe layers grown by MBE with x-values of 0.24, 0.32 and 0.48. The layers had been etched in a Br-based solution, and then patterned with a dense array of small photoresist dots. This pattern is magnified and shown in Fig. 4.11. The samples were inserted into the MBE system and exposed to an atomic hydrogen flux for 60 minutes at 80°C. After stripping the photoresist, the patterns could still be observed using a differential interference-contrast (DIC) microscope, as shown in Fig. 4.12. If steps were present, however, they were too small to be measured optically or with a surface profilometer. The samples were then examined using AFM. The only discernible features were infrequent photoresist remnants that marked the position of the dots. Fig. 4.13 shows that no measurable step height could be detected above the background rms. surface roughness of 2.5 to 2.9 nm. This indicates a step height of less than 5 nm, and a resulting HgCdTe etch rate of less than 0.05 Å/sec. The pattern observed with the DIC microscope was probably due to surface stoichiometry changes occurring with atomic hydrogen cleaning.

4.8 Stability of the Oxide on HgCdTe

Several experiments performed in this study indicated that the oxide present after the Br-methanol etch is relatively unstable. In one experiment, two samples were exposed to the hydrogen-source filament without hydrogen gas being introduced into the chamber, one in the
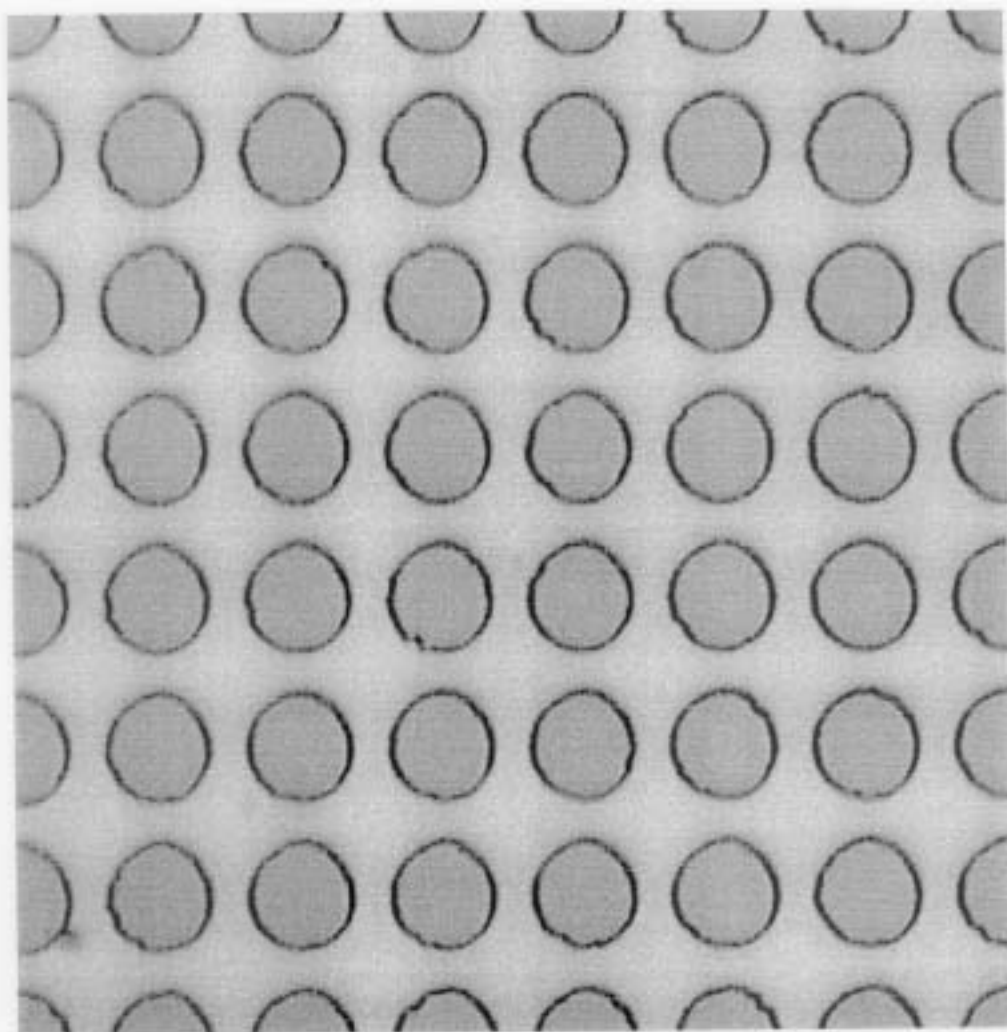
Fig. 4.11   Magnified (1750×) picture of the HgCdTe patterned with photoresist provided by the Norweigen Defence Research Establishment.
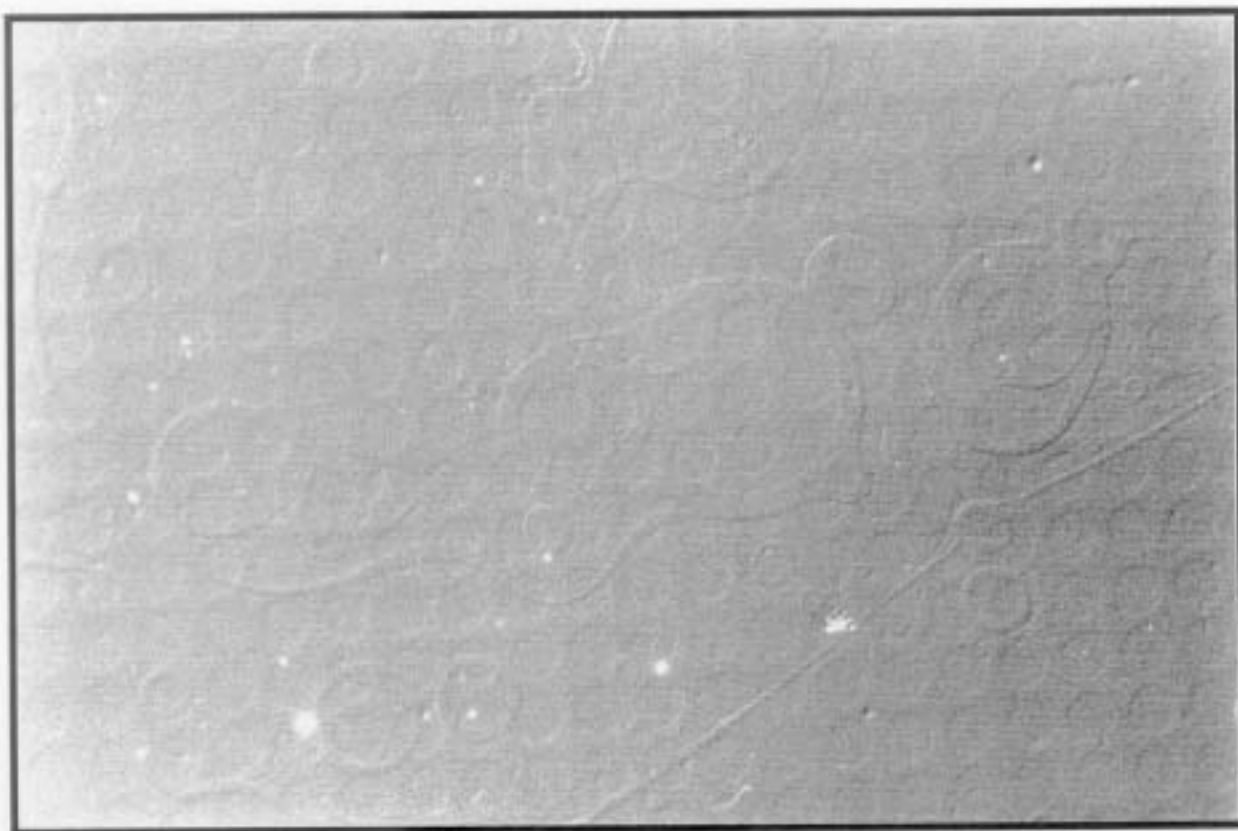
Fig. 4.12   Nomarski interference photographs of the photoresist pattern left after
              hydrogen cleaning and a subsequent acetone dip. (Magnification: × 800.)
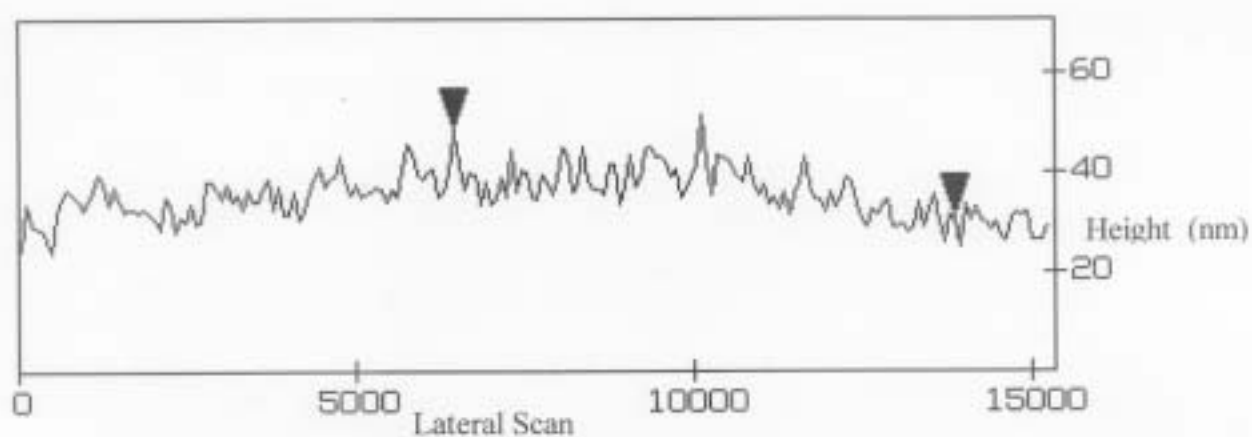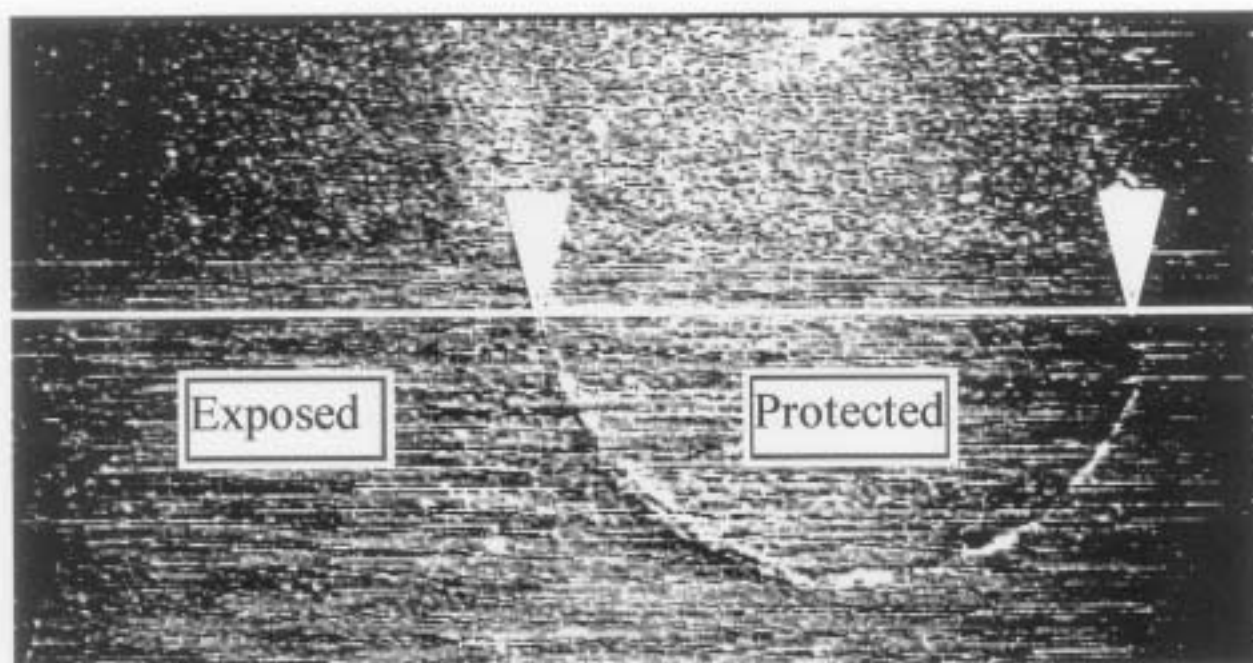
Fig. 4.13   AFM micrograph of patterned HgCdTe after atomic hydrogen cleaning and photoresist stripping. The white line across the micrograph indicates the path of the lateral scan underneath, and the triangle correspond to the locations where an etch step would occur if the HgCdTe had been etched by atomic hydrogen.

XPS chamber and one in the growth chamber. XPS and RHEED data for this experiment are presented in Table 4.1, Table 4.2, Fig. 4.14, and Fig. 4.15. The XPS data in Table 4.2 clearly shows that the oxide thickness does decrease after 30 minutes of exposure to hydrogen gas, and decreases again after 30 minutes of exposure to the filament. Similarly, the diffuse scattering in RHEED associated with oxide is gone after 1 minute of exposure to the filament. Diffuse scattering is best observed near the edge of the RHEED screen, away from the main pattern. Thus, this effect is not clear in Fig. 4.15. Indeed, the surface of the sample whose RHEED is shown in Fig. 4.15b was more ordered and had less diffuse scattering than was typically observed. Note that, in this atypical case, there are also ordered streaks indicating that a part of the surface may indeed be free of overlayers. Continued exposure to the filament, approximately 5 minutes, began to transform the pattern of lines into an irregular spotty pattern, which is believed to be a characteristic of a Te overlayer, as shown in Fig. 4.15c. After 25 minutes the irregular pattern shown in Fig 4.15d indicates that the Te overlayer cannot be removed by filament exposure alone. Results in the XPS system also indicated that the Te overlayer had not been removed, as the spectra still showed a peak with the metallic Te binding energy. The samples in each case were eventually exposed to atomic hydrogen. In the XPS experiment the Te overlayer was readily removed as seen by the disappearance of the metallic Te peak. Similarly, the RHEED pattern began to come back after only one minute of exposure to atomic hydrogen, however it indicated a rougher surface than was seen with a typical hydrogen cleaning procedure.

The desorption mechanism could involve thermal, photon, or electron-stimulated processes. Alternatively, oxide removal may occur simply as the result of etching by atomic hydrogen produced from the residual gases of the system. Several of these possibilities were
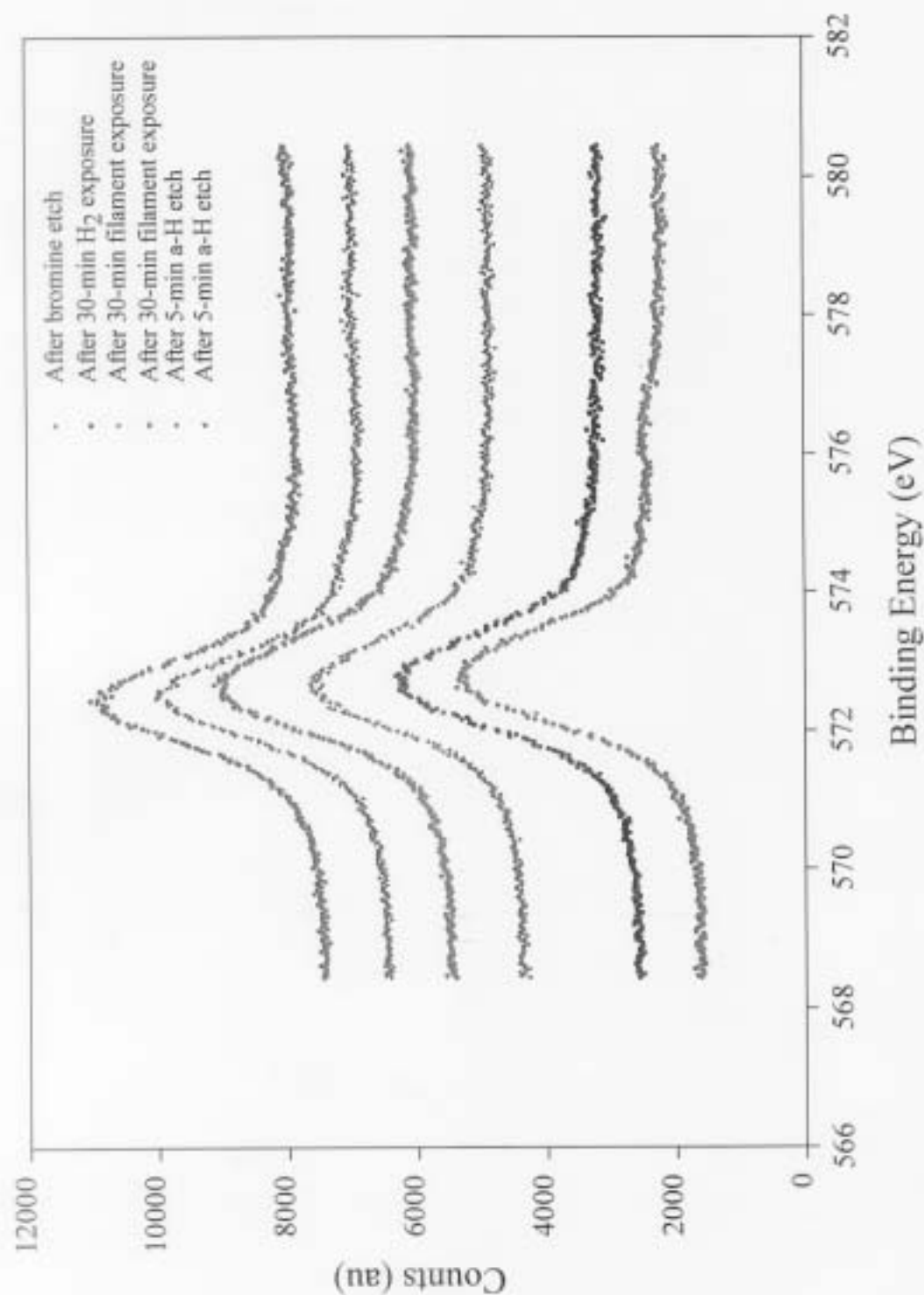
Fig. 4.14 XPS scan of a sample exposed to molecular hydrogen only, followed by an exposure to only the filament. The Te oxide is constantly diminishing, however the binding energy of Te is not representative of tellurium in an HgCdTe matrix until the sample is exposed to atomic hydrogen. For completeness the table on the following page provides peak areas.

61

	Peak Position (eV)	After Br Etch	30 min H_2 Exposure	30 min Filament Only	Overnight	30 min Filament Only	5 min a-H Etch	5 min a-H Etch
Hg 4f$_{7/2}$ Peak	100.2±0.1	3335.8	3428.6	2880.9	1548.1	3387.5	3311.8	3300.7
Cd 3d$_{3/2}$ Satellite.	403.5±0.1	42.7	42.7	37.4	49.8	49.8	86.8	120.1
Cd 3d$_{5/2}$ Peak	405.1±0.05	1120.0	1202.9	1058.0	1100.0	1283.7	1766.8	2159.0
HgCdTe Te 3d$_{5/2}$ Peak	572.4	1891.1 (22.5%)	2705.0 (33.9%)	2790.6 (40.8%)	2814.8 (42.0%)	3404.5 (46.2%)	4874.8 (74.0%)	6327.9 (93.3%)
Metallic Te 3d$_{5/2}$ Peak	572.9	4581.4 (54.5%)	3804.3 (47.7%)	2817.1 (41.2%)	2697.7 (40.2%)	2787.7 (37.8%)	870.0 (13.2%)	0 (0%)
HgCdTe Te 3d$_{3/2}$ Satellite	574.3	459.1 (5.5%)	474.4 (5.9%)	463.7 (6.8%)	506.4 (7.6%)	565.9 (7.7%)	498.0 (7.6%)	457.5 (6.7%)
Metallic Te 3d$_{3/2}$ Satellite	574.8	570.0 (6.8%)	486.4 (6.1%)	385.4 (5.6%)	315.7 (4.7%)	327.6 (4.4%)	126.0 (1.9%)	0 (0%)
Te-Oxide 3d$_{5/2}$ Peak	576.3	728.9 (8.7%)	349.7 (4.4%)	240.3 (3.5%)	215.2 (3.2%)	154.7 (2.1%)	72.6 (1.1%)	0 (0%)
Te-Oxide 3d$_{3/2}$ Satellite	578.1	174.1 (2.1%)	157.6 (1.9%)	145.3 (2.1%)	154.4 (2.3%)	125.8 (1.7%)	144.9 (2.2%)	0 (0%)

Table 4.1   Peak areas for Hg, Cd, Te, and TeO_2 in the XPS spectra of WVU F in Fig. 4.14. All of the peaks in the Te scan also have the percent of the total area of the graph that they represent. This allows one to recognize when a particular peak becomes unnecessary.

	After Br Etch	30 min H₂ Exposure	30 min Filament Only	Overnight	30 min Filament Only	5 min a-H Etch	5 min a-H Etch
Hg % Composition	41.3	42.5	42.0	28.2	43.3	42.1	39.1
Cd % Composition	11.5	12.4	12.8	16.6	13.6	18.6	21.2
HgCdTe Te % Composition	12.4	17.8	21.6	27.2	23.1	32.9	39.7
Metallic Te % Composition	30.1	25.0	21.8	26.0	18.9	5.9	0.0
Oxide Te % Composition	4.8	2.3	1.9	2.1	1.0	0.5	0.0
HgCdTe x-Value	0.22	0.23	0.23	0.37	0.24	0.31	0.35
Oxide Thickness (Å)	1.64	0.74	0.57	0.51	0.32	0.14	0.0
Te-overlayer Thickness (Å)	13.84	8.97	6.89	6.58	5.64	1.47	0.00

Table 4.2   Percent concentrations, x-values, oxide thicknesses, and overlayer thicknesses for the XPS spectra of WVU F in Fig 4.14. This more clearly shows the removal of the oxide. Note that the method for obtaining the oxide and overlayer thicknesses assumes that the layers are flat. However, the surfaces are rough, and so the thicknesses are really just average values over the surface.
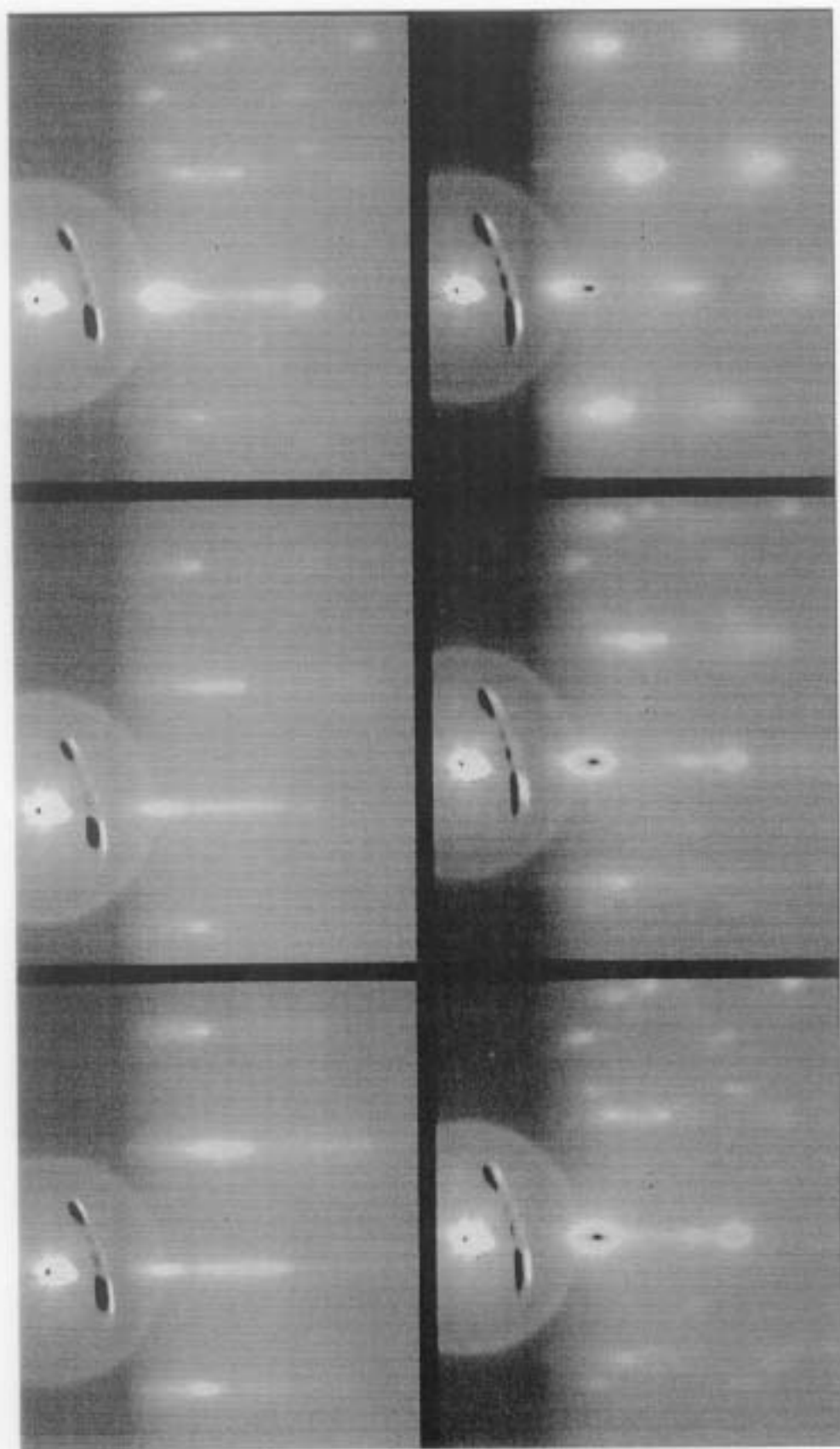
Fig. 4.15   RHEED evolution of HgCdTe (a) as etched (~80°C), (b) exposed to light for 1 minute (~80°C), (c) exposed to light for 5 minutes (~80°C), (d) exposed to light for 25 minutes (~80°C), (e) exposed to hydrogen for 1 minute (~80°C), (f) exposure to hydrogen for 6 minutes (~80°C).

eliminated on the basis of relatively simple experiments. Thermal desorption was ruled out by annealing an oxide-containing surface at temperatures of 80°C, 100°C, and 120°C without removing the oxide. Electron-stimulated desorption was ruled out by observing that the hydrogen source filament-to-substrate current was a factor of 40 lower than the photo-emission current produced during XPS analysis (under which condition the oxide overlayer was stable).

On another occasion, the as-chemically-etched substrate was allowed to remain in the analysis chamber for approximately 48 hours without heating after the as-etched surface had been analyzed indicating a typical TeO peak. Subsequent XPS analysis revealed that the oxide was desorbed during this period which indicates that the oxide is unstable in vacuum.

Preliminary investigations in the MBE system indicate that photo-stimulated desorption may be the underlying mechanism for oxide removal without atomic hydrogen. The output from a 100-W tungsten-halogen lamp was filtered to pass only 400 to 700-nm light and focused on the HgCdTe layer. The as chemically-etched substrate exhibited diffuse scattering observed with RHEED and associated with the oxide overlayer as shown in Fig. 4.16. Fig. 4.17 shows that this cool illumination was found to eliminate the diffuse scattering. However, continued exposure to the light did not degrade the surface of the HgCdTe, as shown in Fig. 4.18 which had been exposed to the white light source for over an hour. In this case, the sample surface appeared to have improved enough with just light exposure that a decision was made to deposit CdTe. Fig. 4.19 is a RHEED pattern of this CdTe layer, exhibiting quite a reasonable pattern. It is noted that this difference, ie. The lack of evidence for a Te overlayer, could be due to the improved polishing process used on these newer HgCdTe pieces. This effect will be the topic of a future study planned for this summer. The Norwegian Defense Research Establishment in
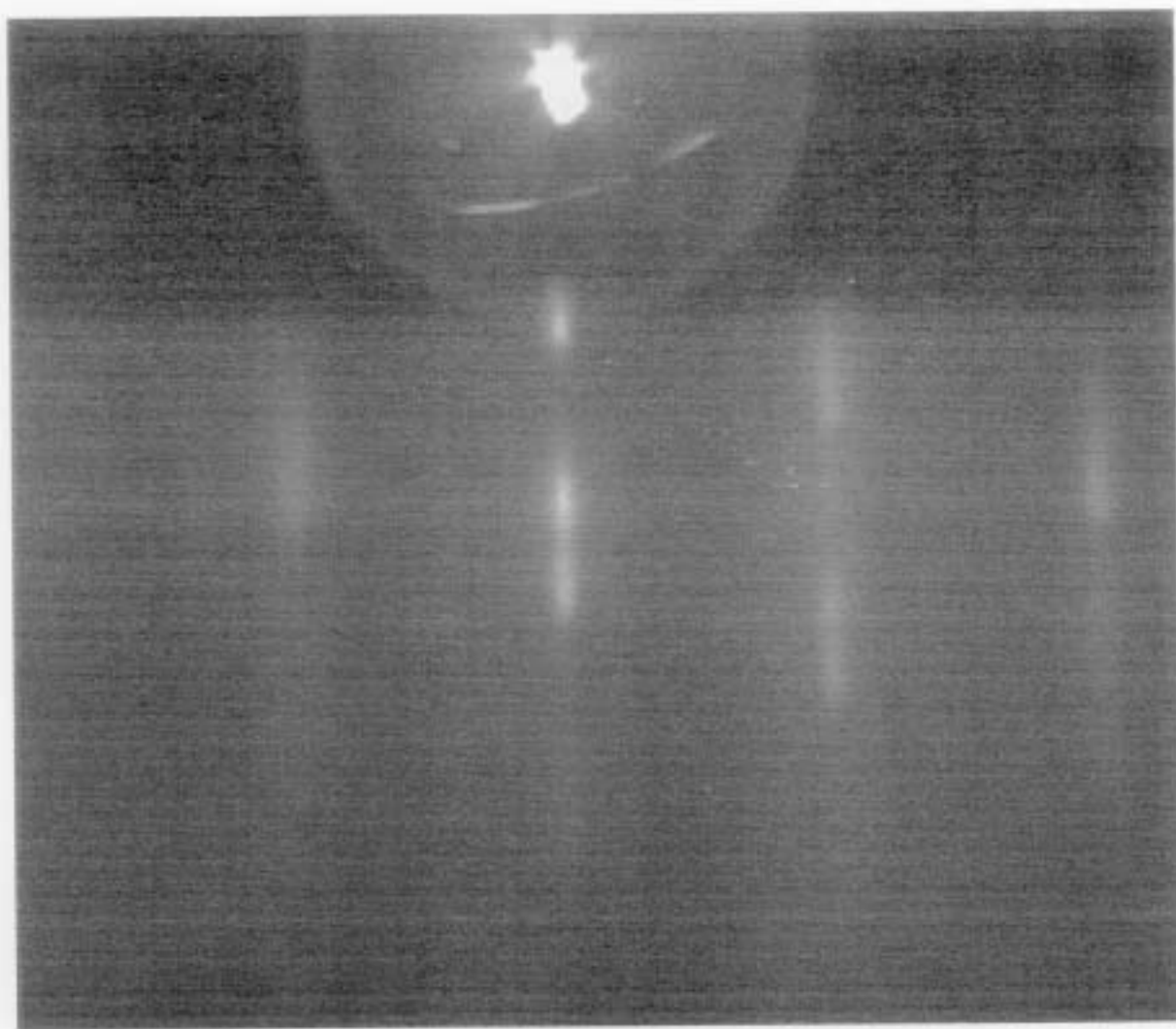
Fig. 4.16   RHEED of as-etched HgCdTe.
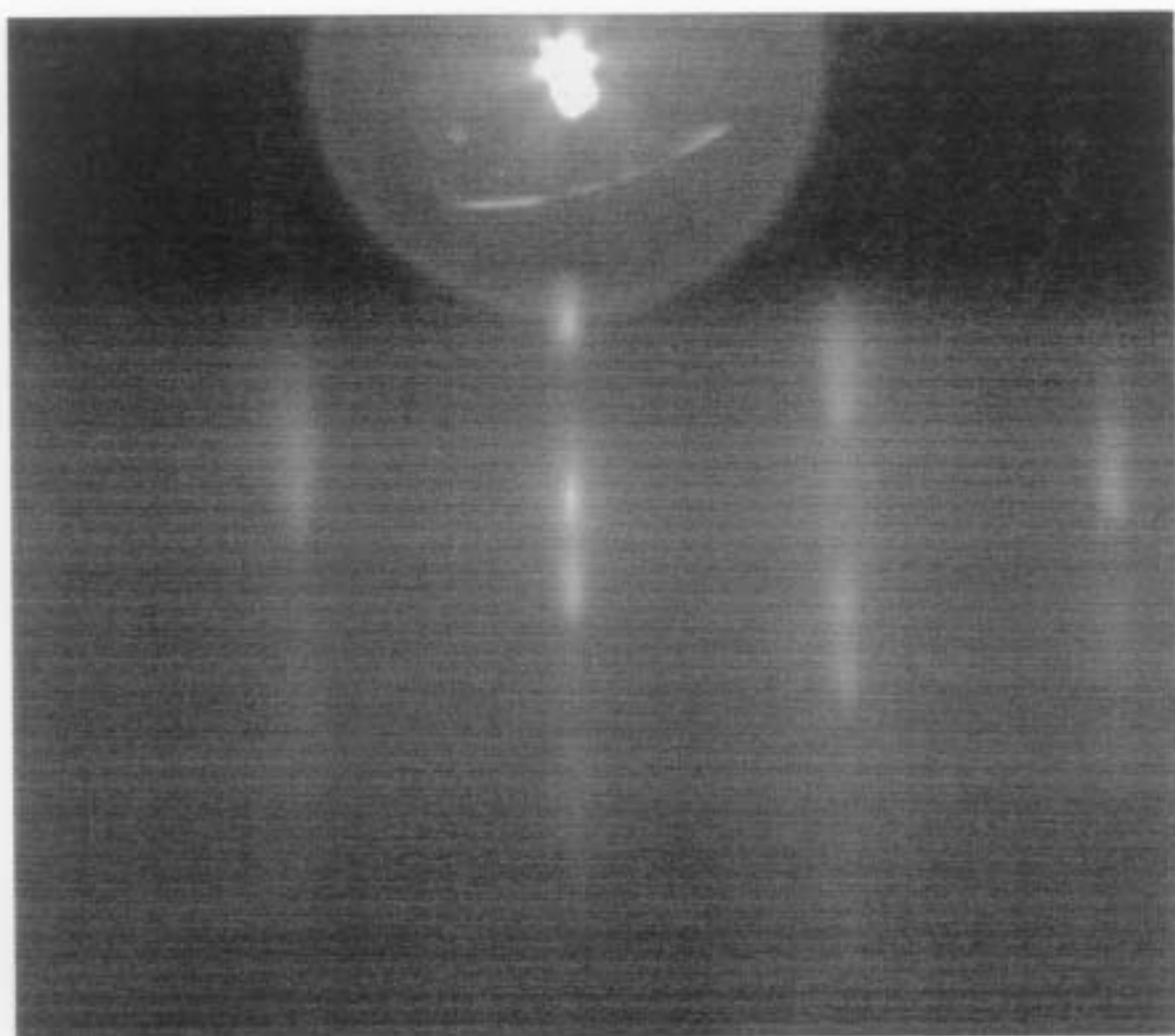
Fig. 4.17   RHEED of HgCdTe exposed to white light source for 5 min.
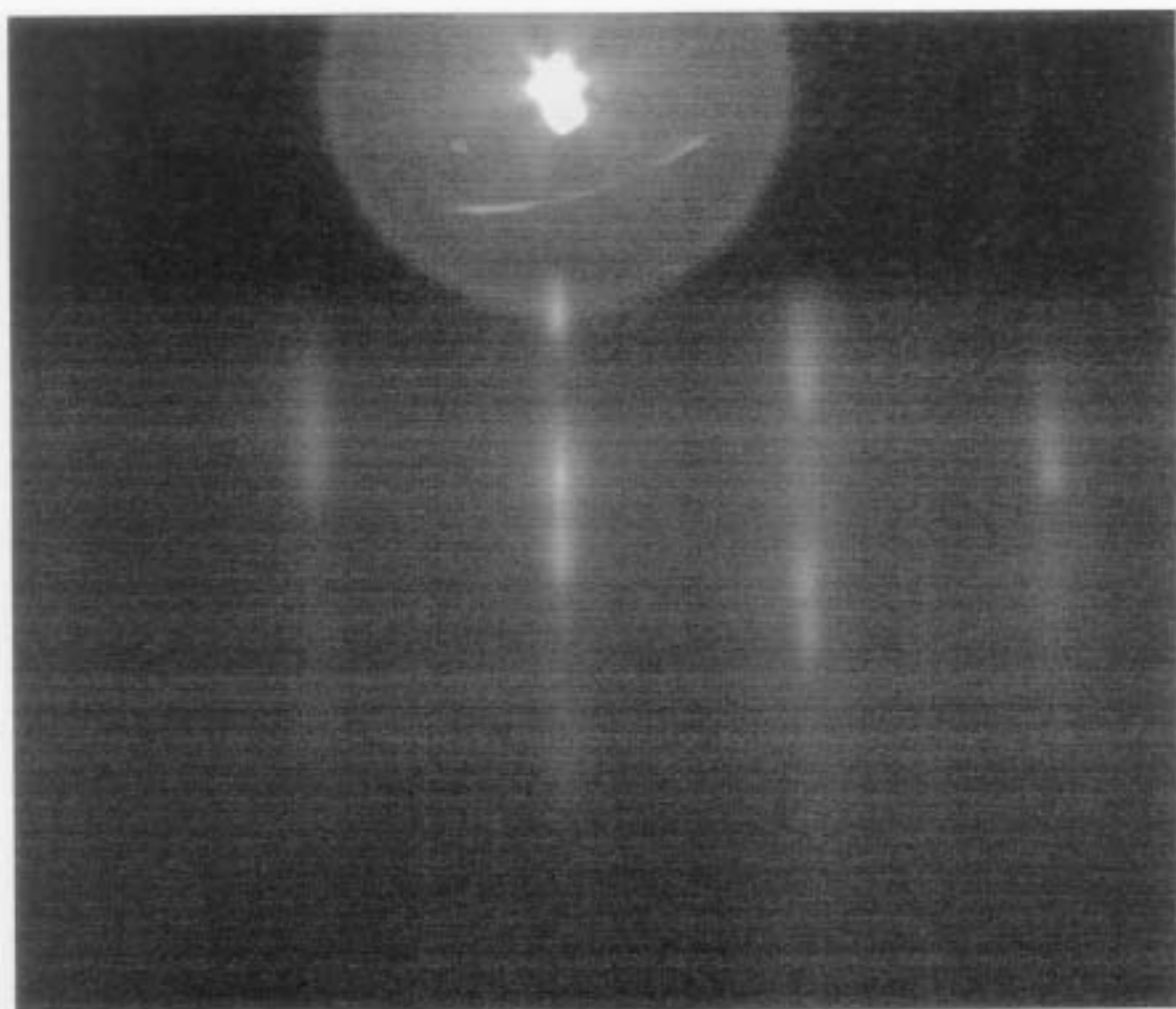
Fig. 4.18   RHEED of HgCdTe after over an hour of exposure to a white light source.
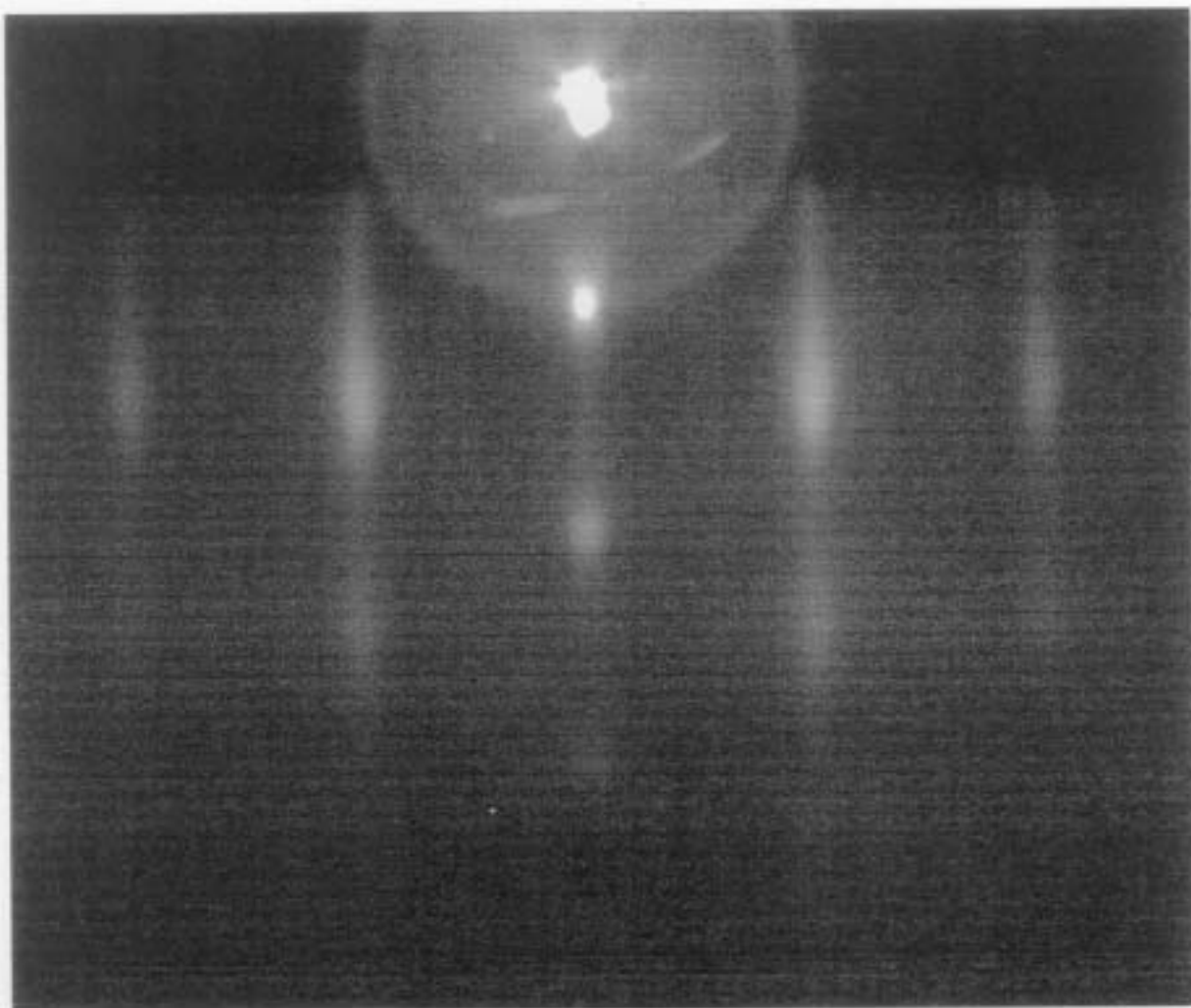
Fig. 4.19   RHEED of CdTe deposited on HgCdTe exposed only to a white light source.

Kjeller, Norway has invited both Dr. T. Myers and me to visit their laboratory and study the effect of atomic hydrogen cleaning on MBE-grown HgCdTe. MBE materials do not require any polishing, and therefore the study will have a further element of control.

4.9 Other Types of Oxide

There is also evidence that oxide can occur in more than one chemical state on HgCdTe. In one hydrogen etching experiment, it became necessary to re-expose the HgCdTe sample to atmosphere for 3 hours after the oxide-Te peak was removed (i.e. after a 5-minute atomic hydrogen etch at room temperature). When this surface was re-analyzed, a more intense oxide-Te peak was observed. As indicated in Fig. 4.20, Table 4.3, and Table 4.4, this new oxide layer was twice as thick as typically observed on the Br-methanol etched samples. It is noted in passing this spectra is more typical of what has been reported in the literature. This thicker layer may have been due to an increase in the number of reactive surface sites produced by surface roughening during this stage of the atomic hydrogen etch. This is consistent with spotty/diffuse RHEED patterns obtained during the initial stages of atomic hydrogen etching. Alternatively, this increase in oxide formation may be caused by more of the underlying HgCdTe matrix being exposed for oxidation. Interestingly, after the air exposure the Te photoelectron peak binding energy was consistent with only metallic Te. It appeared that all the Te in a HgCdTe matrix went to forming the oxide. On only this sample the oxide peak also appeared to be composed of more than one photo electron peak. This particular oxide was also more resistant to atomic hydrogen etching, with an etch rate that varied with thickness. The initial removal rate was 0.23 Å/min, close to a factor of two slower than typical for all Br-methanol etched samples, slowing to a rate of 0.13 Å/min. Both results indicate that there may indeed be more than one type of oxide formed on a HgCdTe surface, depending intimately upon prior surface treatment.
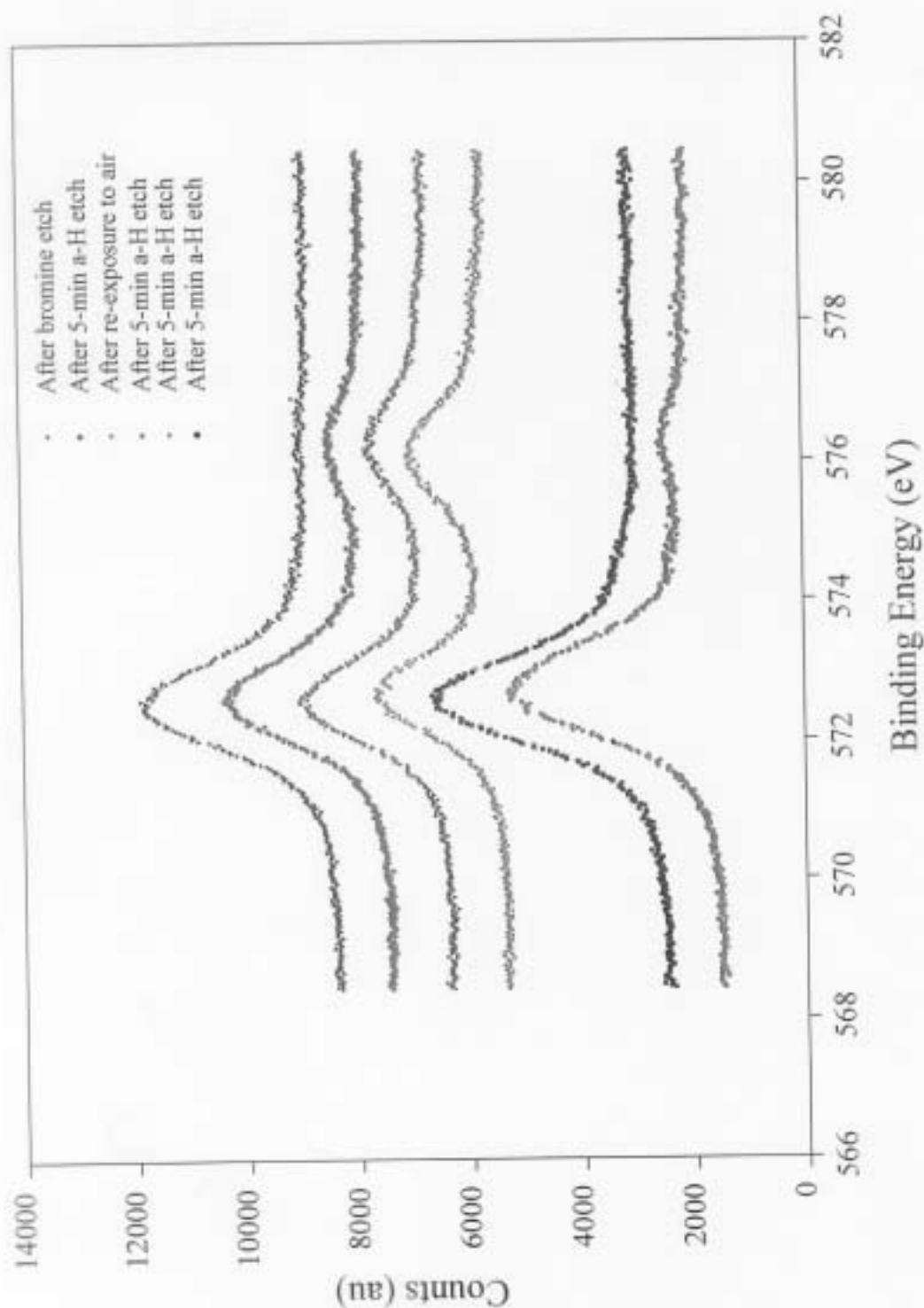
Fig. 4.20   XPS of HgCdTe exposed to hydrogen for 5 minutes to remove the oxide, then exposed to air for 3 hours, which allowed a new, stronger oxide to be form. The peak areas are in the table on the following page.

	Peak Position (eV)	After Bromine Etch	5 min a-H Etch	New Peak Position (eV)	3 hour Air Exposure	5 min a-H Etch	5 min a-H Etch	5 min a-H Etch
Hg 4f$_{7/2}$ Peak	100.3±0.1	2726.1	2820.0	100.3±0.1	2400.5	2404.2	2388.8	2554.8
Cd 3d$_{3/2}$ Satellite	403.45±0.45	19.6	62.0	403.45±0.45	84.8	67.9	57.9	68.4
Cd 3d$_{3/2}$ Peak.	405.05±0.05	880.0	1301.4	405.05±0.05	1257.0	1236.6	1240.4	1257.6
HgCdTe Te 3d$_{3/2}$ Peak	572.4	2833.4 (32.5%)	4828.5 (58.0%)	572.3	0 (0%)	1082.9 (14.5%)	845.4 (12.2%)	2009.8 (27.6%)
Metallic Te 3d$_{3/2}$ Peak	572.9	3787.2 (43.4%)	2370.4 (28.5%)	572.7	3614.3 (53.8%)	3356.9 (44.8%)	3989.7 (57.5%)	3870.7 (53.1%)
HgCdTe Te 3d$_{3/2}$ Satellite	574.3	449.4 (5.2%)	585.7 (7.0%)	574.1	0 (0%)	211.5 (2.8%)	260.8 (3.8%)	367.5 (5.0%)
Metallic Te 3d$_{3/2}$ Satellite	574.8	479.5 (5.5%)	243.2 (2.9%)	574.5	313.2 (4.7%)	422.5 (5.6%)	406.7 (5.9%)	405.6 (5.6%)
Te-Oxide 3d$_{3/2}$ Peak	576.3	936.1 (10.7%)	145.1 (1.7%)	576.0 & 576.2	1199.6 & 1361.7 (17.9% & 20.3%)	24.6 & 2063.8 (0.3% & 27.6%)	15.4 & 1259.0 (0.2% & 18.1%)	0 & 490.3 (0% & 6.7%)
Te-Oxide 3d$_{3/2}$ Satellite	578.1	238.1 (2.7%)	148.3 (1.8%)	577.9 & 578.2	13.1 & 214.5 (0.2% & 3.2%)	76.8 & 246.9 (1.0% & 3.3%)	18.6 & 141.7 (0.3% & 2.0%)	0 & 145.3 (0% & 2.0%)

Table 4.3   Peak areas for Hg, Cd, Te, and TeO$_2$ in the XPS spectra in Fig. 4.20. All of the peaks in the Te scan also have the percent of the total area of the graph that they represent. This allows one to recognize when a particular peak becomes unnecessary.

72

	After Bromine Etch	5 min a-H Etch	3 hour Air Exposure	5 min a-H Etch	5 min a-H Etch	5 min a-H Etch
Hg Percent Composition	36.5	36.2	35.8	34.9	35.9	36.6
Cd Percent Composition	9.8	13.8	15.5	14.9	15.4	14.9
HgCdTe Te % Composition	20.1	32.9	0	8.3	6.7	15.3
Metallic Te % Composition	26.9	16.1	28.5	25.8	31.8	29.4
Oxide Te % Composition	6.7	1.0	20.2	16.1	10.2	3.7
HgCdTe x-Value	0.21	0.28	0.30	0.30	0.30	0.29
Oxide Thickness (Å)	1.87	0.24	9.74	6.08	3.88	1.19
Te-overlayer Thickness (Å)	9.77	3.66	$+\infty$	20.42	22.38	11.58

Table 4.4   Percent concentrations, x-values, oxide thicknesses, and overlayer thicknesses for the XPS spectra in Fig. 4.20. Note the oxide formed after the re-exposure to air is never removed. Also note that the method for obtaining the oxide and overlayer thicknesses assumes that the layers are flat. However, the surfaces are rough, and so the thicknesses are really just average values over the surface.

4.10 Preliminary Device Results

A set of three LPE HgCdTe layers were etched and exposed to atomic hydrogen until a streaky 2-D pattern was obtained. Approximately 0.25 μm of CdTe was then deposited at 80°C at a rate of 0.1 μm/hr. The samples were sent for processing into Hg-diffused devices at Lockheed Martin Microelectronics Center (Nashua, NH). The time between the CdTe passivation step and further processing was longer than six months due to corporate mergers and shifting of laboratory equipment from Syracuse, NY to Nashua, NH. Even so, the processing resulted in >99% yield of working devices. The resulting average R_oA values were 8, 18, and 678 Ω cm², for cut-off wavelengths of 9.9, 8.3, and 8.1 μm, respectively. This can be compared to the results for a control that underwent standard processing in the same "lot", 55 Ω cm² and 9.7 μm. The lower values for the devices fabricated using atomic hydrogen-cleaned HgCdTe may be due to the long ambient exposure (including courier mail shipping) spent between CdTe deposition and other processing, a major departure from the standard diffused diode process. The results are encouraging and additional LPE samples cleaned with atomic hydrogen will be processed in the near future. Importantly, the results of this first process lot indicate that use of atomic hydrogen may indeed be a viable approach to low temperature oxide/overlayer removal.

5. Cleaning of GaAs for ZnSe and CdTe Deposition

5.1 Background

For MBE growth of ZnSe on GaAs substrates, the final step prior to growth is often a thermal cleaning at temperatures ranging from 580 to 650°C to remove the native oxides.[30,31] However, the resulting GaAs surface after this treatment exhibits a Ga-rich surface reconstruction. This gallium-rich surface can lead to the formation of Ga_2Se_3 at the interface[49] which can then serve as nucleation sites for stacking faults. Either heating the substrate under an As-flux or the growth of GaAs epilayers prior to ZnSe growth has been shown to improve the interface quality.[50,51] A recent study by Kuo *et al.* indicates that stacking fault densities less than 10^4 cm^{-2} can be obtained through a combination of GaAs epilayer growth followed by Zn treatment of the surface prior to ZnSe growth.[5] A disadvantage of this approach is that a separate growth chamber is required for the GaAs epilayer deposition to minimize the potential for cross-contamination.

Of interest here is that several studies have demonstrated an As-stabilized GaAs surface after atomic hydrogen cleaning at substrate temperatures between 360 and 400°C.[6,7,8] Prior studies have indicated that such an As-stabilized surface is crucial to a high quality ZnSe/GaAs interface.[50] A former student in this lab, Dr. Zonghai Yu, performed experiments involving growth of ZnSe on GaAs substrates, and his work is presented here as a precursor to the work done involving CdTe growth on GaAs. ZnSe films were grown on semi-insulating, (100)-oriented GaAs substrates using high purity (7N) elemental Zn and Se from conventional MBE furnaces (EPI). The 2 μm-thick layers were grown at 250°C and 300°C with uncorrected Zn-to-

Se beam equivalent pressure (BEP) ratios ranging from 0.5 to 1.5. Doped layers were grown on an undoped 0.4 µm thick buffer layer.

5.2 Substrate Preparation

The substrates were initially rinsed in flowing DI H_2O for five minutes. After being blown dry with high purity nitrogen gas, the substrates were etched in a H_2SO_4:H_2O_2:DI H_2O (8:1:1) solution for 5 minutes at room temperature and rinsed in flowing DI H_2O for 5 minutes. The substrates were then blown dry with nitrogen gas. Prior to growth the substrates were thermally-treated in vacuum in one of two ways. The more conventional treatment involved heating to 580°C for between ten to twenty minutes followed by cooling to the growth temperature. Under the other treatment, the substrate was heated to 360°C and exposed to atomic hydrogen at a system pressure of 2×10^{-6} Torr BEP for 20 minutes, at which point the hydrogen flow is cut off and the substrate is cooled to the growth temperature.

5.3 RHEED During Hydrogen Cleaning

The sample surface was monitored by RHEED during cleaning and growth. Fig. 5.1a is a typical RHEED pattern of a (100) GaAs substrate without *in-situ* cleaning. The RHEED pattern exhibits rings and a spotty pattern indicative of an oxide overlayer. The conventional preheat led to a Ga-rich surface, indicated by a weak (4×2) surface reconstruction which became rough if the heating continued too long. As shown in Fig. 5.1b, the diffraction pattern intensity was not strong, and remained spotty, indicating a rough surface. Subsequent ZnSe growth on this surface did not become two-dimensional (2D) until 10 seconds after growth initiation. The atomic hydrogen cleaning step resulted in an As-stabilized surface, indicated by observation of a weak (2×4) surface reconstruction pattern. A typical bright, streaky RHEED pattern of such a

[100] [110]

(a)

(b)

(c)
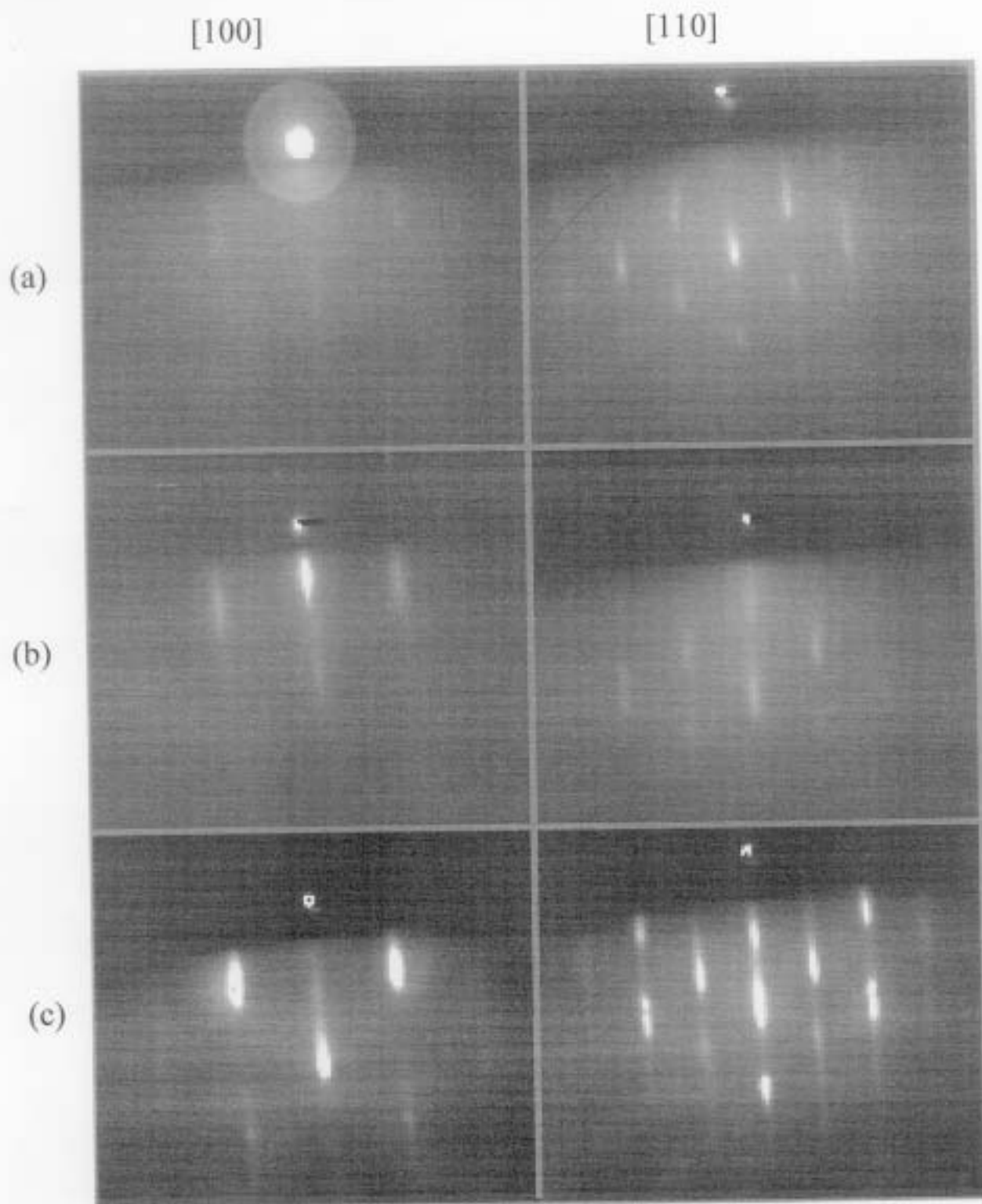
Fig. 5.1   RHEED of the [100] and [110] azimuths of GaAs (a) as etched, (b) thermally cleaned (~580°C), (c) and cleaned with atomic hydrogen (~360°C).

77

surface is shown in Fig. 5.1c. Note also the presence of the Kikuchi lines. ZnSe layers grown on this surface resulted in a 2D growth mode immediately after growth initiation. It is noted in passing that a thermal cleaning under a molecular hydrogen flux was attempted with the cracker turned off, which yielded results similar to the conventional preheat and required a temperature of 580°C to obtain oxide removal.

5.4 ZnSe Deposition

5.4.1 Effect of Atomic Hydrogen Cleaning

Two types of stacking fault defects are observed in ZnSe films grown on GaAs substrates as studied using transmission electron microscopy (TEM).[5,52] These are the same type of defects that have also plagued growth of CdTe and HgCdTe on the (100) orientation.[53-56] Frank-type stacking faults, which are bound by Frank partial dislocations, appear as triangular-shaped twin faults. Shockley-type stacking faults, which are bound by Shockley partial dislocations, are more line-shaped. The radiative efficiency is lower in the region of the stacking fault, allowing the use of techniques such as cathodoluminescence (CL) to image the defects.[5,57,58] Optical fluorescence microscopy can also be used to image these stacking faults. An Olympus BX60M microscope was used with a standard biological fluorescence attachment utilizing a 100 W Hg lamp as the excitation source, resulting in a much simpler system than that required for CL.

Fig. 5.2a is the fluorescence micrograph of a ZnSe film grown on GaAs substrate with conventional thermal cleaning. The dark features are non-radiative regions due to stacking faults, with the short line-shaped features ascribed to Shockley-type stacking faults and the larger triangular-shaped features to Frank-type stacking faults. These images are very similar to those observed under TEM.[5] The density of both types of defects was determined to be greater
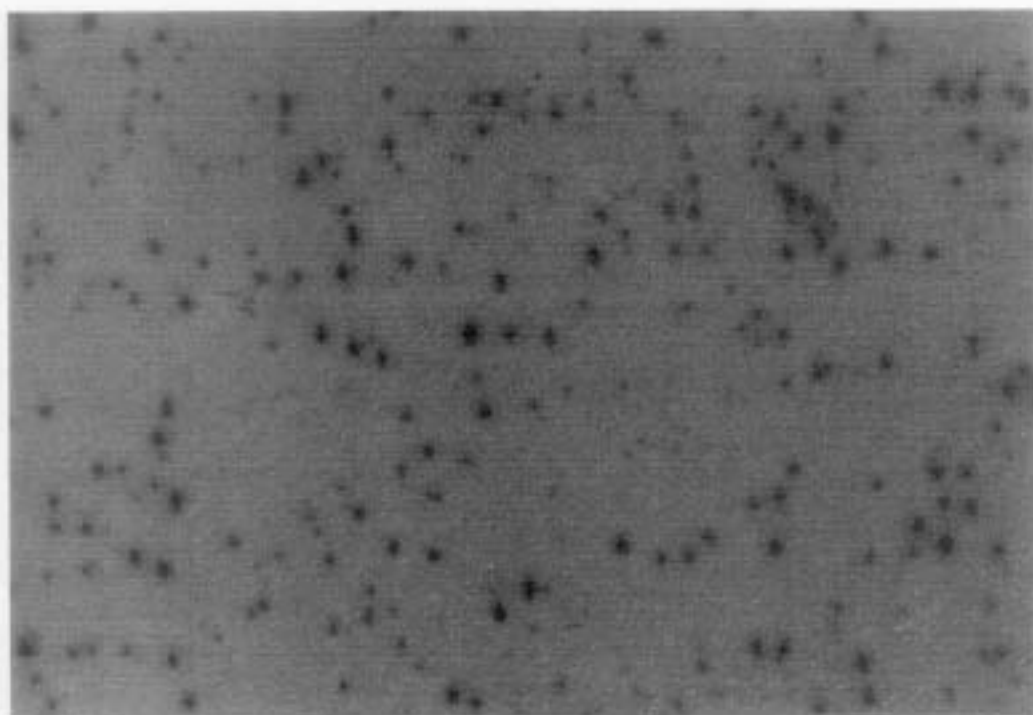
(a)
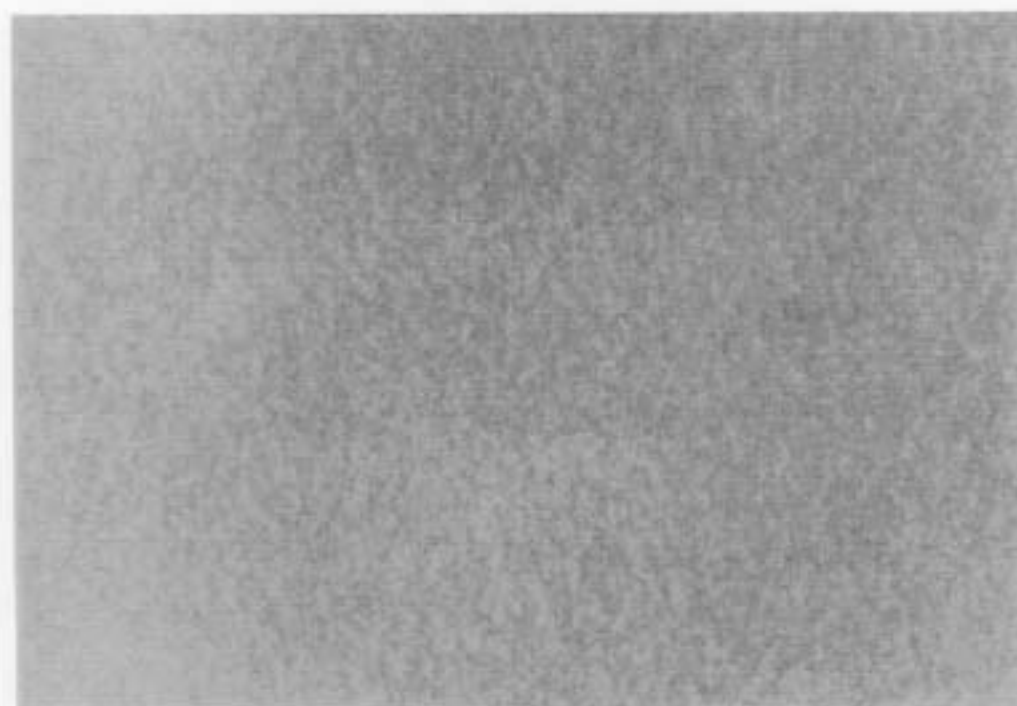
(b)

Fig 5.2   UV florescence micrographs of two different ZnSe films grown on GaAs
representing an area of 125 × 88 μm.   In (a) the GaAs was thermally
cleaned, and in (b) the substrate underwent atomic hydrogen cleaning.

than 10^7 cm^{-2} by simply counting the number of stacking faults in the field of view. Fig. 5.2b shows a typical fluorescence micrograph of a ZnSe film grown on a GaAs substrate cleaned with atomic hydrogen. A significant reduction in defect density is observed. The dark features associated with the stacking faults were isolated and difficult to find on these layers. The density of both types of stacking faults was conservatively estimated to be less than 10^4 cm^{-2} by direct observation. This is comparable to samples grown after the more complex approach of growing a GaAs buffer layer followed by a Zn pre-treatment. A significant difference was not observed for the two different substrate temperatures (250°C and 300°C), the presence of nitrogen-doping, or the growth-flux ratios investigated.

5.4.2 Effect of Zn Pretreatment

After the completion of Dr. Yu's study, the effect of the Zn-pretreatment in addition to hydrogen cleaning was studied. After typical hydrogen cleaning, the substrate was lowered to the growth temperature of 300°C. Once the substrate temperature settled, the Zn oven was opened for approximately ten seconds. After that time the Se oven was opened and growth commenced.

It was shown that the Zn pretreatment further improved the ZnSe film by reducing the number of defects. Photoluminescence (PL) experiments were performed by Monica Moldovan in Dr. N. Giles' lab at WVU comparing ZnSe films grown with and without the Zn-pretreatment. M. Moldovan et. al. reported the results at the 1997 US Workshop on the Physics and Chemistry of II-VI Materials.[58] Fig. 5.3 shows a low temperature (4.8K) PL spectra of two ZnSe films grown under the same conditions, the only difference being that (a) was grown without a Zn pre-treatment, and (b) was grown with a Zn-pretreatment.[59] The so-called I_v line at 2.775 eV, which

80
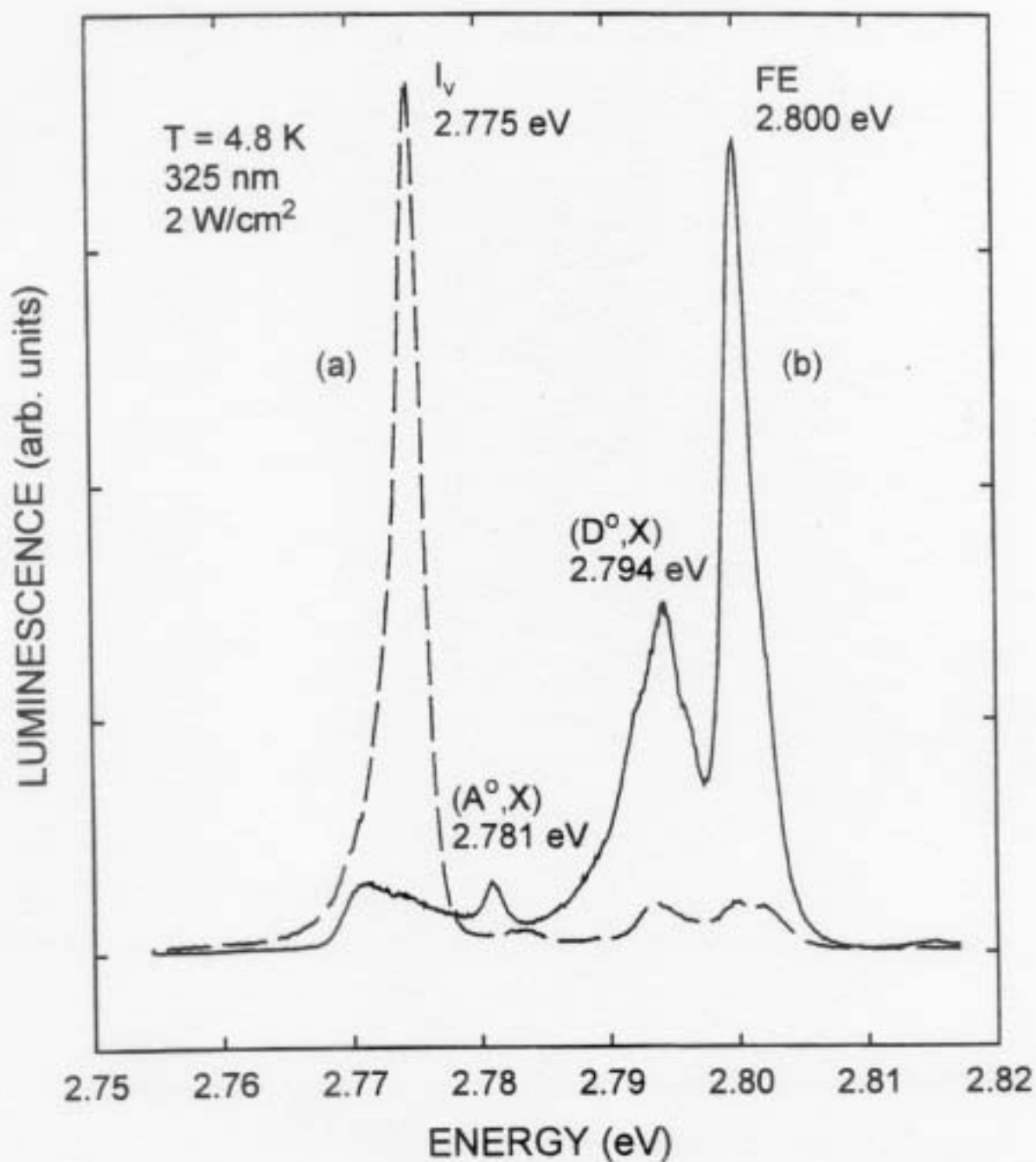
Fig. 5.3   PL of ZnSe at 4.8K showing the reduction of the I_v line in samples (b) with a Zn
            pretreatment, as opposed to those (a) without a Zn pretreatment.
            (Taken from Ref. 59)

is very prominent in the sample grown without the Zn pretreatment, has been attributed to selenium-site-related defects.[60,61] Plot (b)'s scale is magnified compared to that of (a), to demonstrate the reduction of the I_v line due to the Zn pretreatment. Thus, we take the dramatic reduction in intensity of the I_v line to indicate reduced Se-related defects in the film.

5.5 CdTe Deposition

The growth of CdTe is also susceptible to twin-related defects, resulting in a surface feature often referred to as a "pyramidal hillock". Thus, CdTe was also grown on (100)-oriented GaAs cleaned using atomic hydrogen to investigate if atomic hydrogen cleaning led to a significant reduction of those features. The CdTe thickness was nominally 2.0 μm, and the RHEED of the CdTe film during growth, shown in Fig. 5.4, was streaky during the 300°C growth, indicating a relatively smooth surface. A picture taken with the DIC microscope of the hillocks on this sample is shown in Fig. 5.5. The resulting pyramidal hillock density was 1×10^4 cm^{-2} which is a factor-of-ten lower than what was previously obtained by my advisor's group at General Electronics Laboratory (Syracuse, NY) on GaAs substrates using conventional thermal cleaning. This indicates that the atomic hydrogen cleaning leaves a surface appropriate for CdTe growth as well. This density, 10^4 cm^{-2}, may represent an intrinsic lower limit for twin-related features for CdTe growth, as this is continually seen for (100)-oriented substrates. Indeed, lower densities are only obtained by using CdTe or GaAs tilted off (100) by as much as 10°,[54-56] or other orientations such as (211)B.[53,62] An interesting follow-up to the present study would be an investigation of atomic hydrogen cleaning of such off-axis substrates.
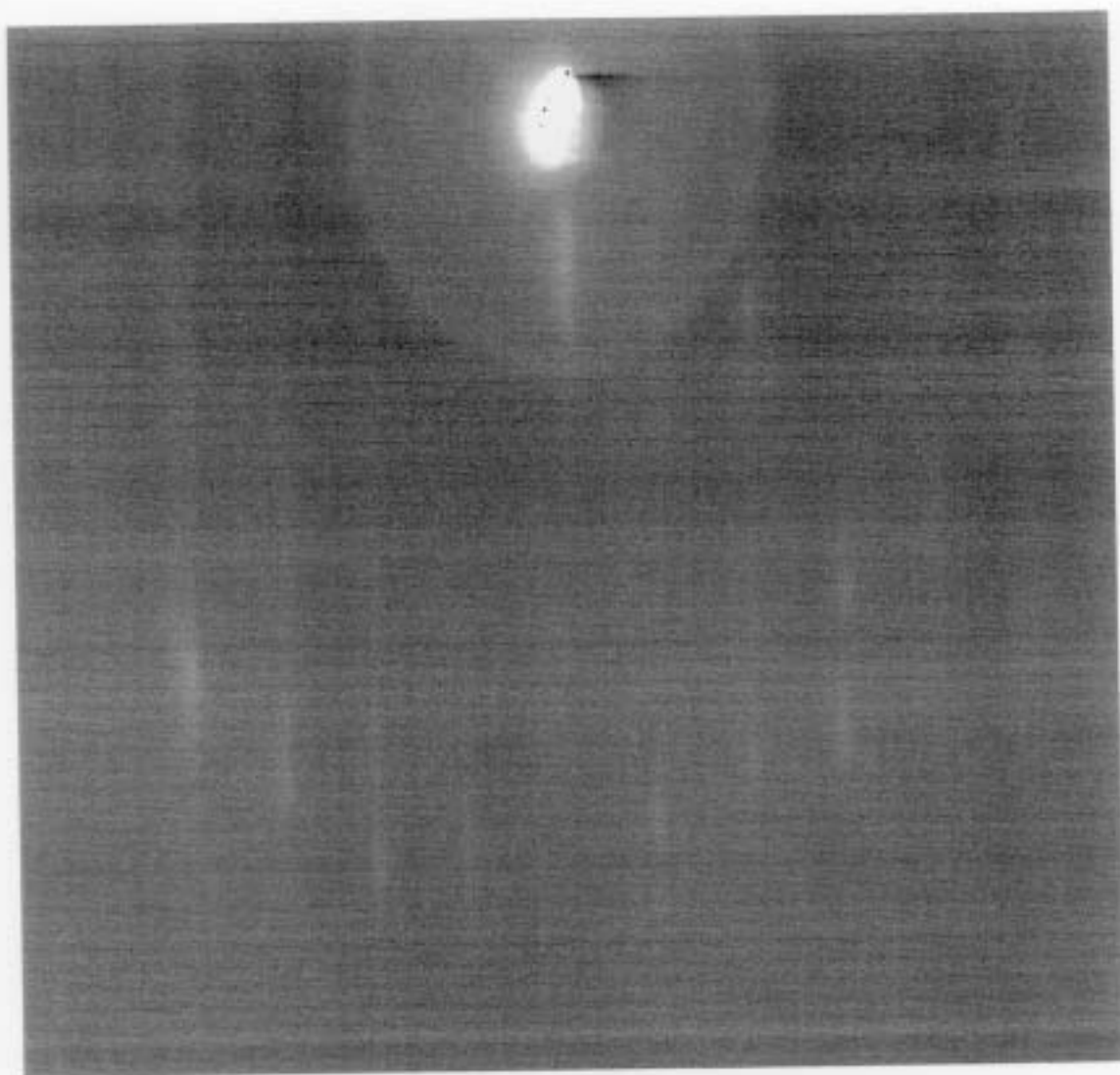
Fig. 5.4   RHEED of CdTe deposited on GaAs
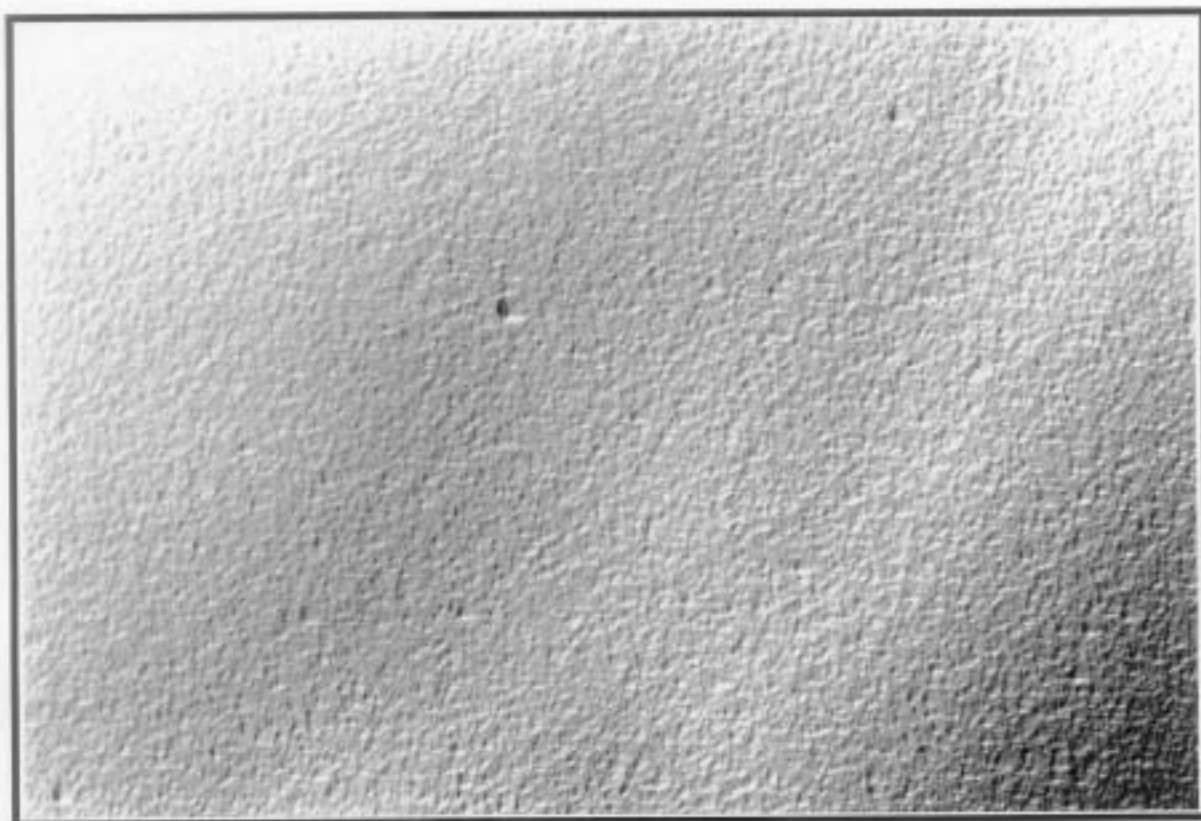
Fig. 5.5   Hillocks on a CdTe film grown on GaAs. The picture represents approximately 250×180 µm, and the approximate density of hillocks is 10^4 cm^{-2}.

5.6 Mechanisms

The mechanism for the removal of the oxide layer has been reported by Yamada *et al.*[8] There are typically three major components of the oxide layer: Ga_2O_3, Ga_2O and As oxides.[8] It is known that the latter two oxides desorb at lower temperatures ($\sim 300°C$-$400°C$) than the Ga_2O_3. Therefore, it is the Ga_2O_3 component that requires the high temperatures in the thermal cleaning. The reason this compound can be removed at lower temperatures under atomic hydrogen is that the hydrogen reacts with the Ga_2O_3 to create the more volatile compound Ga_2O through the following mechanism.[8]

$$Ga_2O_3 + 4H \rightarrow Ga_2O \uparrow + 2H_2O \uparrow$$

The Ga_2O desorption then leaves the surface devoid of oxides, as well as removing Ga to produce an As-rich surface. Note that it takes about 20 minutes to remove the oxide layer although the arrival rate of atomic hydrogen is large enough to provide sufficient atomic hydrogen in less than 4 s. The need for four hydrogen atoms to reduce the Ga_2O_3 may be the factor producing a kinetic limit, resulting in this low efficiency. Even with the low efficiency, however, this process produces a high quality surface for subsequent growth as detailed above.

6. Cleaning of Sapphire for GaN Deposition

6.1 Background

Wide band gap materials, such as GaN, are of interest for many reasons. First, and most obvious, because of their use in the blue and uv wavelength ranges. This smaller wavelength range allows for more compact storage capabilities, as well as full color displays. Secondly this compound is more robust than other semiconductors. It can operate at higher temperatures and is resistant to most chemical etches. Finally, electronic properties such as the predicted electron saturation velocity and potential for low contact resistance[63] indicate that GaN will be a more viable semiconductor for device fabrication than other wide bandgap semiconductors such as SiC or diamond.

The growth of GaN by MBE has been plagued with many problems. The most troublesome of these problems is finding a compatible substrate. Many materials have been studied as possible substrates for GaN. To date the most commonly used substrate has been sapphire, mainly because of its availability and simple preparation for growth. Conversely, one of its biggest drawbacks is its lattice mismatch with GaN of ~ 16%. However, if one instead considers a commensurate lattice where six lattice constants of GaN align with seven lattice constants of the oxygen sub-lattice of the sapphire, the mismatch is brought down to ~ 0.5%. In either case the mismatch is still a considerable barrier to overcome, and the need for the best possible substrate surface is of great importance. Atomic hydrogen cleaning improves the surface of this substrate for GaN growth by MBE.

6.2 Surface Preparation

The sapphire substrate is degreased and then etched for ten minutes in a quartz beaker containing a 3:1 solution of H_2SO_4:H_3PO_4. This acid is kept at a temperature of at least 140°C throughout the etch. The substrate is etched for ten minutes, then the quartz beaker containing the acid and substrate is transferred into a cooling bath for four minutes. After the cooling bath the substrate is rinsed in flowing DI H_2O for five minutes and finally blown dry with high purity nitrogen gas.

While completing this study some disparity was seen in the RHEED of as-etched sapphire, which led to variance in the RHEED of the hydrogen cleaned sapphire. It was determined that the differences in the sapphire RHEED from day-to-day was due to the poorly monitored acid temperature in the *ex-situ* etch. This problem became the topic of a new investigation. The first improvement came with the use of a new hot plate which could approach higher temperatures with more accuracy. The second improvement was the implementation of a teflon-coated thermocouple which could be used to measure the acid temperature directly, instead of the plate temperature which tends to be at a hotter temperature due to thermal losses in the beaker.

In order to determine the minimum acid temperature for a ten-minute etch, several pieces of sapphire were chemically-etched using the process above. Each step of the process but one was identical for each substrate. The only difference was the temperature of the acid during the etch, which was measured with the teflon-coated type-K thermocouple held in the acid, without touching the sides or bottom of the beaker. After being transferred to the system the substrates

were cleaned with atomic hydrogen and monitored with RHEED. Fig. 6.1a shows the RHEED of a sapphire substrate etched at an acid temperature of ~ 110°C. When compared with Fig. 6.1b, which is RHEED of a sapphire substrate etched at an acid temperature of ~ 140°C, it is noted that 6.1b is much brighter, appears to have less contaminants on the surface, and also has a ring of spots. These spots are associated with the first order Laue zone, therefore they are only seen on very flat two dimensional surfaces. These results showed that an acid temperature of at least 140°C for a 10-min etch time is crucial to achieving the best possible diffraction patterns.

6.3 RHEED During Hydrogen Cleaning

Initial RHEED of the etched sapphire shows a diffuse background, Fig. 6.2, once again indicative of contaminants on the surface. After a 15 minute treatment with hydrogen, the scattering disappears, and the surface exhibits a smooth two-dimensional surface with Kikuchi lines as shown in Fig. 6.3.

6.4 GaN Deposition

Subsequent GaN films have been grown on these layers. However, there are a number of unanswered questions concerning the growth process, so many that it would be out of the scope of this thesis to go into great detail on this subject. Therefore only a rather brief description of some of the problems will be outlined here. One of the first problems plaguing researchers is the importance of a nitrided substrate. The ability to produce and the need for a nitrided substrate is one of the current problems being addressed by this lab. Another issue is the requirements of the initial buffer layer. The partial pressure of gallium, and the nitrogen plasma's power and flow settings, as well as the substrate temperature and growth time are all integral to the quality of the buffer layer and GaN film. AFM images of these films typically reveal a rough surface. This
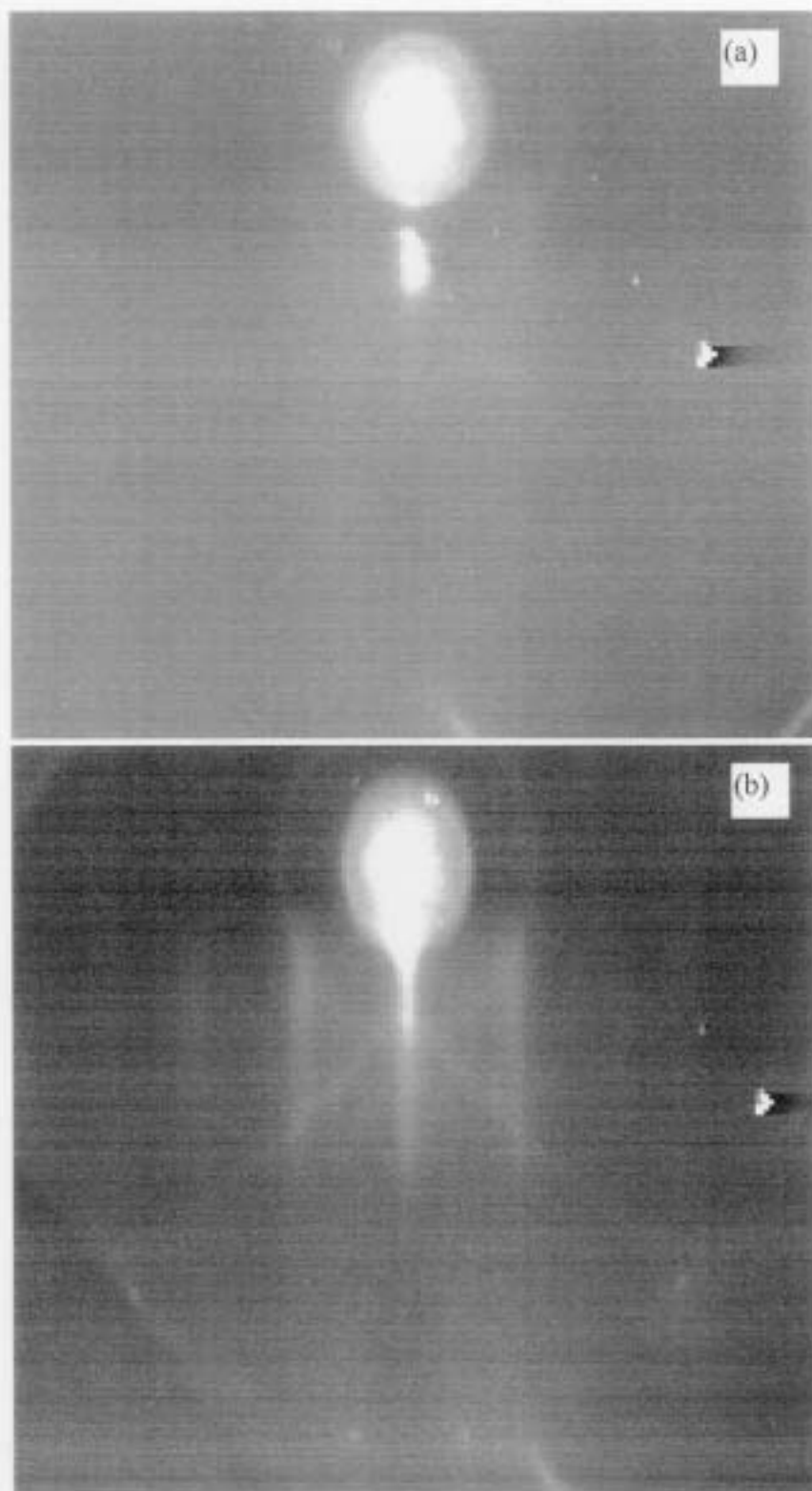
Fig. 6.1   A RHEED comparison of sapphire substrates chemically etched at two different acid temperatures (a) ~114°C and (b) ~143°C. Note the ring of spots near the edge of the pattern in (b) that is not present in (a).
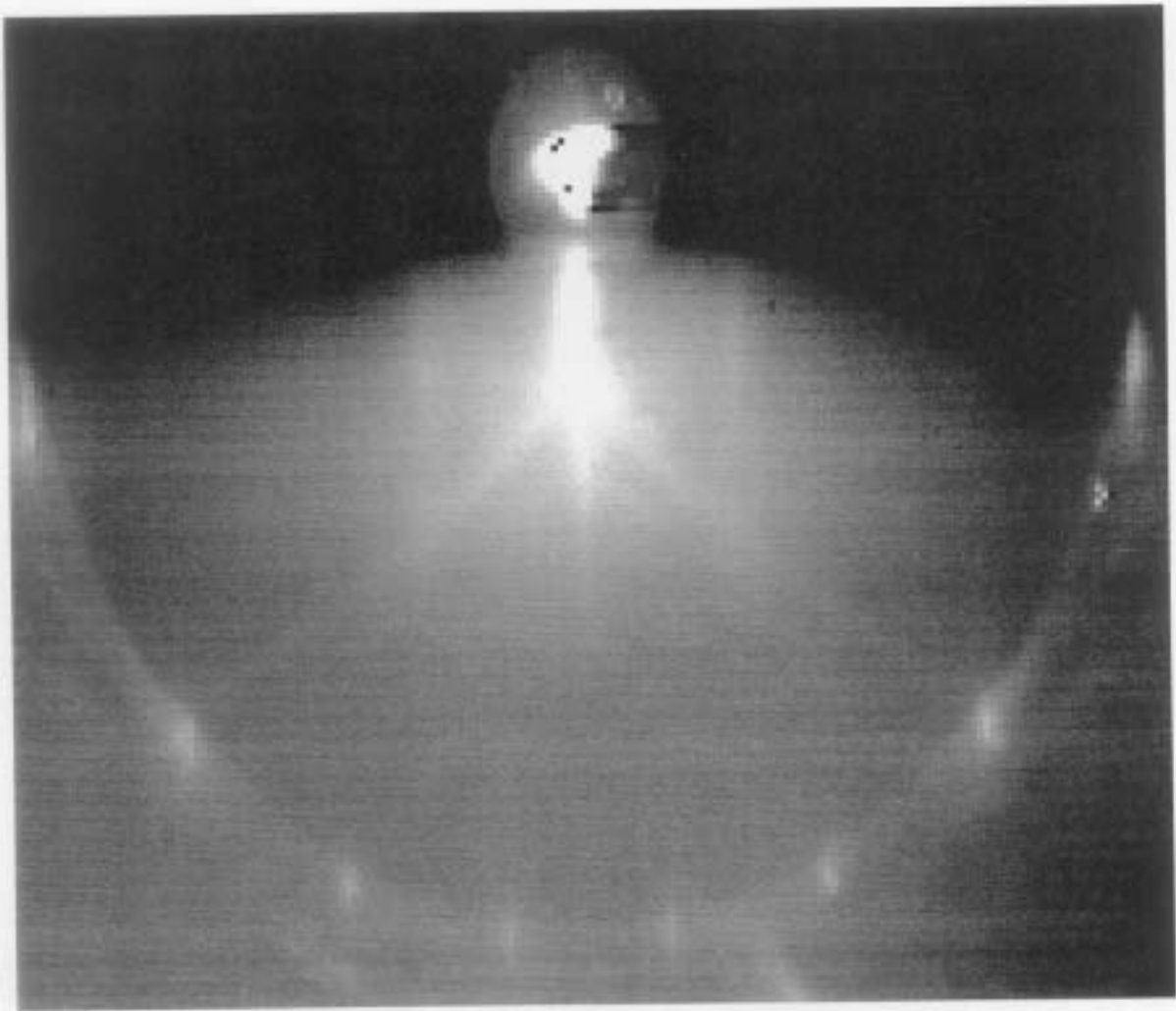
Fig. 6.2   RHEED of chemically etched sapphire.
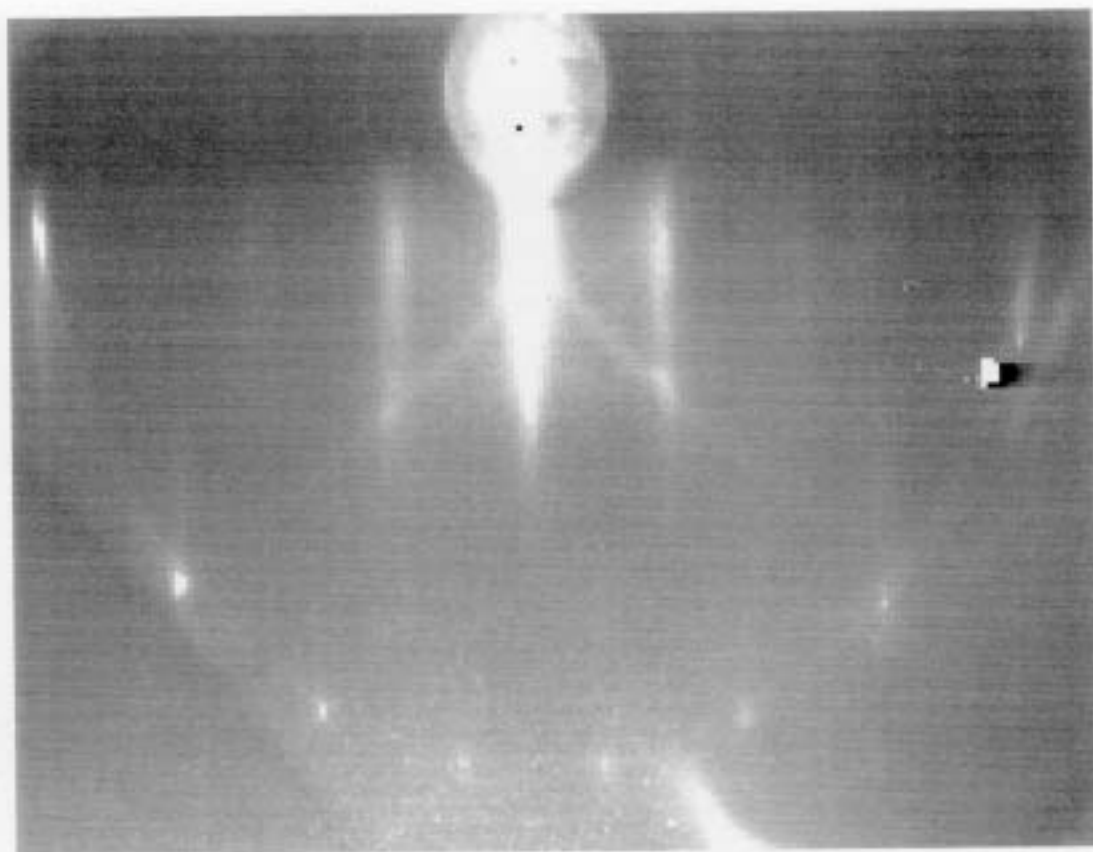
Fig. 6.3   RHEED of sapphire after hydrogen cleaning.

surface roughness tends to be related to the parameters surrounding the buffer layer and film and not the substrate preparation. TEM measurements performed by Linda Romano at Xerox, in Palo Alto, California, show the presence of inversion domains.[64] Again these defects are attributed to growth processes and techniques, and not to poor surface cleaning. Due to these overall issues with the growth process itself, nothing can be said about a direct effect of hydrogen cleaning on subsequent films. However, by understanding the removal of diffuse scattering in RHEED images, and through consideration of the importance of clean atomically-flat substrates for epilayer growth, it is presumed that this process is beneficial to substrate preparation.

7. Cleaning of Si for ZnTe/CdTe Deposition

7.1 Background

HgCdTe, as stated previously, is popular for its performance in the infrared wavelengths. One device currently using HgCdTe is a hybrid IR focal plane array. Presently the HgCdTe/CdZnTe film is grown, then attached to a Si chip containing the integrated circuit. When the device is employed, the thermal mismatch between the Si and the bulk CdZnTe can cause the device to fail.[65] If a CdZnTe or CdTe thin film could be deposited on Si, then used as a substrate for HgCdTe, the thermal mismatch problem could be minimized.

Since the first study of the growth of CdTe on Si by MBE,[66] high temperature (>800°C) thermal desorption has been the primary technique for oxide removal.[67] Recently, techniques have been developed[68] for *ex-situ* oxide removal from Si using etchants based on HF. These procedures result in a hydrogen-terminated surface which is remarkably resistant to further oxidation, at least on (211) surfaces. The hydrogen can be desorbed in the MBE system at temperatures of about 550 to 600°C[65], leaving a clean, ordered Si surface for subsequent epilayer growth. This technique has been successfully used for the growth of ZnTe and CdTe on Si.[65,69] An alternate, low-temperature approach would be to use atomic hydrogen to remove the oxide, as has been demonstrated for GaAs/Si heteroepitaxy.[10]

7.2 Surface Preparation

Based on prior work by Dhar *et al.*[65] and Lyon *et al.*,[69] we decided to focus growth efforts on (211)-oriented Si substrates. The results of this study were reported at the 1996 Materials Research Society Meeting in Boston, Massachusetts.[29] After an extensive review of the literature, it was decided that the Si would be cleaned following the procedure outlined by Fenner

et al.[68] This etch involves many steps. To shorten the description, from this point it is to be assumed that the substrate is blown dry with nitrogen gas after every DI H_2O rinse. After the degrease, the substrate undergoes a five-minute DI H_2O rinse before being submersed for ten minutes in a 5:1:1 DI H_2O:NH_4OH:H_2O_2 solution kept at 80°C. This is followed by a five-minute DI H_2O rinse, then a fifteen-second dip in a 50:1 DI H_2O:HF solution, and then a twenty-second DI H_2O rinse. Next the substrate is immersed in a 6:1:1 DI H_2O:HCl:H_2O_2 solution for ten minutes. This step is followed by a twenty-minute DI H_2O rinse. The final step is a 2.5-minute dip in 1:1:10 HF:DI H_2O:absolute reagent alcohol. In the first part of this study the substrate was rinsed with DI H_2O after this last dip, but towards the end of the study it was discovered by looking at RHEED patterns that better surfaces could be attained if the samples were blown dry after a short reagent alcohol rinse. For example, Fig. 7.1a is a RHEED pattern of a substrate which had undergone a final water rinse. When it is compared to a substrate which had instead been rinsed with reagent alcohol, as in Fig. 7.1c you will notice it is a much stronger pattern. Fig. 7.1b and d represent the same Si surfaces after being heated and exposed to an As flux. Again Fig. 7.1d is stronger than Fig. 7.1b.

7.3 RHEED During Hydrogen Cleaning

The as-prepared Si substrates gave a RHEED pattern exhibiting both diffuse scattering and rings. These features disappeared upon heating the substrate above 200°C, leaving only the sharp, streaky RHEED pattern shown in Fig. 7.2. Note the presence of the strong Kikuchi lines. The disappearance of the rings may correspond to a desorption of residual carbon from the etch, as reported in a prior study.[70] For comparison with the Fenner etch procedure, the use of atomic hydrogen for cleaning the Si surface was also investigated. In particular, it was found that about

94
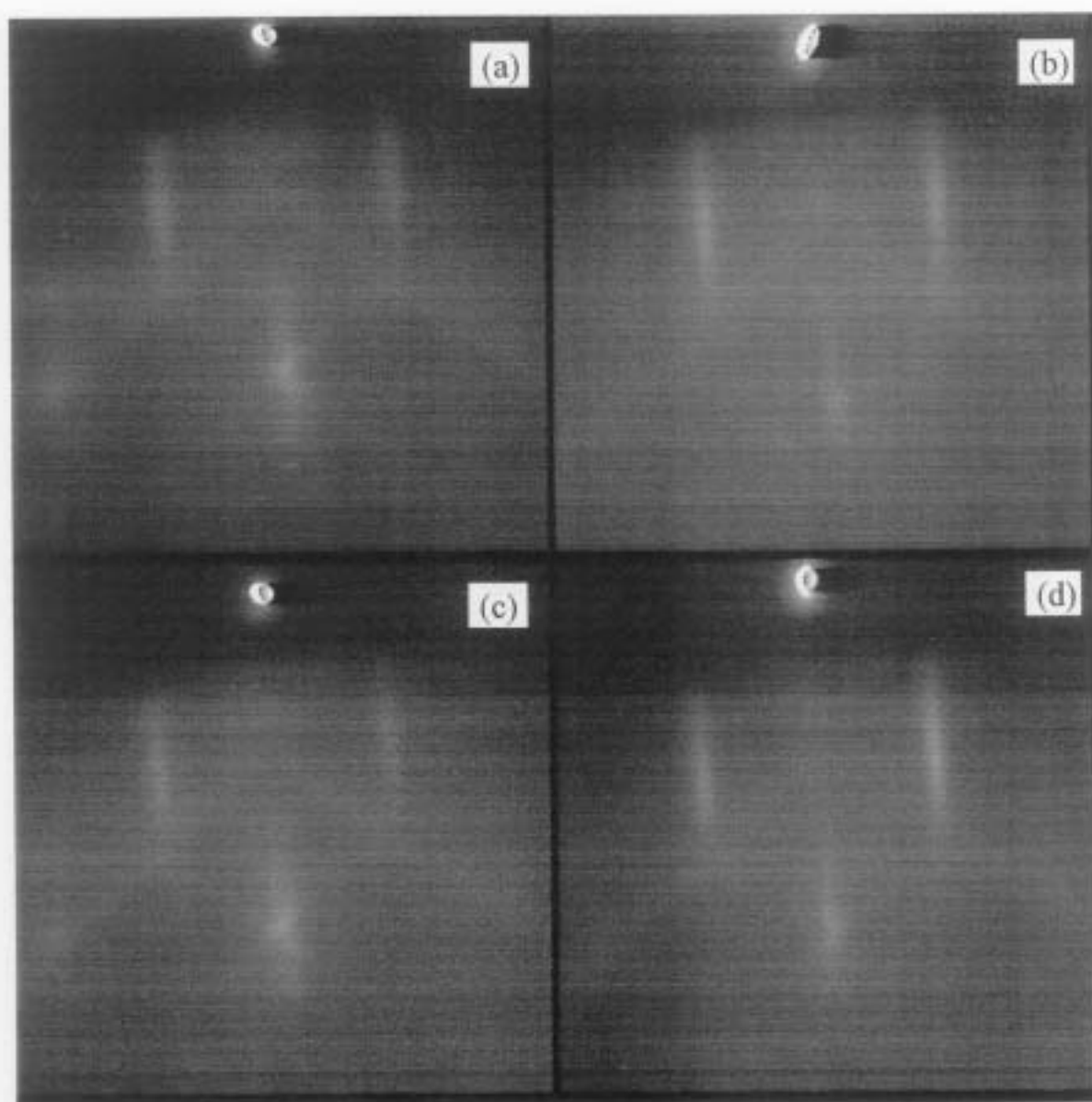
Fig. 7.1   RHEED comparison of Si substrates (after heating to 200°C) that underwent two different *ex-situ* etches. In (a) and (b) the substrate was rinsed in DI H$_2$O after the Fenner etch, and in (c) and (d) the substrate was rinsed for a short time with reagent alcohol. Images (a) and (c) are as etched, and (b) and (d) are after being heated under As and cooled to growth temperature. Note that the pattern in (d) is much stronger than in (b).
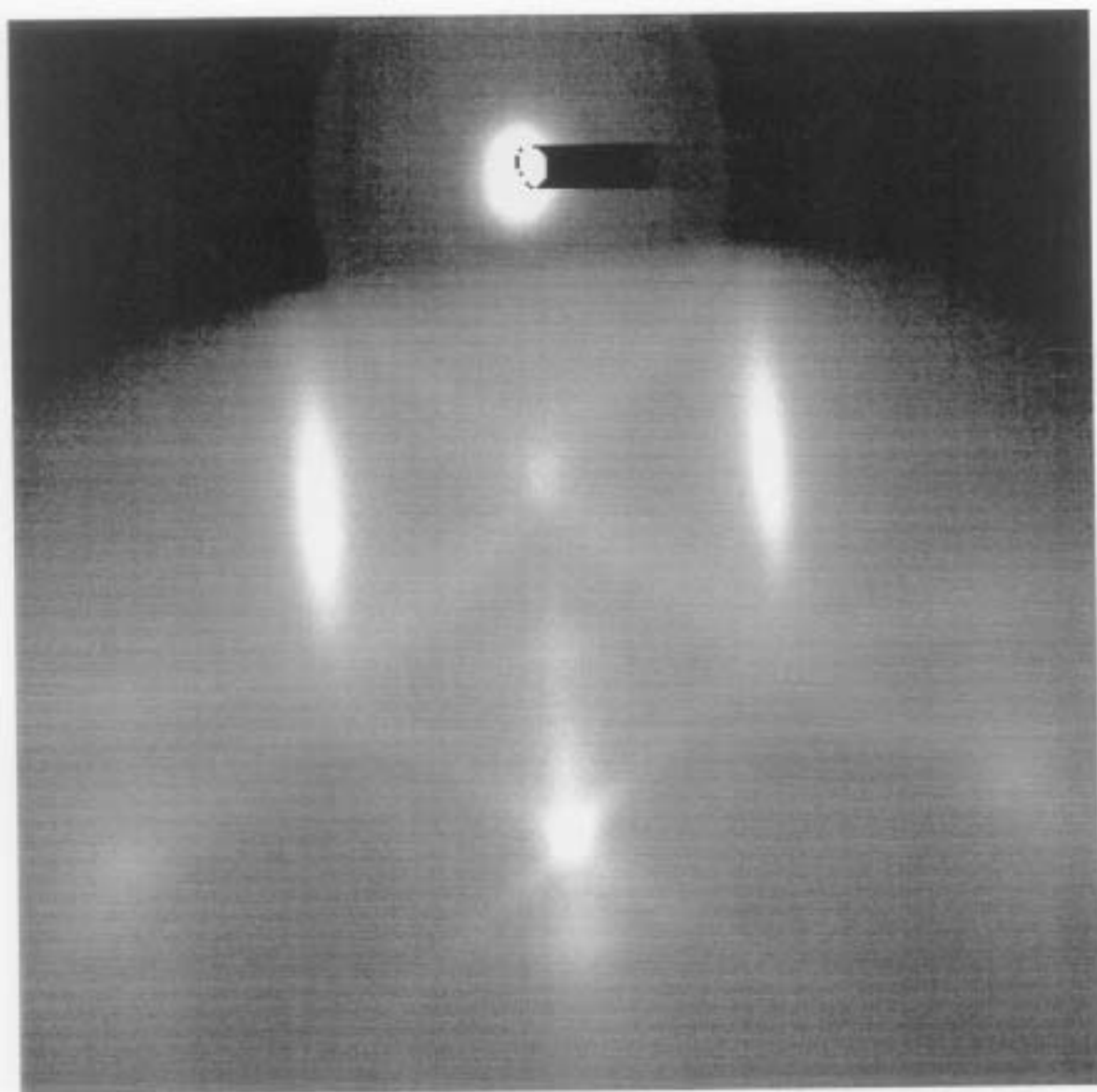
Fig. 7.2   RHEED of Si after the Fenner etch.

a twenty minute exposure of atomic hydrogen at 600°C removed the oxide layer from a Si substrate etched in a HF:H$_2$O solution. A Si substrate cleaned using the Fenner etch was also exposed to atomic hydrogen for an equivalent amount of time. Both hydrogen cleaning procedures resulted in a RHEED pattern equivalent to that obtained by the Fenner etch alone, as shown in Fig. 7.3 with the possible exception of a slight increase in diffuse scattering. In addition samples were heated to temperatures as high as 700°C, well above the desorption temperature for hydrogen on Si,[71] without any observation of change from the bulk-like (1x1) RHEED patterns shown in Figs. 7.2 and 7.3. The lack of change in the RHEED pattern indicates an absence of surface reconstruction.

7.4 ZnTe/CdTe Deposition

All attempts to deposit a film directly on a Si surface prepared by either of the three techniques described resulted in polycrystalline ZnTe and CdTe, as shown by the rings in Fig. 7.4 and Fig. 7.5. It is well known that bare silicon surfaces are highly reactive with the Column VI elements O, S, Se and Te, which all react with similar chemistries. For example, it was demonstrated that one of the difficulties occurring with the growth of ZnSe on Si[72] was the formation of an amorphous SiSe$_2$ layer at the interface, analogous to SiO$_2$. Therefore, it is believed the polycrystalline growth observed in these ZnTe/Si experiments was due to the formation of an amorphous SiTe$_2$ layer upon exposure to flux containing Te, analogous to the results observed with Se. Following the lead of Romano *et al.* and Dhar *et al.*, As was used to passivate the surface of the Si. The substrate was exposed to an As flux while heated to about 550°C. With the As passivation, single crystal growth was obtained on substrates cleaned by the Fenner process as shown by the well-ordered RHEED pattern in Fig. 7.6. However, growth on
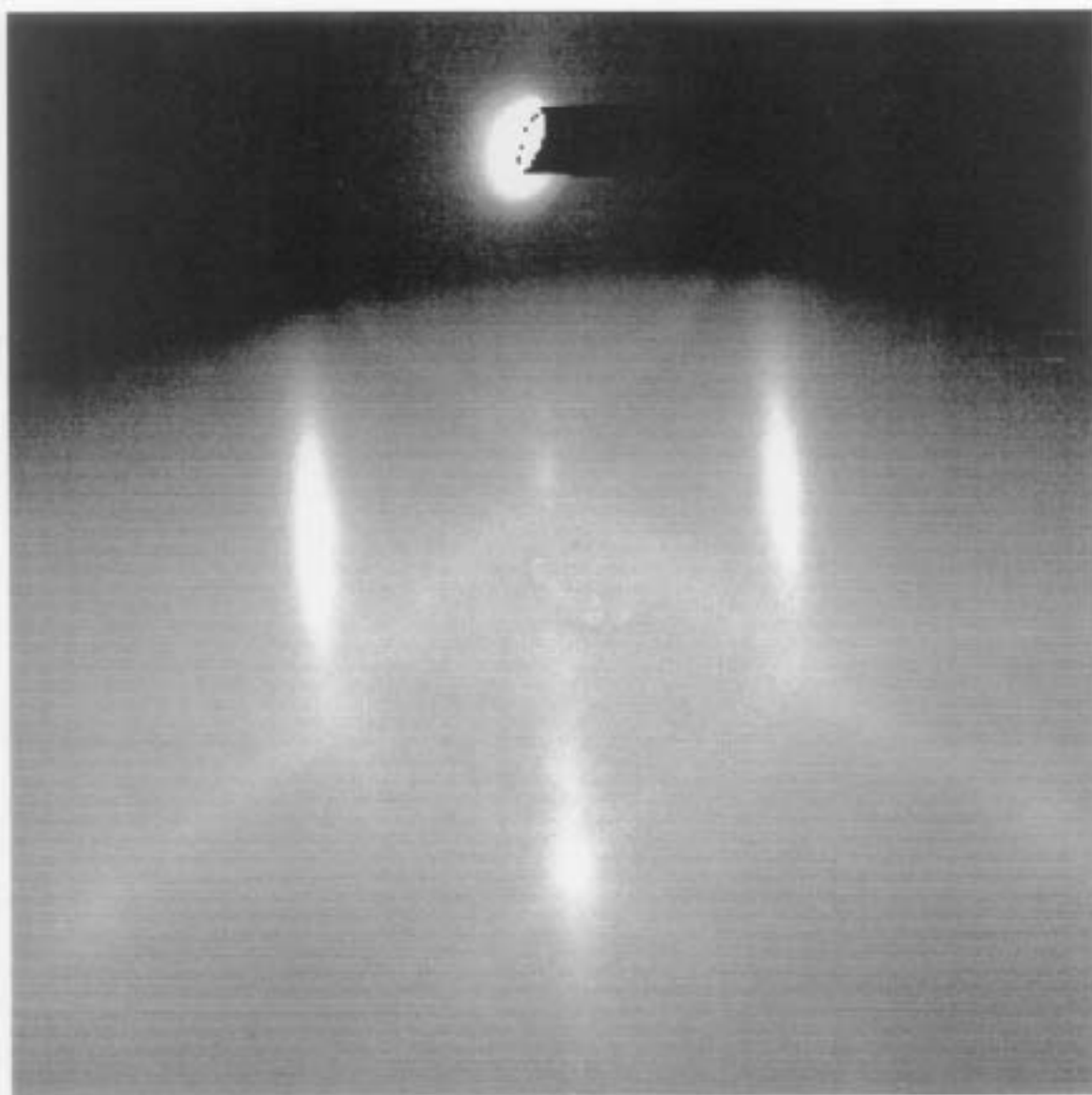
Fig. 7.3　　　RHEED of Si after hydrogen cleaning.
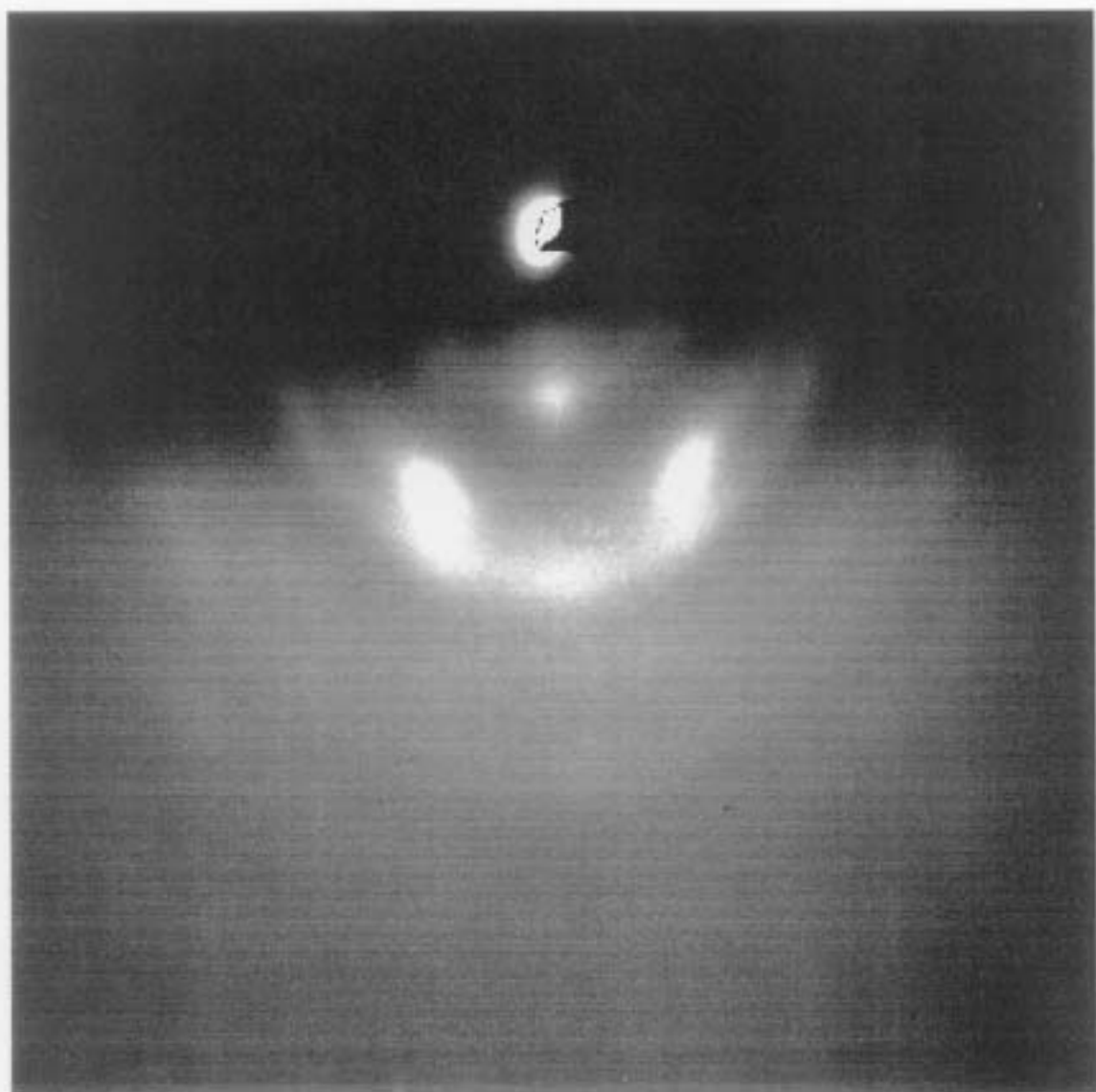
Fig. 7.4   RHEED of ZnTe deposited on Si after the Fenner etch.
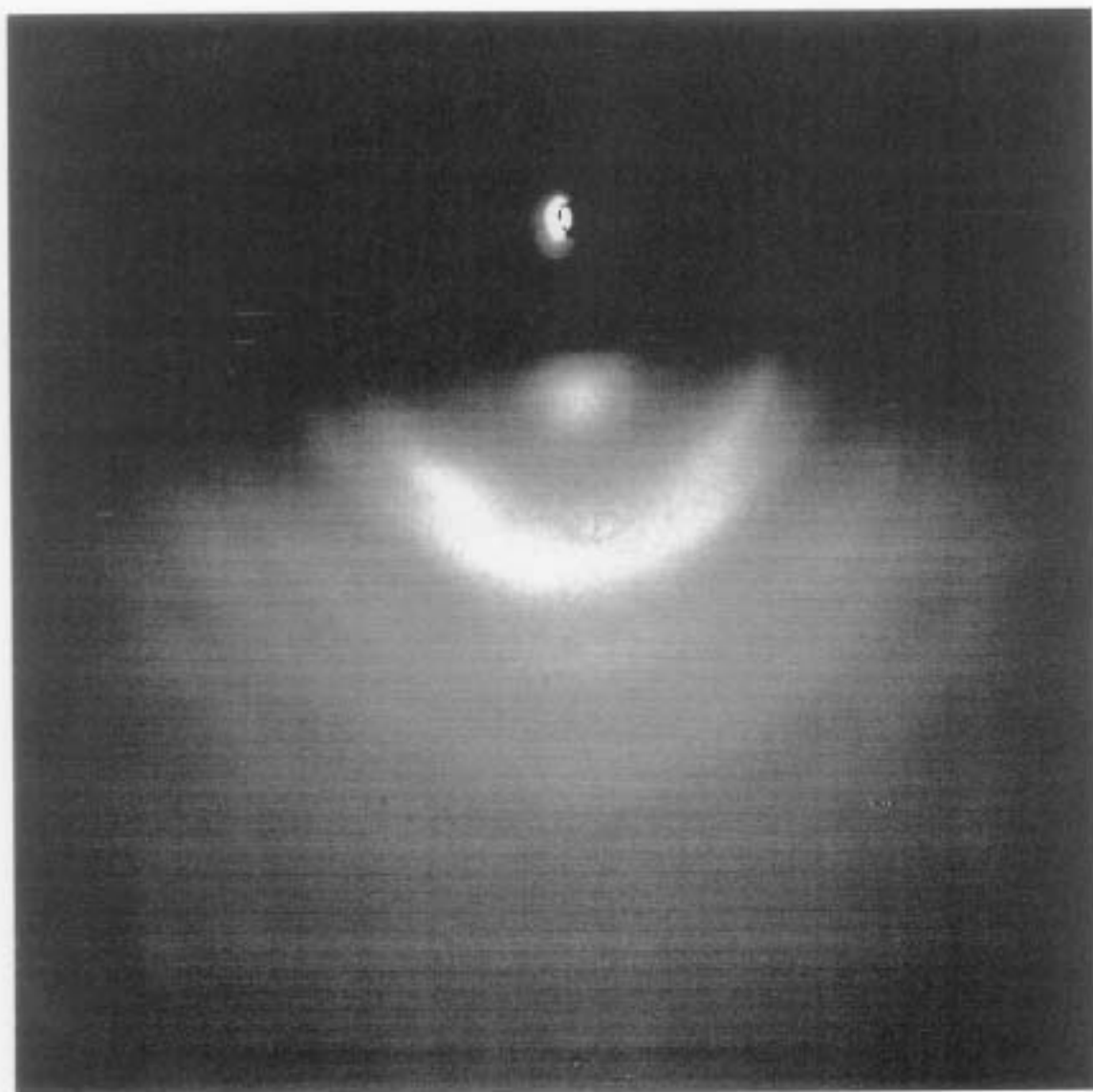
Fig. 7.5   RHEED of ZnTe deposited on Si after hydrogen cleaning.
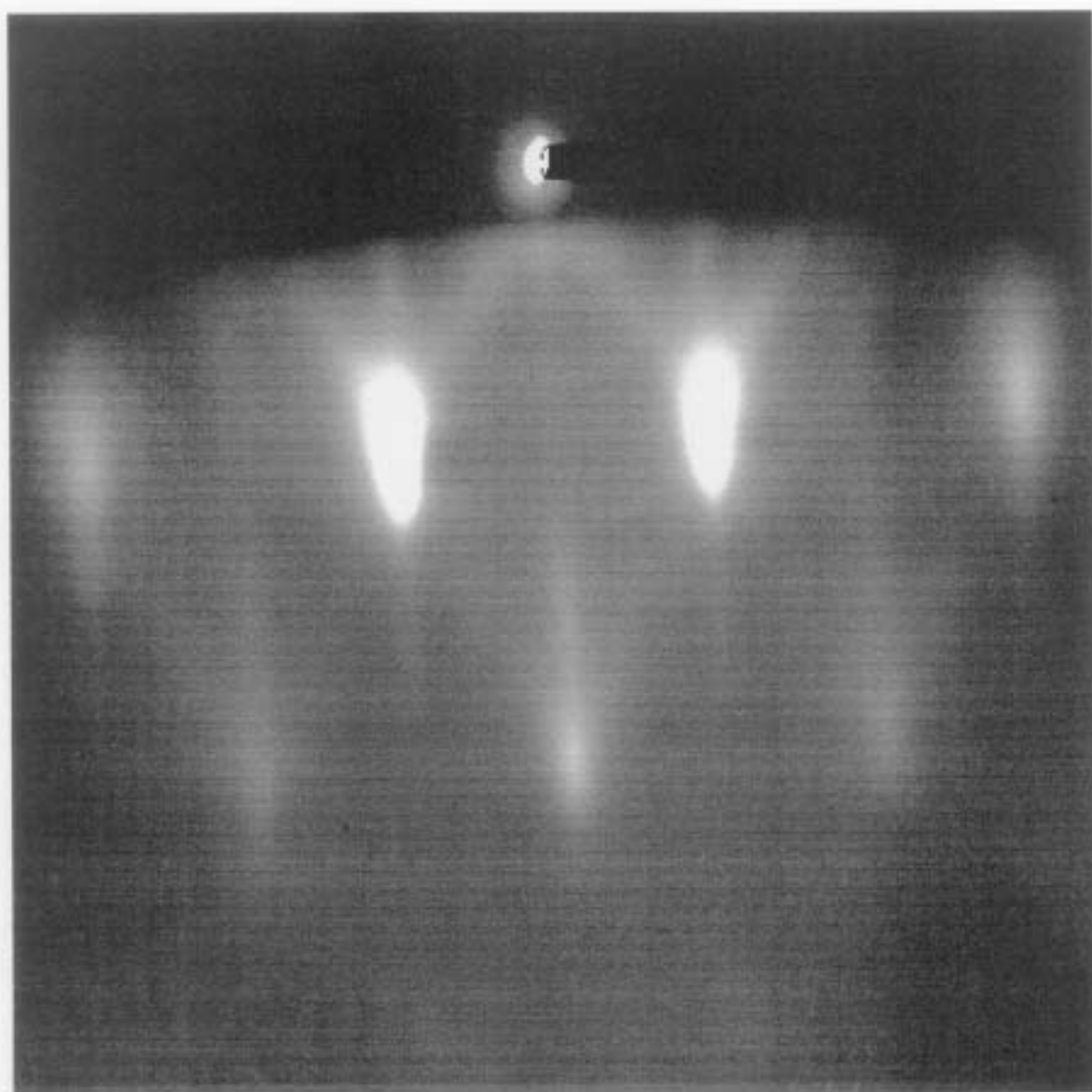
Fig. 7.6   RHEED of ZnTe deposited on Si after the Fenner etch and treated with As.

101

substrates exposed to atomic hydrogen continued to result in polycrystalline material. Further investigation indicated that the problem always occurred if the substrate was exposed to atomic hydrogen prior to As passivation. After As passivation, atomic hydrogen exposure did not present any ill effects.

7.5 Mechanisms

The inability to grow single crystal ZnTe on Si exposed to atomic hydrogen prior to As-passivation may not be directly related to exposure to atomic hydrogen. As discussed earlier, atomic hydrogen can etch Te (and presumably CdTe and ZnTe) at low temperatures with TeH_2 as an etch product. There is a significant coating of Te-bearing compounds in the growth chamber which would be exposed to atomic hydrogen, resulting in a potential background of TeH_2. Any TeH_2 striking the heated Si surface would decompose, allowing Te to react with the surface. Exposure of a Si substrate cleaned with the Fenner process directly to Te did not lead to observable changes in the RHEED pattern. In addition there are no analytical capabilities on our growth chamber to investigate such surface contamination. Thus this speculation could not be directly confirmed. Thus, our study may indicate that atomic hydrogen cannot be used for oxide removal from Si substrates inside a II-VI MBE chamber. However, cleaning in an external preparation chamber may still be feasible. This topic is under continued investigation in our laboratory.

8. Conclusions

Thermally-produced atomic hydrogen is shown to be effective in preparing substrate surfaces for subsequent growth. Each substrate is unique and therefore reacts differently with the hydrogen. The results of this study are delineated here.

(1)   CdTe treated with atomic hydrogen exhibits an atomically-flat surface indicated by both RHEED images and AFM measurements. This *in-situ* treatment can be performed at lower temperatures than were previously needed for thermal cleaning, and leaves the substrate surface free from oxides and other contaminants that may remain behind after *ex-situ* cleaning. In addition the CdTe remains stoichiometric, and subsequent CdTe films deposited on this surface retain a two-dimensional flat surface.

(2) Hydrogen cleaning is an effective method for cleaning HgCdTe.   Again the temperatures required are lower than conventional methods. This is of particular importance since high temperatures are known to degrade HgCdTe. After cleaning, the HgCdTe surface exhibits an rms. roughness of less than 0.5 nm. Furthermore, the CdTe used to passivate the surface exhibited a streaky RHEED pattern indicative of a two-dimensional surface. An XPS study showed both the removal of oxides and a shift of stoichiometry.   This shift in stoichiometry may not limit the fabrication of devices after atomic hydrogen cleaning since it is towards higher x-values. Importantly, reflectance measurements indicated the shift is a surface effect. Most importantly hydrogen cleaned samples were later processed into working devices, showing that hydrogen cleaning does not limit fabrication.

(3)   Treatment of GaAs for the growth of II-VI compounds can be difficult and tedious. With the use of atomic hydrogen, the oxides and other surface contaminants are removed at reduced temperatures, and the defect density in the resulting film is greatly reduced.

103

Additionally, hydrogen cleaning of GaAs followed by a Zn-pretreatment further reduces the number of these defects. A second advantage of hydrogen cleaning of GaAs substrates is that this approach may eliminate the need for the growth of a GaAs epilayer, resulting in a less complicated growth process for subsequent manufacture of layers for light-emitter fabrication.

(4)   Removal of the diffuse background in RHEED images of sapphire is possible with atomic hydrogen. RHEED images taken before and after hydrogen cleaning show that the treatment removes this diffuse scattering which indicates the removal of surface contaminants, and brings out a very bright two dimensional RHEED pattern exhibiting streaks and Kikuchi lines.

(5)   The results for the hydrogen cleaning of silicon are inconclusive. While the oxide can be removed, the hydrogen may also be reacting with the walls of the chamber, which could result in the premature deposition of Te on the surface of the silicon. Future studies are planned to investigate the cleaning of silicon with atomic hydrogen in an environment that has not been exposed to elemental tellurium.

To summarize, there are advantages in using atomic hydrogen for cleaning over other types of substrate preparation. The first is the lower substrate temperature needed to perform the cleaning. One advantage of the lower temperature, is that it can result in less cross-contamination from heated surfaces. For GaAs surfaces, the atomic hydrogen cleaning can be accomplished at a temperature less than 400°C, while thermal cleaning must be carried out around 600°C. A similar change is also seen for CdTe. Thermal treatments typically require temperatures near 300°C, but with atomic hydrogen cleaned surfaces can be obtained as low as 80°C. Perhaps the substrate most affected by this lower temperature is HgCdTe. With thermal treatments the Hg

could easily be desorbed seriously degrading of the HgCdTe, and hence adversely affecting the performance of the subsequent device. Hydrogen cleaning, however, only effects the stoichiometry of the first monolayer of material, which will not affect the bandgap and subsequent detection wavelength of the device, since that will be determined by the bulk material.

Atomic hydrogen can also make a substrate more suitable for subsequent growth. It has been shown to be effective at removing carbon and other surface impurities as well as oxides, resulting in a cleaner surface.[7,13] For GaAs substrates the atomic hydrogen cleaning results in an appropriate As-stabilized GaAs surface for subsequent ZnSe or CdTe growth, eliminating the need for an As-flux. In HgCdTe and CdTe, Te overlayers have been shown to be removed. Additionally, the mercury depletion in the first monolayer may help to more closely lattice match the CdTe passivation layer. And in sapphire diffuse background scattering on the RHEED is removed.

It is clear that atomic hydrogen solves some of the fabrication problems that have plagued industry in the past. These surfaces can now be cleaned effectively and efficiently. The processing steps can be performed at more desirable temperatures, and in some cases, like GaAs, the processing can be done even with one system rather than two. As these new techniques are integrated into use in more and more facilities many more problems may be solved, and even better techniques may be developed.

References

1.   Nichia Surpasses 10,000 Hours, Compound Semiconductors **3**, No. 6, p4 Nov/Dec 1996.

2.   G. F. Neumark, R. M. Park, and J. M. DePuydt, Physics Today **47**, 26 (June 1994).

3.   S. Guha, J. M. DePuydt, M. A. Haase, J. Qiu, and H. Cheng, Appl. Phys. Lett. **63**, 3107 (1993).

4.   G. C. Hua, N. Otsuka, D. C. Grillo, Y. Fan, J. Han, M. D. Ringle, R. L. Gunshor, M. Hovinen, and A. V. Nurmikko, Appl. Phys. Lett. **65**, 1331 (1994).

5.   L. H. Kuo, L. Salamanca-Riba, B. J. Wu, G. Hofler, J. M. DePuydt, and H. Cheng, Appl. Phys. Lett. **67**, 3298 (1995).

6.   E. J. Petit and F. Houzay, J. Vac. Sci. Technol. B **12**, 547 (1994).

7.   T. Sugaya and M. Kawabe, Jpn. J. Appl. Phys. **30**, L402 (1991).

8.   M. Yamada, Y. Ide, and K. Tone, Jpn. J. Appl. Phys. **31**, L1157 (1992).

9.   Y. Okada, T. Fujita, and M. Kawabe, Appl. Phys. Lett. **67**, 676 (1995).

10.   H. Shimomura, Y. Okada, and M. Kawabe, Jpn. J. Appl. Phys. **31**, L628 (1992).

11.   H. Shimomura, Y. Okada, H. Matsumoto, M. Kawabe, Y. Kitami, and Y. Bando, Jpn. J. Appl. Phys. **32**, 632 (1993).

12.   Y. J. Chun, Y. Okada, and M. Kawabe, Jpn. J. Appl. Phys. **32**, L1085 (1993).

13.   C. M. Rouleau and R. M. Park, J. Appl. Phys. **73**, 4610 (1993).

14.   N. Kondo, Y Nanishi, Jap. J Appl. Phys. **28**, L7 (1989).

15.   Y. Luo, D. A. Slater, and R. M. Osgood, Jr., Appl. Phys. Lett. **67**, 55 (1995).

16.   Zhonghai Yu, S.L.Buczkowski, M. C. Petcu, N. C. Giles, and T. H. Myers, Appl. Phys. Lett. **68**, 529 (1996)

17.   Zhonghai Yu, S.L.Buczkowski, N. C. Giles, and T. H. Myers, Appl. Phys. Lett. **69**, 82 (1996)

18.   Zhonghai Yu, S.L.Buczkowski, L.S. Hirsch, and T. H. Myers, J. Appl. Phys. **80**, 6425 (1996)

19.   KSA 400 User Manual, k-Space Associates, Inc. (Ann Arbor, MI), 1997

20.   Atomic Hydrogen Source: Users Guide, EPI (Minneapolis, MN), February 1995.

21.   Fisons Instruments Operating Instructions, Fisons Instruments (United Kingdom), 1995.

22.   Rich Bresnahan, EPI engineer private communication.

23.   G.L. Weissler and R.W. Carlson, editors, Methods in Experimental Physics, New York:Academic Press, 1979.

24.   EPI Application Note, August/September, 1994.

25.   EPI Application Note, January, 1996.

26.   Cryo-Torr 100, 7, 8, and 8F High-Vacuum Pumps Manual, Helix Technology Corporation (Mansfield, MA), 1995.

27.   C. D. Stinespring, J. M. Lannon Jr., J. S. Gold, M. Guntu, and S. Kumar in Surface Modification Technologies IX, eds. T.S. Sudarshan, W. Reitz, and J. Stiglich, The Minerals, Metals, and Materials Society (Warrendale, PA) 565 (1996).

28.   Osaka Turbo Pump Manual, Osaka Vacuum Ltd. (Japan).

29.   L.S. Hirsch, Zhonghai Yu, M.R. Richards-Babb, and T.H. Myers, Mat. Res. Soc. Symp. Proc. **450**, 263 (1997).

30.   J. M. DePuydt, H. Cheng, J. E. Potts, T. L. Smith, and S. K. Mohapatra, J. Appl. Phys. **62**, 4756 (1987).

31. M. Ohishi, H. Saito, H. Torihara, Y. Fujisaki, and K. Ohmori, J. Cryst. Growth **111**, 792 (1991).

32. L.S. Hirsch, Zhonghai Yu, S.L. Buczkowski, T. H. Myers, and M.R. Richards-Babb, J. Electron. Mat. **26**, 534 (1996).

33. L.S. Hirsch, K.S. Ziemer, M.R. Richards-Babb, C.E. Stinespring, and T.H. Myers, to be published in J. Electron. Mat. (1997).

34. J. F. Moulder, W. F. Stickle, P.E. Sobol, K. D. Bomben, Handbook of X-ray Photoelectron Spectroscopy, Physical Electronics, Inc. (Eden Prairie, MN), 25, (1995).

35. H. M. Nitz, O. Ganschow, U. Kaiser, L. Wiedmann, and A. Benninghoven, Surface Sci. **104**, 365 (1981)

36. A.B. Christie, I Sutherland, and J.M. Walls, Surface Sci., **135**, 225 (1983).

37. W. E. Swartz, K. J. Wynne, and D. M. Hercules, Anal. Chem. **43**, 1884 (1971).

38. T. S. Sun, S.P Buchner, and N.E. Byer, J. Vac. Sci. Technol. **17**, 1067 (1980).

39. S. W. Garentroom and N. Winograd, J. Chem. Phys. **67**, 3500 (1977).

40. S. Svensson, N. Martensson, E. Basilier, P. A. Malmquvist, J. Electron. Spectrosc. Relat. Phenom. 9, 51 (1976).

41. D. Briggs and M.P. Seah, Practical Surface Analysis, Volume 1, John Wiley and Sons (Chichester, England), 207 (1990).

42. R. C. Keller, M.Seelmann-Eggbert and H. J. Richter, Appl. Phys. Lett **67**, 3750 (1995); R. C. Keller, M.Seelmann-Eggbert and H. J. Richter, J. Electron. Mat. **24**, 1155 (1995)

43. G. D. Davis, N.E Byer, R.A. Riedel, R.R. Daniels G. Margaritondo, J. Vac. Sci. Technol A3, 203 (1985)

44.   T. H. Myers, A. N. Klymachyov, C. M. Vitus, N. S. Dalal, D. E. Endres, K. A. Harris, R. W. Yanka, and L. M. Mohnkern, Appl. Phys. Lett. **66**, 224 (1995)

45.   P. M. Raccah, J. Vac. Sci. Technol. A1, 1587 (1983)

46.   J. G. Werthen, J. P. Haring, and R. H. Bube, J. Appl. Phys. **54**, 1159 (1983)

47.   U. Slosbach and H. J. Richter, Surf. Sci. **97**, 191 (1980)

48.   M. K. Bahl, R. L. Watson, and K. J. Irgolic, J. Chem. Phys. **66**, 5526 (1977)

49.   D. Li, M. Gonsalves, N. Otsuka, J. Qiu, M. Kobayashi, and R.L. Gunshor, Appl. Phys. Lett. **57**, 449 (1990).

50.   M. C. Tamargo, R. E. Nahory, B. J. Skromme, S. M. Shibli, A. L. Weaver, R. J. Martin, and H. H. Farrell, J. Cryst. Growth **111**, 741 (1991).

51.   R. Ruppert, D. Hommel, T. Behr, H. Heinke, A. Waag, and G. Landwehr, J. Cryst. Growth **138**, 48 (1994).

52.   K. Shahzad, J. Petruzzello, D.J. Olego, D.A. Cammack and J.M. Gaines, Appl Phys. Lett. 57, 2452 (1990)

53.   R. J. Koestner and H. F. Shake, J. Vac. Sci. Technol. **A6**, 2834 (1988)

54.   W. Wang, H. Ehsani, and I. Bhat, J. Electron. Mat. **22**, 873 (1993)

55.   D. W. Snyder, S. Mahajan, E. J. Ko and P.J. Sides, Appl. Phys. Lett. **58**, 848 (1991)

56.   W. J. Hamilton, J. A. Vigil, W. H. Konkel, V. B. Harper, and S. M. Johnson, J. Electron. Mat. **22**, 879 (1993)

57.   G. M. Williams, A.G. Cullis, K. Prior, J. Simpson, B.C. Cavenett and S.J.A. Adams, Int. Phys. Conf. Series **134**, 671 (1993).

58.   H.T. Lin, D.H. Rich and D.B. Wittry, J. Appl. Phys. **75**, 8080 (1994).

59. M.Moldovan, L. S. Hirsch, A. J. Ptak, C. D. Stinespring, T. H. Myers, and N. C. Giles, to be published in J. Ele. Mat.

60. K. Shahzad, D. J. Olego and D. A. Cammack, Phys. Rev. **B39**, 13016 (1989).

61. M. Yoneta, M. Oshishi, H. Kobashi, and H. Saito, J. Cryst. Growth **159**, 148 (1996).

62. J.M. Arias, M. Zandian, J.G. Pasko, R.E. Dewames and E.R. Gertner, J. Appl. Phys. 65, 1747 (1989).

63. H. Morkoc, S. Strite, G.B. Gao, M.E. Lin, B. Sverdlov, and M. Burns, J. Appl. Phys. **76**, 1363 (1992)

64. L.T. Romanno and T.H. Myers, Appl. Phys. Lett. 71, 3486 (1997)

65. N.K. Dhar, C.E.C. Wood, A. Gray, H.Y. Wei, L. Salamanca-Riba and J.H. Diana, J. Vac. Sci. Technol. B **14**, 2366 (1996).

66. Y. Lo, R.N. Bicknell, T.H. Myers, J.F. Schetzina, and H.H. Stadelmeier, J. Appl. Phys. **54**, 4238 (1983).

67. R. Sporken, S. Sivananthan, K.K. Mahavadi, G. Monfroy, M. Boukerche and J.P. Faurie, Appl. Phys. Lett. **55**, 1879 (1989).

68. D.B. Fenner, D.K. Biegelsen and R.D. Brigans, J. Appl. Phys. **66**, 419 (1989).

69. T.J. de Lyon, J.A. Roth, O.K. Wu, S.M. Johnson and C.A. Cockrum, Appl. Phys. Lett. **63**, 818 (1993)

70. P.J. Granthaner, F.J. Granthaner, R.W. Fathauer, T.L. Lin, M.H. Hecht, L.D. Bell, W.J. Kaiser, F.D. Schowengendt and J.H. Mazur, Thin Solid Films **183**, 197 (1989).

71. See, for example, B.S. Meyerson, F.J. Hipsel, and K. J. Uram, Appl. Phys. Lett. **57**, 1034 (1990).

72.   L.T. Romano, R.D. Brigans, X. Zhou and W.P. Kirk, Phys. Rev. B. **52**, 11,201 (1995)

73.   R.C. Weast, Editor, <u>CRC Handbook of Chemistry and Physics</u>, CRC Press Inc. (Boca Raton, FL), B68-161, 1985.

Appendix A: *Ex-situ* Preparation

This section is designed to give a quick reference on *ex-situ* cleaning of each substrate discussed in the thesis. In the flow charts provided, rectangles are for submersions of a substrate in a beaker of solution, diamonds are for rinsing the substrates in a flowing liquid, and ovals are for use of high purity nitrogen gas. Some acids require the beaker and substrate to be placed in a bath of cool water. These cooling baths are labled in a rectangle containing the rectangle with the acid information. All temperatures given are for the hot plate unless otherwise indicated.
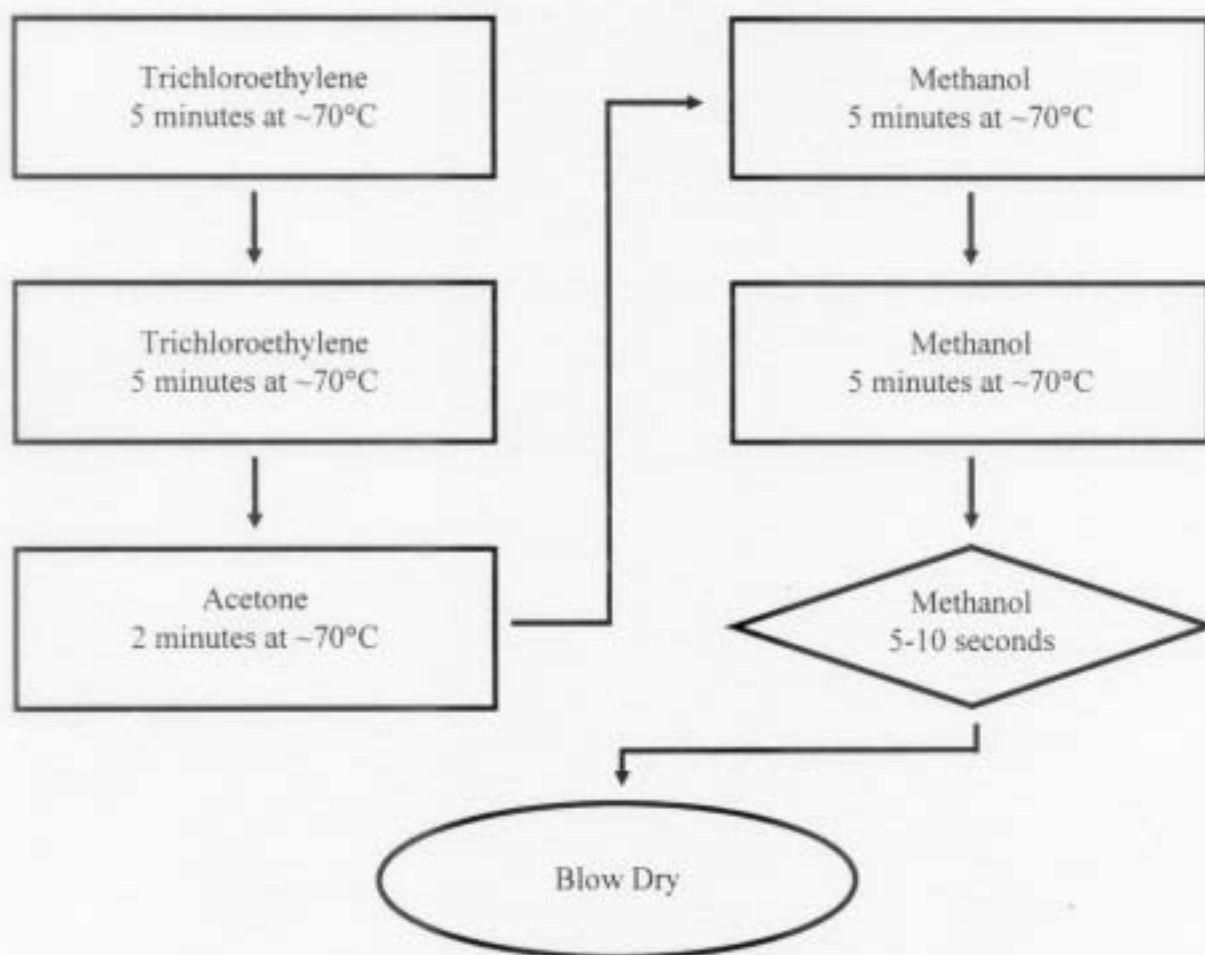
Fig. A.1 Flow chart for the degreasing procedure that is performed before each etch.

Fig. A.2 Flow chart of *ex-situ* CdTe etch.

Fig. A.3 Flow chart of *ex-situ* HgCdTe etch.

```
  ┌─────────────────┐                      ┌──────────────────────────┐
  │   DI H₂O        │                      │      DI H₂O              │
  │   5 minutes     │                      │ 10 seconds while agitating│
  └─────────────────┘                      └──────────────────────────┘
          │                                            │
          ▼                                            ▼
  ┌─────────────────┐                          ┌─────────────────┐
  │    Blow Dry     │                          │     DI H₂O      │
  └─────────────────┘                          │    5 minutes    │
          │                                     └─────────────────┘
          ▼                                            │
  ┌─────────────────────────┐                          ▼
  │ 8:1:1 H₂SO₄:H₂O₂:H₂O    │                  ┌─────────────────┐
  │      5 minute           │                  │    Blow Dry     │
  └─────────────────────────┘                  └─────────────────┘
          │
          ▼
  ┌─────────────────────────┐
  │    Cooling bath         │
  │ 8:1:1 H₂SO₄:H₂O₂:H₂O    │
  │      1 minute           │
  └─────────────────────────┘
```

Diamond: DI H_2O / 5 minutes

Ellipse: Blow Dry

Rectangle: 8:1:1 H_2SO_4:H_2O_2:H_2O / 5 minute

Rectangle: Cooling bath / 8:1:1 H_2SO_4:H_2O_2:H_2O / 1 minute

Rectangle: DI H_2O / 10 seconds while agitating
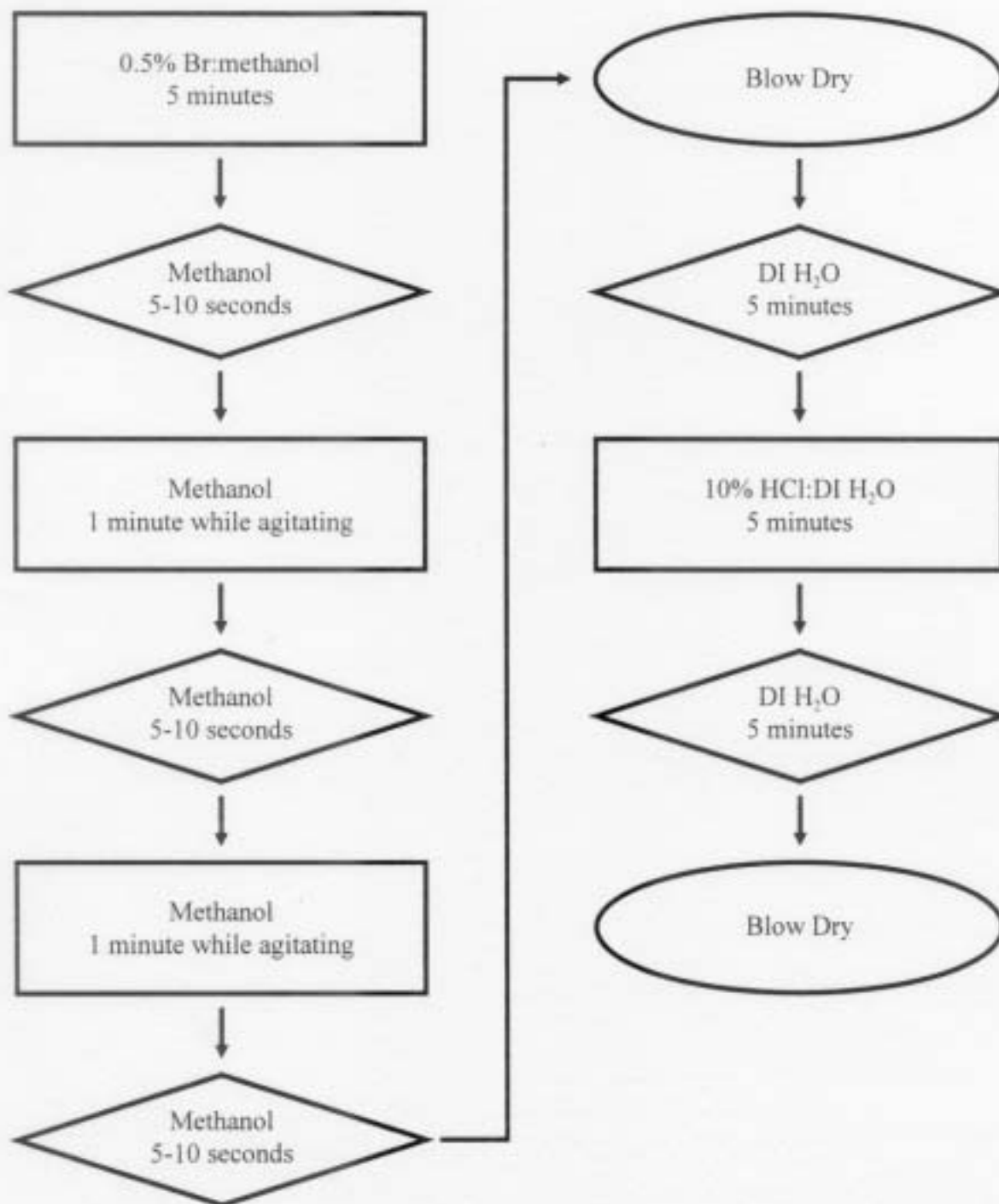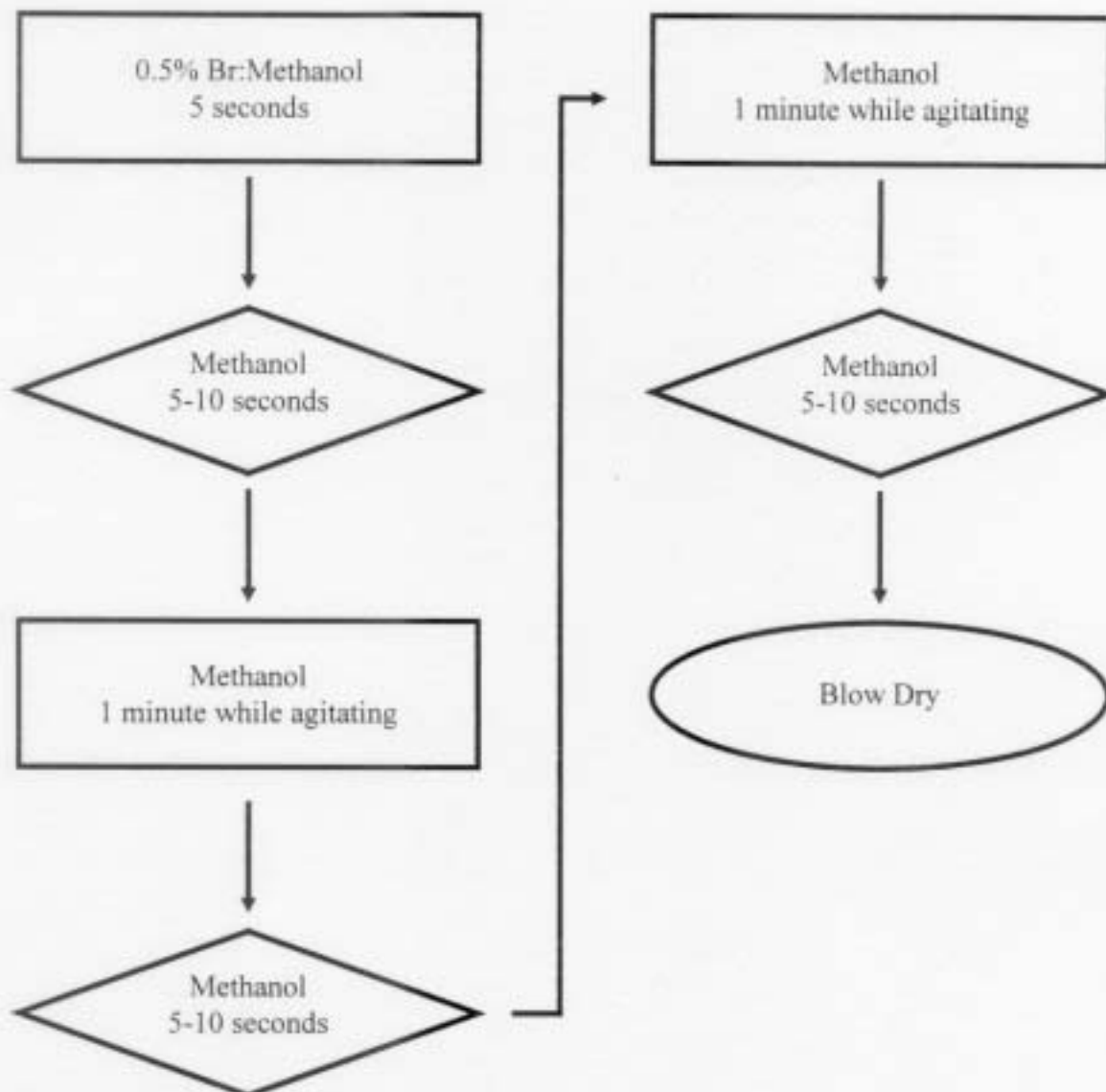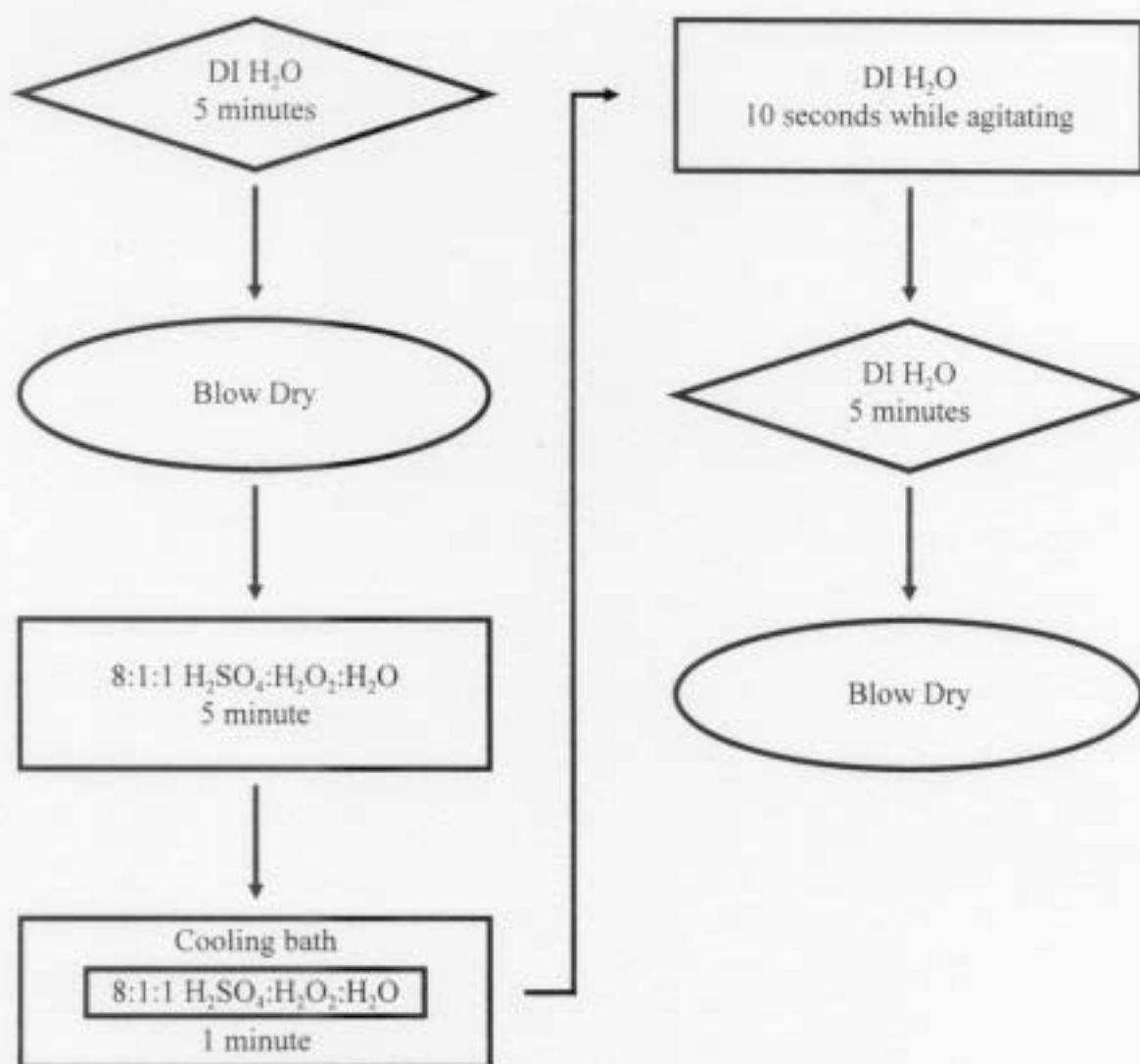
Diamond: DI H_2O / 5 minutes

Ellipse: Blow Dry

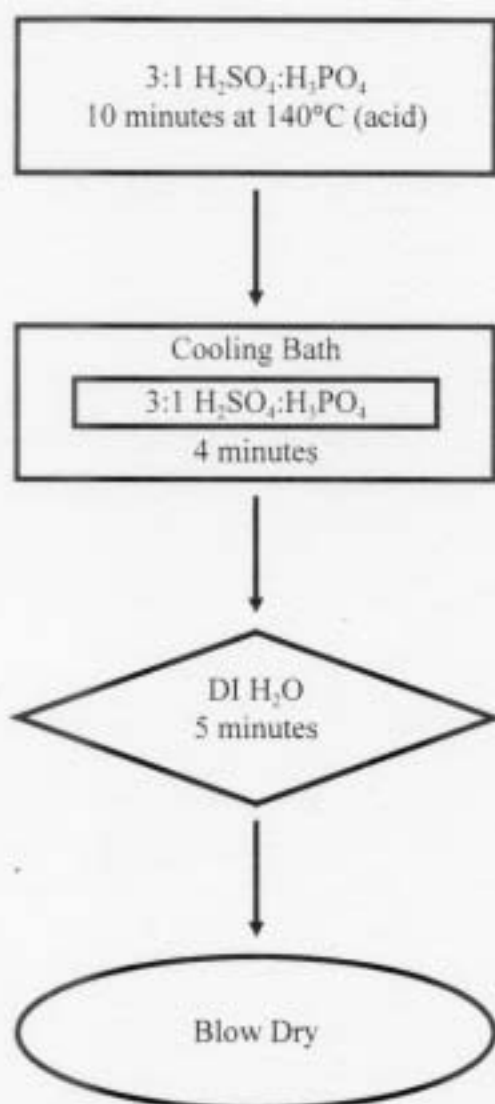Fig. A.4 Flow chart of *ex-situ* GaAs etch.
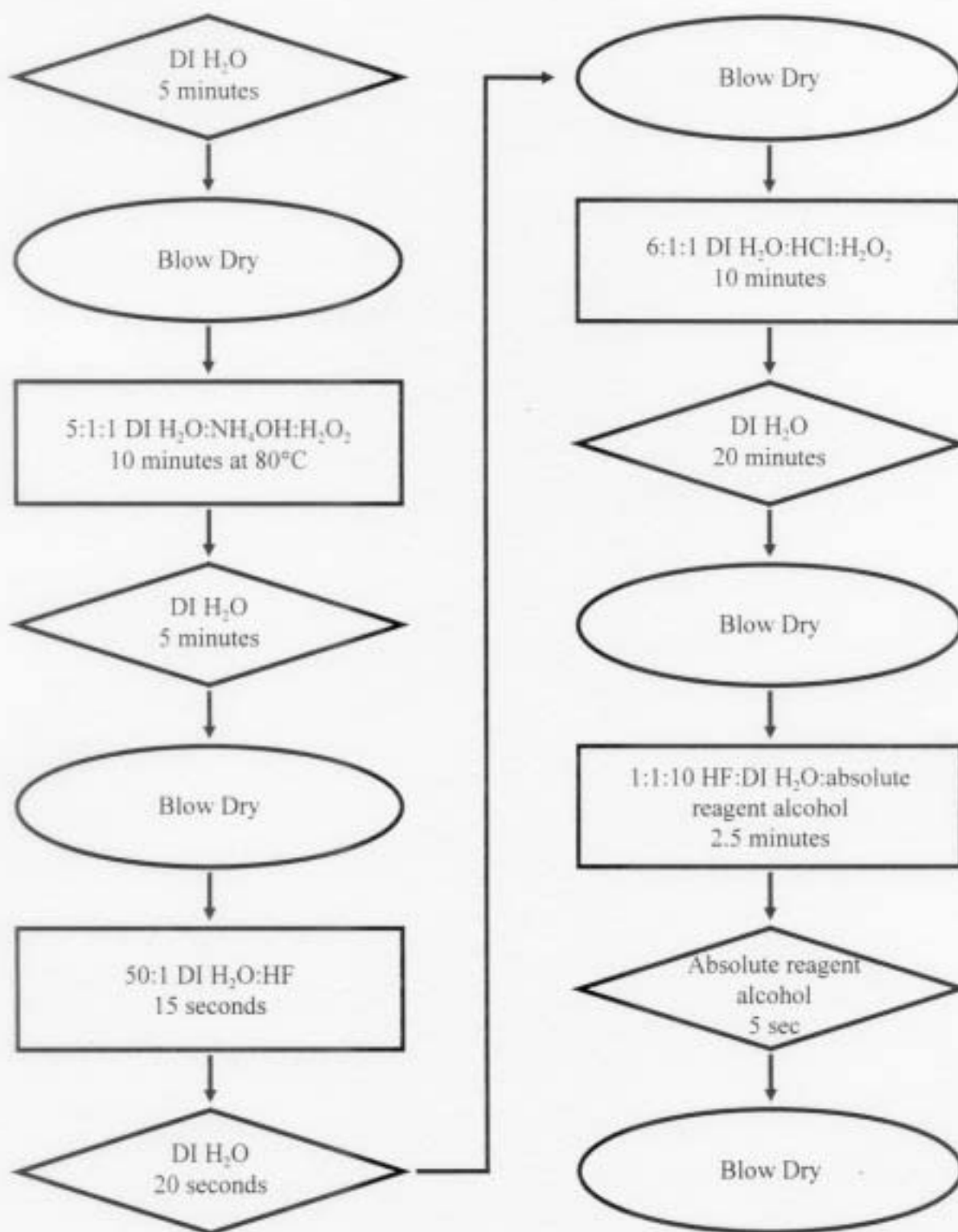
Fig. A.5 Flow chart of *ex-situ* sapphire etch.

Fig. A.6 Flow chart of *ex-situ* Si etch.

Appendix B: XPS Theory

One type of information which can be obtained from XPS measurements is the relative concentrations of the elements in the material. One way of determining this information is to compare peak areas of the individual constituents. The derivation of this method[14] as well as the analysis for two of the HgCdTe samples are given here.

The area under the peak can be calculated from the data by fitting a peak with a specific curve and integrating. The area under the curve is representative of the electron current due to the photoelectron process. The equation for the electron current for a specific transition i from a volume element located at a depth x within the sample is

$$dI_i = AI_p N_i S_i e^{-\frac{x}{\lambda_{pi}}} dx \qquad \text{(B.1)}$$

where A is the area of the x-ray beam, I_p is the incident beam's intensity, N_i is the number density of atoms producing the transition i, and S_i is the sensitivity factor. The sensitivity factor depends on a number of variables. The photoelectron cross section of the atomic orbital of interest, the angular efficiency factor for the instrumental arrangement based on the angle between the photon path and the detected electron, the efficiency of the formation of photoelectrons of a particular energy, and the detection efficiency are all hidden in S_i. The last variable in equation B.1, λ_{pi}, is a function of the absorption depth of the x-rays, λ_p (which is determined by the escape depth of the electron) and the transition electron, λ_i, as follows

$$\frac{1}{\lambda_{pi}} = \frac{1}{\lambda_p \cos\theta} + \frac{1}{\lambda_i \cos\alpha} \qquad \text{(B.2)}$$

The angles θ and α are angles made between a line perpendicular to the surface and the initial and reflected beams respectively.

For a thick slab equation B.1 should be integrated over x from zero to infinity. The integration proceeds as follows. (The superscript c is for constituent.)

$$I_i^c = \int_0^\infty AI_p N_i^c S_i^c e^{-\frac{x}{\lambda_{pi}^c}} dx \qquad \text{(B.3)}$$

$$I_i^c = AI_p N_i^c S_i^c (-\lambda_{pi}^c) e^{-\frac{x}{\lambda_{pi}^c}} \Big|_0^\infty \qquad \text{(B.4)}$$

$$I_i^c = AI_p N_i^c S_i^c \lambda_{pi}^c \qquad \text{(B.5)}$$

Now the equation can be solved for N_i^c, or the number of atoms producing this transition.

$$N_i^c = \frac{I_i^c}{AI_p S_i^c \lambda_{pi}^c} \qquad \text{(B.6)}$$

The concentration of one element in a compound, say mercury in HgCdTe, is the number of mercury atoms divided by the total number of atoms. This ratio looks like

$$\frac{N_i^{Hg}}{\sum N_i^c} = \frac{I_i^{Hg}/S_i^{Hg}}{\sum I_i^c/S_i^c \lambda_i^c} \times \frac{AI_p}{AI_p \lambda_i^{Hg}} \qquad \text{(B.7)}$$

At this point it is obvious that A and I_p will cancel. It should be noted that although λ_i^{Hg}, λ_i^{Cd}, and λ_i^{Te} will all vary slightly, it is a reasonable approximation to assume that they are equal. Because

119

of this approximation, λ_i^c can be pulled from the summation in equation B.8, and canceled with λ_i^{Hg}. The final equation then looks like

$$C_{Hg} = \frac{N_i^{Hg}}{\sum_i N_i^c} = \frac{I_i^{Hg} / S_i^{Hg}}{\sum_i I_i^c / S_i^c} \qquad (B.8)$$

Figures B.1-B.6 contain XPS data for two HgCdTe samples. The first sample was cleaned at ~80°C and the peak areas are given in table B.1. The sensitivity factors are found in literature, and vary slightly from paper to paper. These sets were all normalized to Te, and had ranges of sensitivity for Hg and Cd from 0.58 to 0.76 and from 0.46 to 0.62 respectively[36]. In order to determine which set of factors to use, XPS data from a CdTe sample believed to be stoichiometric was analyzed using several different sets of sensitivity factors. The results which best fit the known concentration levels were then used to determine the concentrations for the rest of the samples. These values, after being normalized to Te, are $S^{Te} = 1$, $S^{Hg} = 0.53$, and $S^{Cd} = 0.64$.[35]

As an example, the concentration levels of MCTT1B after being cleaned for 150 minutes with atomic hydrogen are determined as follows.

$$C_x = \frac{I^x / S^x}{I^{Hg} / S^{Hg} + I^{Cd} / S^{Cd} + I^{Te} / S^{Te}} \qquad (B.9)$$

$$C_{Hg} = \frac{139.22 / 0.53}{139.22 / 0.53 + 253.19 / 0.64 + 546.2 / 1} \qquad (B.10)$$

$$C_{Hg} = \frac{262.68}{262.68 + 395.61 + 546.2} \qquad \text{(B.11)}$$

$$C_{Hg} = 0.22 \qquad \text{(B.12)}$$

$$C_{Cd} = \frac{395.61}{262.68 + 395.61 + 546.20} \qquad \text{(B.13)}$$

$$C_{Cd} = 0.33 \qquad \text{(B.14)}$$

$$C_{Te} = \frac{546.20}{262.68 + 395.61 + 546.20} \qquad \text{(B.15)}$$

$$C_{Te} = 0.45 \qquad \text{(B.16)}$$

In addition to concentrations, the oxide thickness and the tellurium overlayer thickness can both be obtained from equation B.1. In this case the integral must be split into three parts. The first part is the integral over the oxide, which must extend from zero to the oxide thickness, t'. The second integral is over the tellurium overlayer, and extends from t' to t". Finally the substrate is integrated from t" to infinity. The three integrals are then

$$I_i^O = \int_0^{t'} AI_p N_i^O S_i^O e^{-\frac{x}{\lambda_{pi}}} dx \qquad \text{(B.17a)}$$

$$I_j^T = \int_{t'}^{t''} AI_p N_j^T S_j^T e^{-\frac{x}{\lambda_{pj}}} dx \qquad \text{(B.17b)}$$

$$I_k^S = \int_{t''}^{\infty} AI_p N_k^S S_k^S e^{-\frac{x}{\lambda_{pk}}} dx \qquad \text{(B.17c)}$$

In this case the superscripts o and s are to distinguish the oxide from the substrate. Solving these integrals gives

$$I_i^O = AI_p N_i^O S_i^O \lambda_{pi}^O (1 - e^{-\frac{t'}{\lambda_{pi}^O}})$$

(B.18a)

$$I_j^T = AI_p N_j^T S_j^T \lambda_{pi}^T (e^{-\frac{t'}{\lambda_{pi}^T}} - e^{-\frac{t''}{\lambda_{pi}^T}})$$

(B.18b)

$$I_k^S = AI_p N_k^S S_k^S \lambda_{pk}^S (e^{-\frac{t''}{\lambda_{pk}^S}})$$

(B.18c)

Taking the ratios of B.18a to B.18c and B.18b to B.18c, and making the approximation that the mean free paths are equal, the following two equations are obtained

$$\frac{I_i^O}{I_k^S} = \frac{N_i^O S_i^O}{N_k^S S_k^S} \left(\frac{1 - e^{-\frac{t'}{\lambda}}}{e^{-\frac{t''}{\lambda}}} \right)$$

(B.19a)

$$\frac{I_j^T}{I_k^S} = \frac{N_j^T S_j^T}{N_k^S S_k^S} \left(\frac{e^{-\frac{t'}{\lambda}} - e^{-\frac{t''}{\lambda}}}{e^{-\frac{t''}{\lambda}}} \right)$$

(B.19b)

Another approximation can now be made. This approximation is for the specific case in this thesis in which there is a tellurium oxide on a tellurium overlayer. It is assumed that the sensitivity factors for the oxide, the overlayer, and the substrate are equal for the following reason. As stated earlier, the elements that determine the sensitivity factor are the photoelectron cross section of the atomic orbital of interest, the angular efficiency factor for the instrumental arrangement based on the angle between the photon path and the detected electron, the efficiency of the formation of photoelectrons of a particular energy, and the detection efficiency. First of all, the photoelectron cross-section will be the same since all of the electrons are from the same

orbital. Secondly, the angular efficiency will obviously be constant during a scan, since it is due to the experimental setup. The efficiency of formation, and detection efficiency are functions of the binding energy of the electron. In this case the three components' binding energies differ in energy by only a few electron volts, hence the efficiencies will be equivalent. Since all of these components are similar, the ratios of the sensitivity factors is approximately one. Now, rearranging equations B.19a and B.19b yields

$$\frac{I_i^O N_k^S}{I_k^S N_i^O} = \frac{1 - e^{-\frac{t'}{\lambda}}}{e^{-\frac{t''}{\lambda}}}$$

(B.20a)

$$\frac{I_j^T N_k^S}{I_k^S N_j^T} = \frac{e^{-\frac{t'}{\lambda}} - e^{-\frac{t''}{\lambda}}}{e^{-\frac{t''}{\lambda}}}$$

(B.20b)

In completing the next steps it is useful to let the left hand side of equations B.20a and B.20b equal β and η respectively. Simple algebra gives

$$\beta e^{-\frac{t''}{\lambda}} = 1 - e^{-\frac{t}{\lambda}}$$

(B.21a)

$$e^{-\frac{t''}{\lambda}} = \frac{e^{-\frac{t'}{\lambda}}}{\eta + 1}$$

(B.21b)

and then solving for t' and t"

$$t' = -\lambda \ln\left(\frac{\eta + 1}{\beta + \eta + 1}\right)$$

(B.22a)

$$t'' = -\lambda \ln\left(\frac{1}{\beta + \eta + 1}\right) \tag{B.22b}$$

Again λ is the mean free path of the electrons, and β and η are a combination of the ratios of the peak areas and the number densities, or the number of atoms per cubic centimeter. The ratio of number densities is the same as the ratio of mass densities divided by the atomic weight. For example,

$$\frac{N^S}{N^O} = \frac{\rho^S A^O}{\rho^O A^O} \tag{B.23}$$

The value for the number density can be found in the CRC handbook.

The densities for Te in a HgCdTe matrix, amorphous Te, and Te-O are 7.7, 6.0, and 5.6 cm^3 respectively.[73] (The value for HgCdTe is actually approximated from values for CdTe and HgTe.) Again, as an example, the oxides and overlayer thicknesses after the Br:methanol etch on sample WVU B are computed in the following manner.

$$\beta = \frac{I^O N^S}{I^S N^O} \tag{B.24}$$

$$\beta = \frac{1068.1 \times 7.7}{1540.2 \times 5.6} \tag{B.25}$$

$$\beta = 0.95 \tag{B.26}$$

$$\eta = \frac{I^T N^S}{I^S N^T} \tag{B.27}$$

$$\eta = \frac{2458.8 \times 7.7}{1540.2 \times 6.0} \tag{B.28}$$

$$\eta = 2.05 \tag{B.29}$$

Using the universal curve the escape depth, λ_p, can be estimated to be 15 Å for each of the constituents. The penetration depth of the x-rays, λ_f, is much deeper than the sampling volume and can be taken to be infinite here. Thus, the λ in the above equations (λ_p, from Eq. B.2) is 15Åcosθ, where θ=10° is the approximate angle our XPS detector makes with the sample normal. Substitution of these values into equation B.22 gives

$$t' = -15 \ln\left(\frac{2.05+1}{0.95+2.05+1}\right) \tag{B.30}$$

$$t' = 4.02 \text{ Å} \tag{B.31}$$

$$t'' = -15\left(\frac{1}{0.95+2.05+1}\right) \tag{B.32}$$

$$t'' = 20.74 \text{ Å} \tag{B.33}$$

Appendix C

The following pages give the XPS graphs as a function of time for mercury, cadmium, and tellurium for two standard samples. The first sample was cleaned using atomic hydrogen at "room-temperature", and the other was cleaned with atomic hydrogen at 80°C. Following the graphs is a complete set of analyzed data. This data includes the x-values, oxide thicknesses, and tellurium overlayer thicknesses as functions of time.

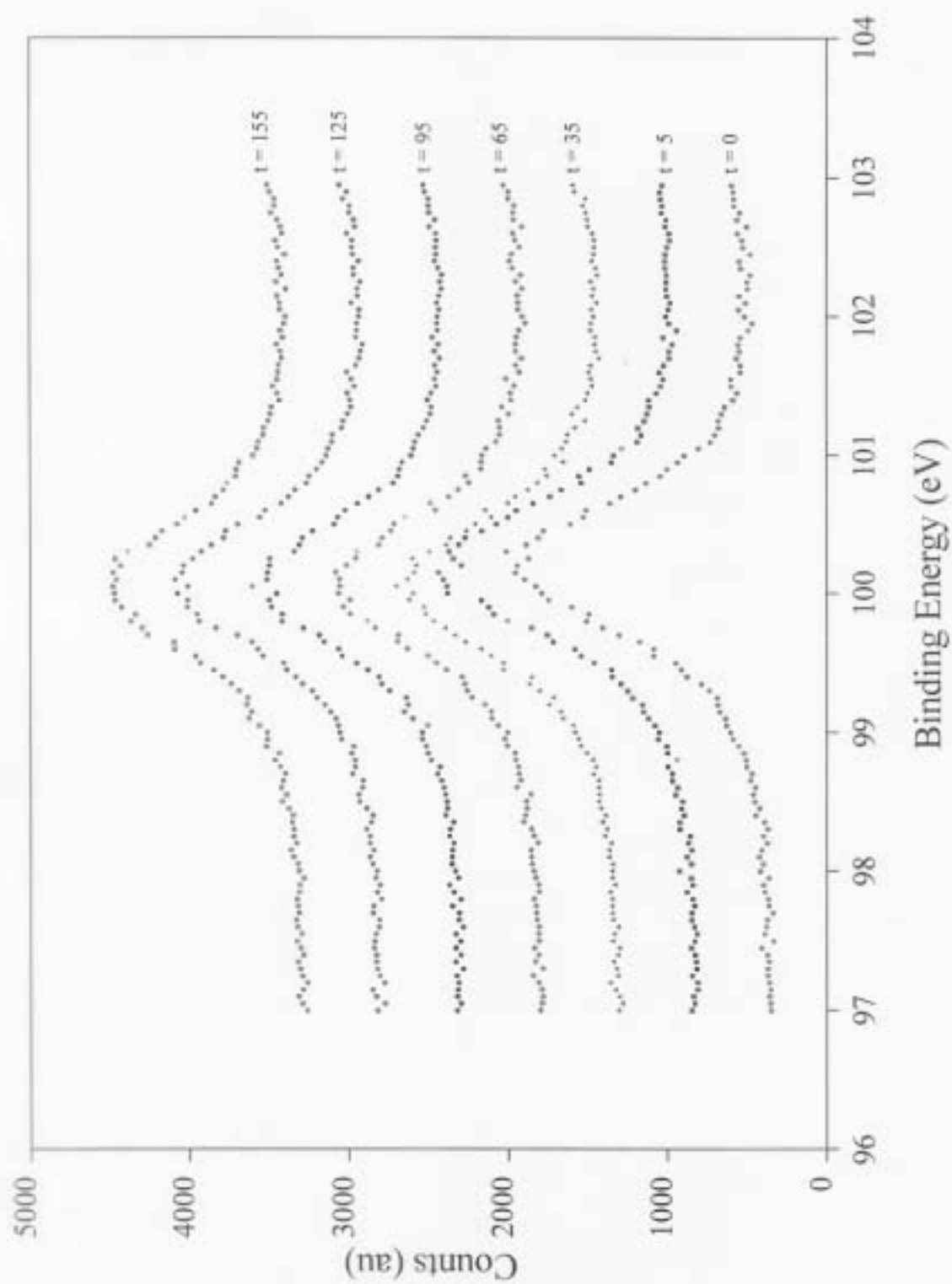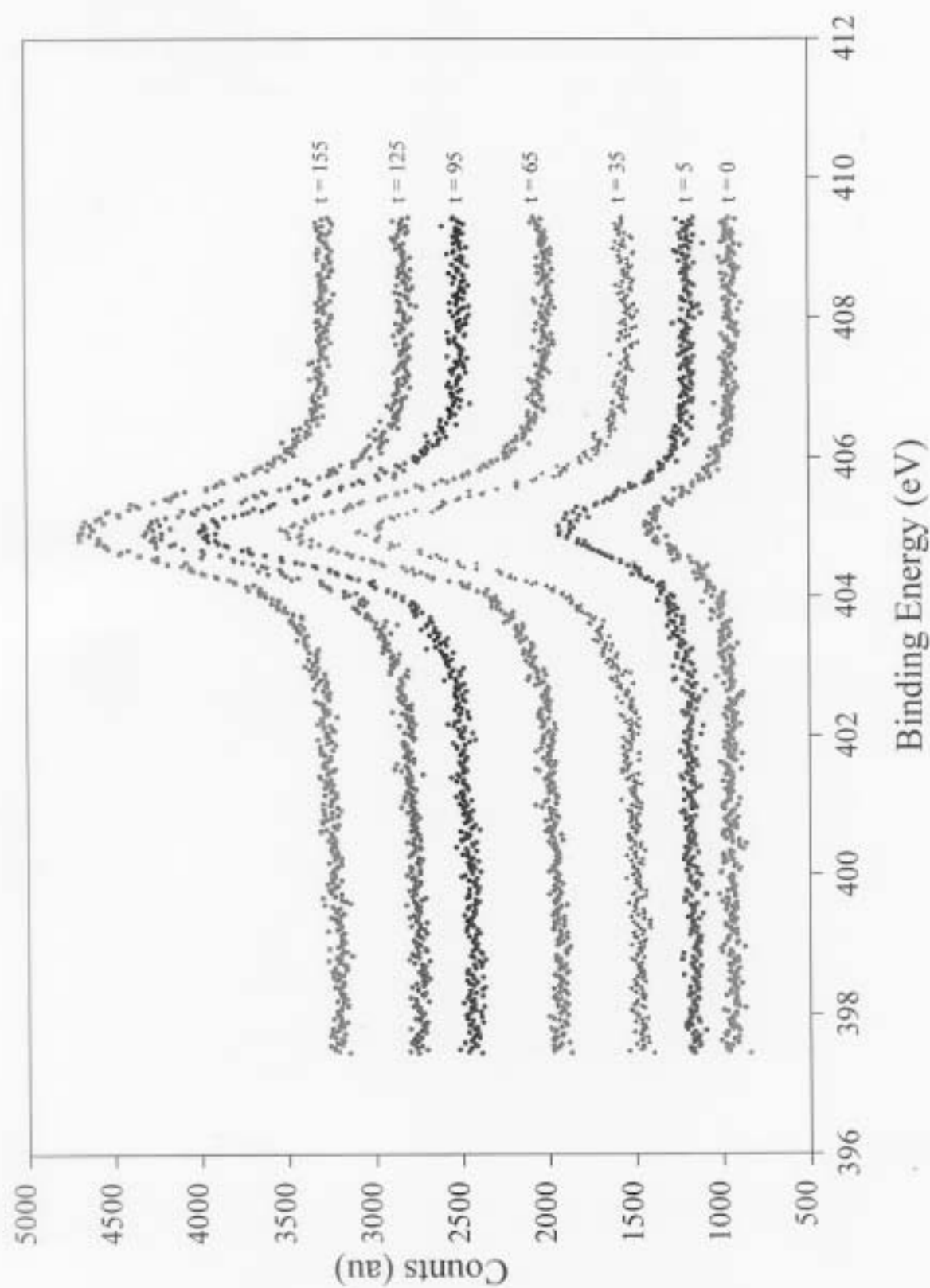Fig. C.1   XPS scans of Hg on WVUG as a function of hydrogen cleaning time at ~80°C.

Fig. C.2 XPS scans of Cd on WVUG as a function of hydrogen cleaning time at ~80°C.
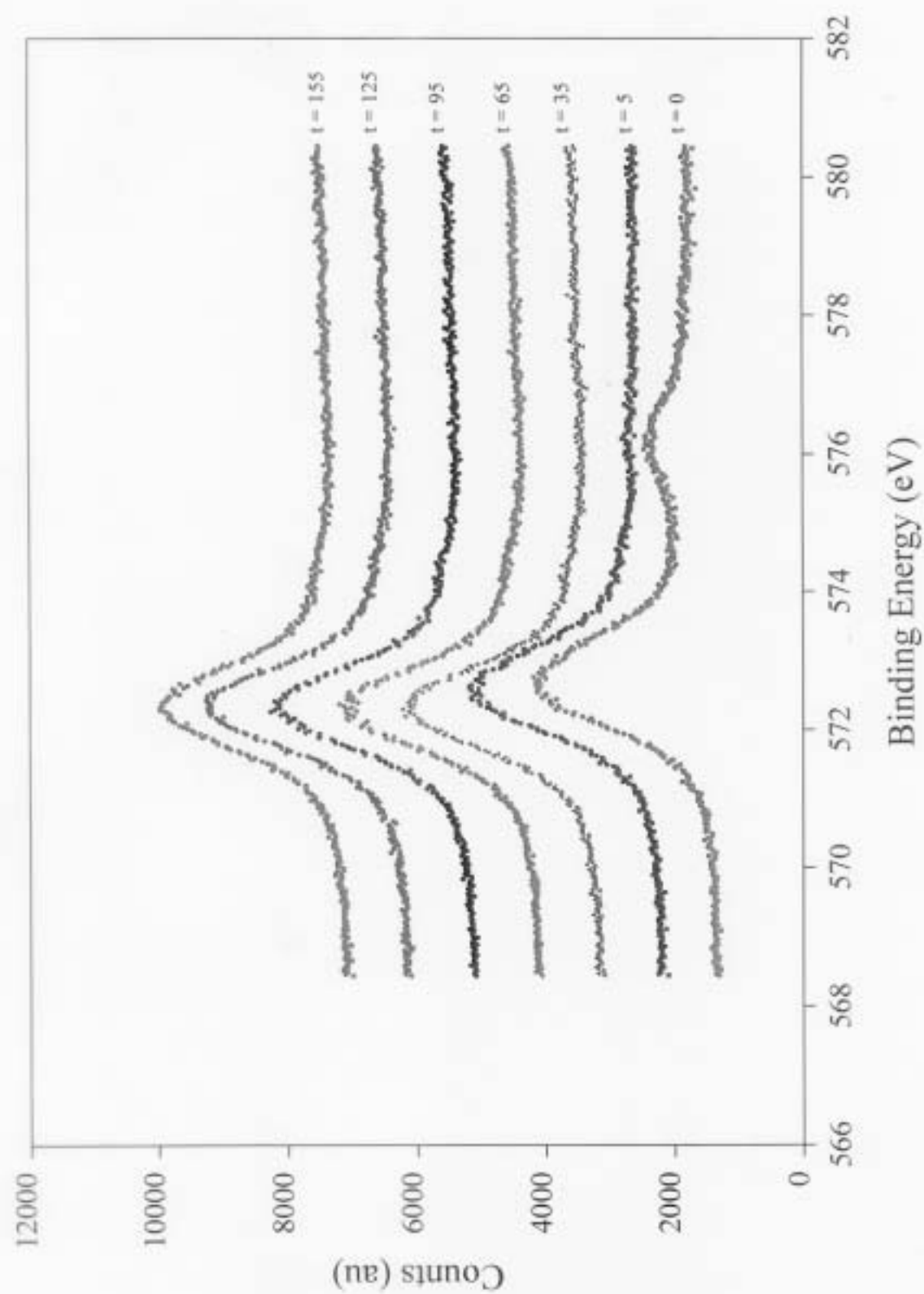
Fig. C.3   XPS scans of Te and Te-O on WVUG as a function of hydrogen cleaning time at ~80°C.

	Peak Position (eV)	After Br Etch	5 min a-H Etch	30 min a-H Etch	48 Hour Break	30 min a-H Etch	30min a-H etch	30 min a-H Etch	30 min a-H Etch
Hg $4f_{7/2}$ Peak	100.15 ±0.05	2269.8	2274.5	1939.8	1790.6	1822.4	1796.5	1823.7	1756.8
Cd $3d_{5/2}$ Satellite	403.85 ±0.15	61.6	61.8	207.4	206.4	209.2	190.8	152.9	208.0
Cd $3d_{5/2}$ Peak	405.05 ±0.05	671.0	990.8	2153.5	2025.4	2159.6	2129.9	2136.6	2035.5
HgCdTe Te $3d_{5/2}$ Peak	572.3	910.7 (13.2%)	2077.1 (34.0%)	4877.0 (86.8%)	4667.6 (92.6%)	4995.2 (92.6%)	5069.7 (91.9%)	5189.3 (92.4%)	4733.1 (93.5%)
Metallic Te $3d_{5/2}$ Peak	572.8	3905.0 (56.8%)	3023.0 (49.4%)	153.0 (2.7%)	0 (0%)	0 (0%)	0 (0%)	0 (0%)	0 (0%)
HgCdTe Te $3d_{5/2}$ Satellite	574.1	238.6 (3.5%)	184.4 (3.0%)	464.5 (8.3%)	370.8 (7.4%)	395.5 (7.3%)	444.9 (8.1%)	426.8 (7.6%)	327.1 (6.5%)
Metallic Te $3d_{5/2}$ Satellite	574.6	480.8 (7.0%)	447.6 (7.3%)	24.5 (0.4%)	0 (0%)	0 (0%)	0 (0%)	0 (0%)	0 (0%)
Te-Oxide $3d_{5/2}$ Peak	576.2	1131.2 (16.5%)	260.2 (4.3%)	9.2 (0.2%)	0 (0%)	0 (0%)	0 (0%)	0 (0%)	0 (0%)
Te-Oxide $3d_{5/2}$ Satellite	578.1	210.3 (3.1%)	125.0 (2.0%)	89.5 (1.6%)	0 (0%)	0 (0%)	0 (0%)	0 (0%)	0 (0%)

Table C.1   Peak areas for Hg, Cd, Te, and TeO_2 in the XPS spectra of WVUG in Fig. C.1-3. All of the peaks in the Te scan also have the percent of the total area of the graph that they represent.

	After Br Etch	5 min a-H Etch	30 min a-H Etch	48 Hour Break	30 min a-H Etch	30 min a-H etch	30 min a-H Etch	30 min a-H Etch
Hg Percent Composition	38.0	38.3	30.3	30.1	29.1	28.8	28.7	29.5
Cd Percent Composition	9.3	13.8	27.9	28.2	28.6	28.2	27.9	28.3
HgCdTe Te % Composition	8.1	18.5	40.4	41.6	42.3	43.0	43.4	42.2
Metallic Te % Composition	34.6	27.0	1.3	0.0	0.0	0.0	0.0	0.0
Oxide Te % Composition	10.0	2.3	0.1	0.0	0.0	0.0	0.0	0.0
HgCdTe x-Value	0.20	0.27	0.48	0.48	0.50	0.50	0.49	0.49
Oxide Thickness (Å)	3.47	0.71	0.02	0.0	0.0	0.0	0.0	0.0
Te-overlayer Thickness (Å)	20.97	9.15	0.26	0.0	0.0	0.0	0.0	0.0

Table C.2   Percent concentrations, x-values, oxide thicknesses, and overlayer thicknesses for the XPS spectra in Fig.C.1-3.
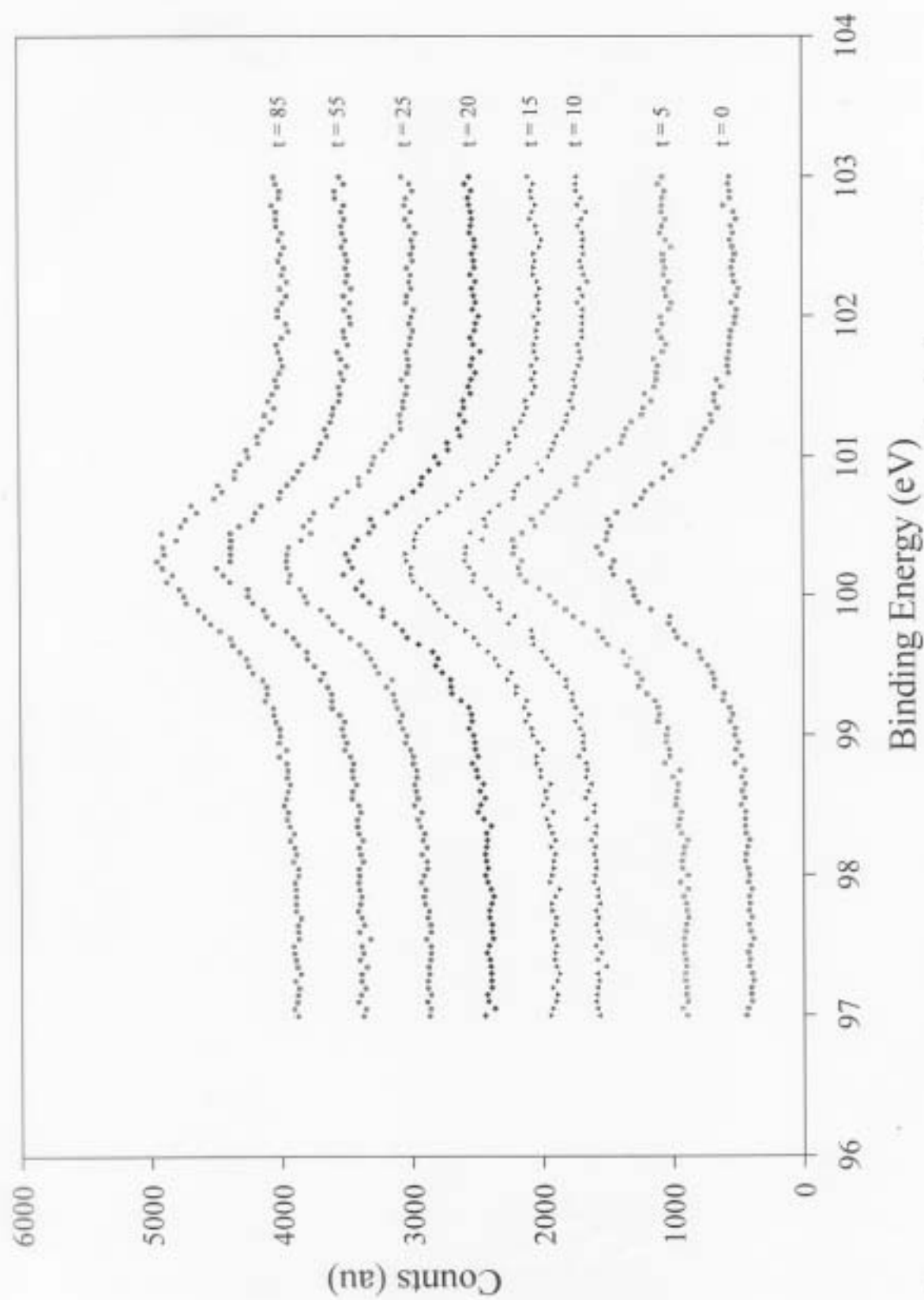
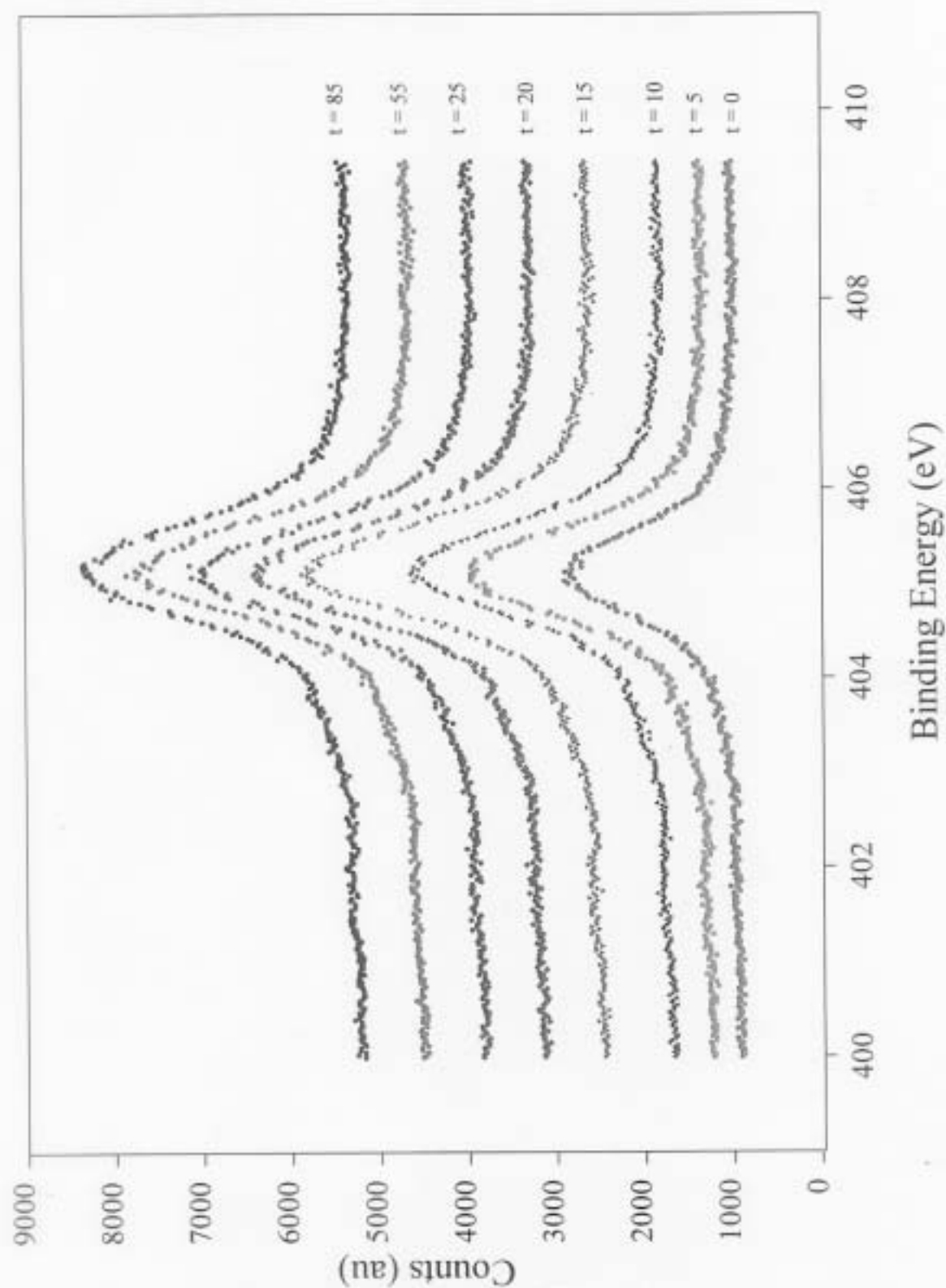Fig. C.4 XPS scans of Hg on WVUD as a function of hydrogen cleaning time at ~50°C

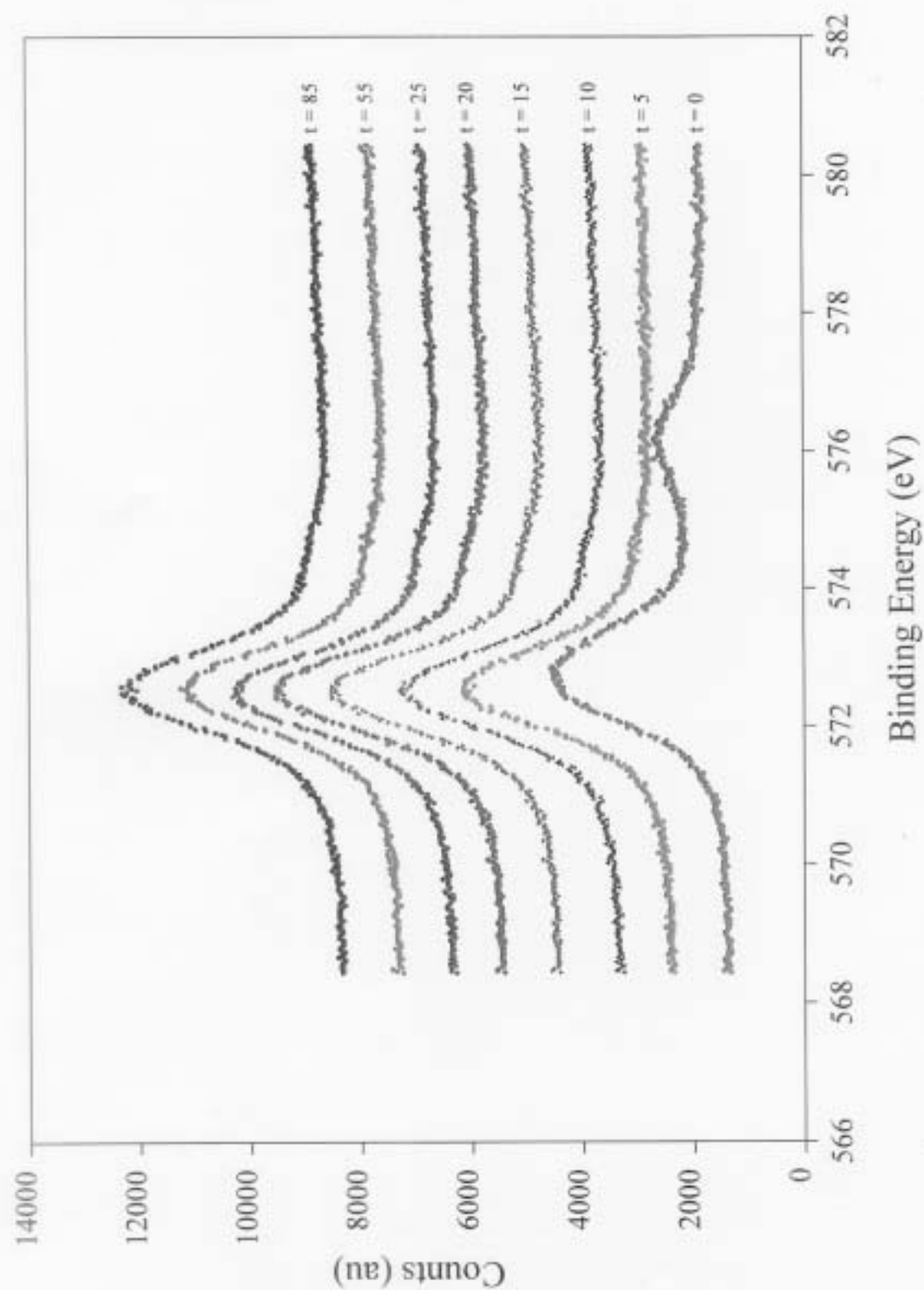Fig. C.5 XPS scans of Cd on WVUD as a function of hydrogen cleaning time at ~50°C

Fig. C.6 XPS scans of Te and Te-O on WVUD as a function of hydrogen cleaning time at ~50°C

	Peak Position (eV)	After Br Etch	5 min a-H Etch	5 min a-H Etch	5 min a-H Etch	5 min a-H Etch	5 min a-H etch	30 min a-H Etch	30 min a-H Etch
Hg 4f$_{7/2}$ Peak	100.25 ±0.05	1617.6	1943.6	1448.4	1653.6	1566.6	1551.1	1540.1	1473.4
Cd 3d$_{3/2}$ Satellite	403.8	175.7	275.6	297.1	343.3	365.0	343.5	392.2	368.3
Cd 3d$_{3/2}$ Peak	405.15 ±0.05	2657.0	3792.8	4183.5	4847.0	4705.3	4670.1	4686.4	4574.1
HgCdTe Te 3d$_{5/2}$ Peak	572.5	3026.0 (37.5%)	5530.7 (77.9%)	6298.3 (86.3%)	6589.6 (88.7%)	6617.9 (91.6%)	6560.4 (93.7%)	6448.3 (94.2%)	6515.2 (94.4%)
Metallic Te 3d$_{5/2}$ Peak	573.1	2749.1 (34.0%)	878.2 (12.4%)	444.2 (6.1%)	326.5 (4.4%)	115.1 (1.6%)	0 (0%)	0 (0%)	0 (0%)
HgCdTe Te 3d$_{5/2}$ Satellite	574.3	337.5 (4.2%)	374.6 (5.3%)	373.3 (5.1%)	489.5 (6.6%)	488.3 (6.8%)	441.3 (6.3%)	398.9 (5.8%)	389.0 (5.6%)
Metallic Te 3d$_{3/2}$ Satellite	574.9	346.4 (4.3%)	150.6 (2.1%)	112.3 (1.5%)	11.9 (0.2%)	6.2 (0.1%)	0 (0%)	0 (0%)	0 (0%)
Te-Oxide 3d$_{5/2}$ Peak	576.2	1419.8 (17.6%)	96.6 (1.4%)	0.7 (0.0%)	4.7 (0.1%)	0 (0%)	0 (0%)	0 (0%)	0 (0%)
Te-Oxide 3d$_{3/2}$ Satellite	578.1	195.0 (2.4%)	65.8 (0.9%)	69.0 (0.9%)	10.6 (0.1%)	0 (0%)	0 (0%)	0 (0%)	0 (0%)

Table C.3   Peak areas for Hg, Cd, Te, and TeO$_2$ in the XPS spectra of WVUDin Fig. C.4-6. All of the peaks in the Te scan also have the percent of the total area of the graph that they represent.

	After Br Etch	5 min a-H Etch	5 min a-H Etch	5 min a-H Etch	5 min a-H Etch	5 min a-H etch	30 min a-H Etch	30 min a-H Etch
Hg Percent Composition	21.2	22.8	22.0	17.7	17.3	17.4	17.4	16.9
Cd Percent Composition	28.8	36.8	52.7	43.0	43.1	43.5	43.9	43.5
HgCdTe Te % Composition	21.0	34.4	21.7	37.4	38.8	39.1	38.7	39.6
Metallic Te % Composition	19.1	5.5	3.6	1.9	0.0	0.0	0.0	0.0
Oxide Te % Composition	9.9	0.6	0.0	0.0	0.0	0.0	0.0	0.0
HgCdTe x-Value	0.58	0.62	0.71	0.71	0.71	0.71	0.72	0.72
Oxide Thickness (Å)	2.95	0.17	0.00	0.00	0.00	0.00	0.00	0.00
Te-overlayer Thickness (Å)	8.75	1.36	0.54	0.39	0.14	0.00	0.00	0.00

Table C.4   Percent concentrations, x-values, oxide thicknesses, and overlayer thicknesses for the XPS spectra in Fig.C.4-6.
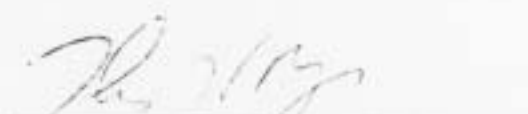
APPROVAL OF EXAMINING COMMITTEE

Preparation of Substrates for Semiconductor Growth Using Atomic Hydrogen

By Lauren S. Hirsch

Submitted to the Eberly College of Arts and Sciences of West Virginia University
In Partial Fulfillment of the Requirements for
The Degree of Master of Science
in Physics

_____   4/7/99
Charter D. Stinespring, Ph.D.   Date

_____   4/7/95
David Lederman, Ph.D.   Date

_____
Thomas H. Myers, Ph.D.   Date
(Committee Chair)

137